ABSTRACT

Title of dissertation: INTERFACIAL CONSIDERATIONS FOR DROPLET PCR LAB-ON-CHIP DEVICES

Kunal Ryan Pandit, Doctor of Philosophy, 2015

Dissertation directed by: Professor Ian White
Fischell Department of Bioengineering

Professor Srinivasa Raghavan
Department of Chemical & Biomolecular Engineering

Lab-on-chip devices have the potential to decentralize the current model of diagnostics to point-of-care diagnostics. Easy to use, low cost, rapid infectious disease diagnostic tools could especially impact and improve healthcare in low resource areas. Micro-total-analytical-systems could also enable smarter medical decisions, quicker patient recoveries, and cheaper healthcare costs in fully developed settings. Significant innovations to standard technologies used today will help realize the promise of lab-on-chip devices. In this work, innovative technologies compatible with current lab-on-chip devices were investigated to simplify their operation, decrease their complexity, and reduce their cost. The interfacial aspects that dominate microfluidic systems, and in particular droplet polymerase chain reaction (PCR) devices, are emphasized.

Droplet PCR utilizing microfluidic technology has largely been automated, but sample preparation methods prior to amplification remains a laborious process. We have developed particles that condense the many steps of sample preparation into a single

buffer protocol. The particles were made by crosslinking chitosan, a pH responsive biopolymer. DNA was electrostatically and sterically adsorbed to the beads at pH 8.5. Furthermore, amplification of DNA directly off the beads was demonstrated eliminating the need to desorb DNA into solution. Implementation of these particles will drastically simplify droplet PCR lab-on-chip devices.

We also characterized the adsorption of polymerase at the oil-water interfaces of droplets and identified a surfactant to prevent the loss of polymerase in solution. The pendant drop technique was used to observe the change in interfacial tension due to adsorption of Taq Pol and/or surfactants to the interface. PCR performance of two surfactants, Brij L4 and ABIL EM90, were predicted from equilibrium interfacial tension measurements. Brij L4, a surfactant that had never been used with PCR, prevented polymerase adsorption and enabled more efficient PCR than ABIL EM90, a popular PCR surfactant.

Lastly, we ambitiously designed a system to conduct droplet PCR without oil or surfactants. Droplets were generated on-chip by adapting a co-flow droplet generating device previously developed in our group. Then droplets were immobilized on-chip in hydrodynamic traps. Two different modes of trapping were demonstrated, indirect and direct. Also, all aspects of an air continuous phase droplet PCR device were considered such as protein adsorption to channel walls and droplet evaporation during thermal cycling.

# INTERFACIAL CONSIDERATIONS FOR DROPLET PCR LAB-ON-CHIP DEVICE

by

Kunal Ryan Pandit

Dissertation submitted to the Faculty of the Graduate School of the
University of Maryland, College Park in partial fulfillment
of the requirements for the degree of
Doctor of Philosophy
2015

Advisory Committee:

Professor Srinivasa R. Raghavan, Chair & Co-Advisor
Associate Professor Ian M. White, Advisor
Professor Don L. DeVoe
Professor Richard V. Calabrese
Assistant Professor Amy J. Karlsson

# Acknowledgements

First I'd like to express my gratitude to Prof. Ian White and Prof. Srini Raghavan for guiding me the past 3 years. Thank you Ian for giving me the freedom to investigate my ideas that were rational as well as my ideas that were out of the box. And thank you Srini for your critical eye that helped to improve all facets of my work.

This dissertation was a result of interdisciplinary collaboration across multiple research groups on campus and with the gracious funding from Canon U.S. Life Sciences. I'd especially like to thank Prof. Richard Calabrese and his former student Dr. Paul Rueger for use of his pendant drop equipment, software to translate droplets images into interfacial tension measurements, and helpful discussions. I'd also like to acknowledge the support and helpful discussion in multiple areas of this dissertation from Prof. Don DeVoe and his research group especially Dr. Eric Kendall, Alex Sposito as well as Dr. Kunqiang Jiang and Annie Lu (co-advised with Srini). Droplet qPCR experiments would not be possible without the use of Prof. Keith Herold's equipment and Dr. Alex Blake's advice. My microfabrication skills were a direct result of continuous advice from Dr. Debalina Chatterjee, Dr. Jeffery Burke, and the facilities and staff at the UMD FabLab. And similarly I'd like to thank Dr. Eric Hoppmann and Dr. Niketa Jani for advice with PCR. I'd also like to thank Dr. Weidong Cao for his ongoing discussion of chitosan particles.

I am also immensely grateful for my current and past colleagues in Ian's lab: Dr. Veemoon Yu, Dr. Eric Hoppmann, Dr. Soroush Yazdi, Stephen Restaino, Sean Virgile, John Goertz, and Hieu Nguyen. As well as in Srini's lab: Dr. Chanda Arya, Dr. Vishal Javvaji, Dr. Kunqiang Jiang, Dr. Hyuntaek Oh, Kevin Diehn, Veena Rao, Jasmin Athas,

Annie Lu, Charles Kuo, Ankit Gargava, Ian MacIntire, and Brady Zarket. And a very special thank you to Imaly Nanayakkara for your extremely valuable help in pushing me to the finish line. You all have aided me in so many tangible and intangible ways.

Finally a special thanks to my family, especially my parents and Liza for your unwavering love and support.

# Contents

## List of Figures

# Chapter 1 INTRODUCTION AND OVERVIEW

## 1.1 Motivation

Point-of-care diagnostic tests that can be performed in low-infrastructure settings are a crucial component missing in the combat against infectious diseases in developing countries (Urdea et al. 2006; Peter et al. 2008). Lab-on-chip products have been envisioned as a solution to meeting the demands of diagnostic needs for monitoring disease progression and treatment efficacy (Chin et al. 2011; Gubala et al. 2012) due to their projected portability, ease of use, and quick sample to answer time. In particular, there is a strong clinical demand of nucleic acid point-of-care detection (Niemz, Ferguson, and Boyle 2011; Ahmad and Hashsham 2012). However, nucleic acid assays are some of the most challenging to develop due to numerous steps in sample preparation, instability, signal amplification, and target contamination (Chin, Linder, and Sia 2012).

Nevertheless, a few semi lab-on-chip nucleic acid diagnostic devices that require instrument support have been commercialized. For example, BD (BD MAX™), Cepheid (GeneXpert®), Micronics (PanNAT®), and BioFire Diagnostics (FilmArray) sell cartridges to be used in large benchtop control systems for nucleic acid diagnostic detection. The cartridges are designed with microfluidic channels to perform sample preparation, reagent mixing, and amplification assays. The benchtop systems heat/cool the reactions, control the fluidics in the cartridges, and house optics for fluorescence detection. Continuous flow microfluidic channels are used in the cartridges where independent operation of different areas in the cartridge are impossible without valves. Thus an

increased number of separate buffer or solvent steps requires more involved microfluidic channel designs and complex fluidic controls (Sista et al. 2008). In general, these commercial systems are not portable and developed for a central lab paradigm.

In contrast to continuous flow, discrete or digital microfluidics break up a fluid into droplets in channels using multiphase flows or in open structures (although droplets are still covered in oil in nucleic acid amplification methods) using technologies such as electrowetting (Cho, Moon, and Kim 2003; Pollack, Shenderov, and Fair 2002) or surface acoustic waves (Ding et al. 2013; Guttenberg et al. 2005). Droplet microfluidics apportions fluids into discrete microreactors which raises local concentrations of nucleic acids and enables high-throughput processing through massive parallelization. (Pompano et al. 2011). However, very few digital microfluidic devices have hit the market. One of the few successful technologies are multiphase droplet generators from BD and RainDance that are only approved for research use to absolutely quantify DNA. Also, Illumina has very recently commercialized a droplet based next generation sequencing library preparation chip. One barrier holding back commercialization of nucleic acid diagnostic digital lab-on-chip devices is the loss of enzymes to oil-water interfaces.

There clearly is a need for improvements to realize the potential of true lab-on-chip devices for point-of-care testing. In general they need to be less complex and cheaper. One strategy to achieve this would be to simplify assay protocols before designing a device to integrate and automate them. As stated earlier, on-chip nucleic acid assays are difficult to design because of complex sample preparation. Simpler nucleic acid purification technologies would eliminate the need for nucleic acid elution from solid phases, decrease the number of buffers necessary, and optimize the buffers to be compatible with PCR as

well as nucleic acid extraction. Novel and simpler solid phase extraction schemes would be enabled by engineering the interfacial interaction of nucleic acids with surface of the solid material. Another strategy to make lab-on-chip devices inexpensive would be to minimize the adsorption of enzymes to oil-water interfaces. Assay costs due to enzyme adsorption or specialty reagents to prevent enzyme adsorption in water in oil droplet microfluidics is prohibitive. Specifically for nucleic acid diagnostics, the most basic polymerase accounts for more than 95% of the cost of each bulk reaction. Novel PCR compatible surfactants that completely prevented Taq Pol adsorption in mineral oil would keep costs of droplet PCR low. A more drastic approach would be to remove the oil interface. However, reliable generation of droplets without breaking apart in confined microfluidic channels has not been demonstrated. Aqueous droplets break apart on surfaces with contact angles as large as 100°. Also, evaporation during PCR is a major concern because droplets evaporate faster than bulk phases due to their larger surface area and higher curvature. Furthermore, protein adsorption may still remain an issue because the droplets would still be in contact with hydrophobic channel walls.

## 1.2 Overview

This dissertation focuses on three different research projects to improve lab-on-chip devices, (i) extraction of DNA using a single buffer, (ii) prevention of Taq Pol adsorption to oil-water interfaces and (iii) droplet microfluidics without oil or surfactants. The remainder of Chapter 1 presents the proposed approach and significance of the research projects. In Chapter 2, PCR is reviewed in detail. Further background information specific to the research projects is reviewed in their respective chapters. DNA extraction with chitosan particles using only one buffer that is optimal for PCR is examined in Chapter 3.

In Chapter 4, characterization of Taq Pol adsorption and prediction of surfactant performance in PCR is presented. Droplet microfluidics and hydraulic trapping with an air continuous phase is demonstrated in Chapter 5. Finally in Chapter 6, the research findings are summarized and future work to advance the research is proposed.

## 1.3 Proposed approach

In Chapter 3, an extremely simple DNA extraction method is presented. Whole magnetic chitosan particles were manufactured without surface modifications to adsorb DNA. The extraction method made use of a single aqueous buffer that is optimal for nucleic acid amplification. Solutions of plasmid and genomic DNA were mixed with the particles in microcentrifuge tubes. DNA remaining in the supernatant was quantified using qPCR. DNA products were amplified directly from adsorbed plasmid or genomes. The mechanism of DNA extraction was elucidated by measuring the adsorption of dyes through UV-VIS spectroscopy.

In Chapter 4, the adsorption of Taq Pol to an oil-water interface was characterized and a novel surfactant to prevent protein adsorption was identified. Protein was indirectly characterized by measuring interfacial tension decrease through the pendant drop method. Surfactant and combined protein and surfactant adsorption were also characterized to select a superior surfactant to prevent Taq Pol adsorption. Superior surfactant performance was confirmed through droplet PCR, emulsion PCR, and qPCR.

In Chapter 5, a co-flow device was adapted to generate droplets on-chip. Hydraulic traps were designed using analytical equations and simulations as a guide. Droplets were hydraulically captured on-chip by two different modes of trapping, direct and indirect.

Droplet generation and manipulation with minimal satellite droplet formation was achieved by ensuring the channel walls were superhydrophobic.

## 1.4 Significance

All of the innovations presented in this dissertation improve upon currently used methods, and can easily be integrated into lab-on-chip devices. The chitosan beads in Chapter 3 simplifies DNA extraction so that only a single buffer is used. Current DNA/RNA solid phase extraction kits require at least two buffers, one to adsorb DNA and another to elute DNA. Our chitosan beads eliminate the elution step because DNA can be amplified directly off the chitosan beads. This has only be shown with one other commercial product (DYNA direct beads, Life Technologies) using an isothermal nucleic acid amplification technique, i.e. not PCR (Yi Sun et al. 2015). In the field of DNA extraction, our chitosan beads are the easiest to use in bulk scale protocols and to implement in microfluidic devices because they challenge the current two step solid phase extraction paradigm. Also this innovating enables sample preparation to be easily integrated into lab-on-chip devices. Current lab-on-chip devices are difficult to design and operate because of numerous buffer washes and valve manipulation. Reduction of sample preparation to a single buffer could realize the potential of lab-on-chip devices. The potential to perform point-of-care diagnostics in low resource setting, bringing quality health care to at risk populations. And also the potential to increase the efficiency of health care in high resource settings by decentralizing diagnostics. The permanent of adsorption of DNA to whole chitosan could also enable serial nucleic acid diagnostics on the same exact sample thereby

reducing the number and quantity of samples collected from patients. All patients would welcome less needles, prodding, and hospital visits.

Characterization of Taq Pol adsorption to oil-water interfaces in Chapter 4 has sorely been lacking from the literature. Previous attempts to calculate the loss of Taq Pol to the interface assumed the process was diffusion limited. Our results strongly indicate that assumption was false, and that the rate limiting step is kinetic adsorption into a high surface pressure film. We showed a surfactant that would prevent loss of Taq Pol to the interface could be identified without performing PCR. Prior to this work, a trial and error method was used to optimize surfactant and oil mixtures. Using the pendant drop, surfactant and oil mixtures can now be optimized quickly and inexpensively. Furthermore, successful droplet PCR in mineral oil with minimal Taq Pol and minimal surfactant was demonstrated for the first time. This was enabled by a surfactant, Brij L4, which had never been used before with PCR. This innovation could be replace ABIL EM90, which is commercially not available to laboratories, in PCR protocols. Using Brij L4 decreases the cost of droplet PCR, especially digital PCR. Currently, digital PCR, which is capable of identifying extremely rare targets, is only used for research purposes. Cheaper amplification could enable digital PCR for immensely valuable diagnostic purposes.

Droplet microfluidics with an air continuous phase in a confined microchannel has largely been unexplored by the literature. Our demonstrations of droplet generation and manipulation on-chip with minimal satellite droplet formation are the first. Successful droplet PCR amplification without oil would be an incredibly ambitious achievement. It would defy the notion that droplets need to be surrounded by oil to prevent evaporation during thermal cycling. Also, it could spur more innovation in the field droplet

microfluidics with a gaseous continuous phase and challenge the benefits of using an oil continuous phase.

# Chapter 2 PCR BACKGROUND

## 2.1 Polymerase chain reaction

Polymerase chain reaction (PCR) is a powerful biochemical technique to amplify, quantify, and identify specific genes related to cancers (Moltzahn et al. 2011), infectious diseases (Strain et al. 2013), forensics (P. Liu et al. 2011; Lounsbury et al. 2013), and hereditary disorders (Pekin et al. 2011). There are several variants of PCR, but each type utilize an enzyme, Taq polymerase (Taq Pol). The polymerase is an enzyme that polymerizes nucleotides in a specific sequence complementary to the DNA segment targeted. Specificity in PCR is achieved by designing two primers that define the beginning and end of the DNA segment of interest. DNA is exponentially amplified by repetitive cycles of splitting double stranded DNA (dsDNA) into single stranded DNA (ssDNA), binding primers to ssDNA, and then extending bound primers into dsDNA with Taq Pol. The amount of DNA is roughly doubled every cycle and can be measured in real time with fluorescent methods.

## 2.2 PCR variants

Widely used PCR techniques include end point (conventional), quantitative or real time, droplet, emulsion, digital, and reverse transcription PCR. In end point PCR, DNA is only measured at the end of the reaction. Therefore, an end point assay can only confirm if the targeted gene is present (when the targeted gene has been exponentially amplified at the end of the reaction) or not (there is only the initial amount of DNA present). Quantitative or real time PCR (qPCR) fluorescently measures DNA amplification during

PCR. Although, actual quantification is determined by relating the cycle at which the reaction surpasses a fluorescent threshold to a calibration curve of standards with the same amplification efficiency.

The fluorescent threshold is determined from the baseline of the amplification plot, where there little change in the fluorescence in the first few cycles (Figure 2.1). The threshold is normally set as 10 times the standard deviation of the baseline. This sets the threshold early in the exponential phase of amplification. The threshold could be set at a different point in the exponential phase except near the plateau region. Reactions with different initial concentrations of DNA plateau at around the same fluorescence intensity because the maximum DNA amplified is limited by primers and free nucleotides. The cycle at which the fluorescence crosses the threshold is recorded as the cycle threshold ($C_t$) or quantitative cycle. Cycle thresholds from amplifications of DNA standards are plotted against the standard DNA amounts on semi-log axes to provide a standard curve (Figure 2.2). Thus, the DNA in a reaction with the same conditions or amplification efficiency as a standard curve can be quantified just from the $C_t$ value. This method of qPCR is the leading tool to detect and measure DNA and RNA, and was the preferred method to quantify DNA in this dissertation.

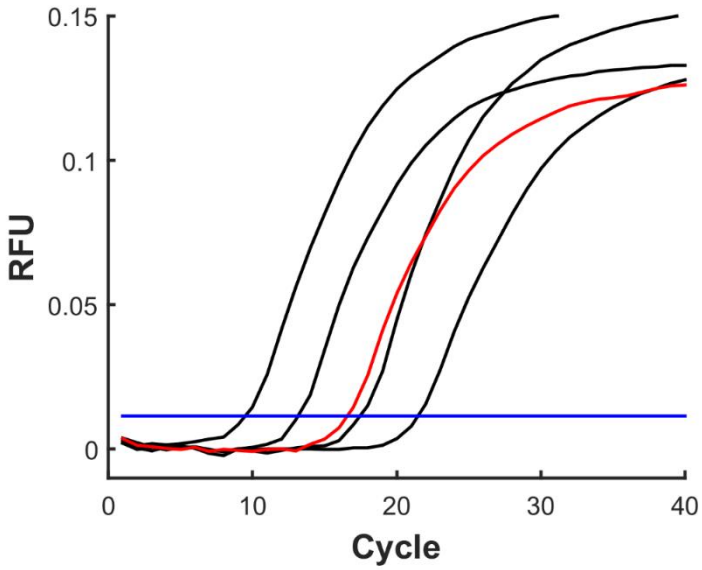


**Figure 2.1 qPCR amplification plot.** The number of cycles a reaction requires to reach the exponential phase of fluorescence increase depends on the initial concentration of DNA. Fluorescence from reactions with pUC19 standards (*black curves*) and an unknown pUC19 sample (*red curve*) were plotted as a function of thermal cycles. From left to right the standard samples had initial concentrations of 1e9, 1e8, 1e7, and 1e6 pUC19 copies per µL. The fluorescence threshold (*blue line*) was set as 10 times the standard deviation of all curves from cycles 1 to 5. Cycle thresholds were determined as the point at which the fluorescence from reactions crosses the fluorescence threshold.

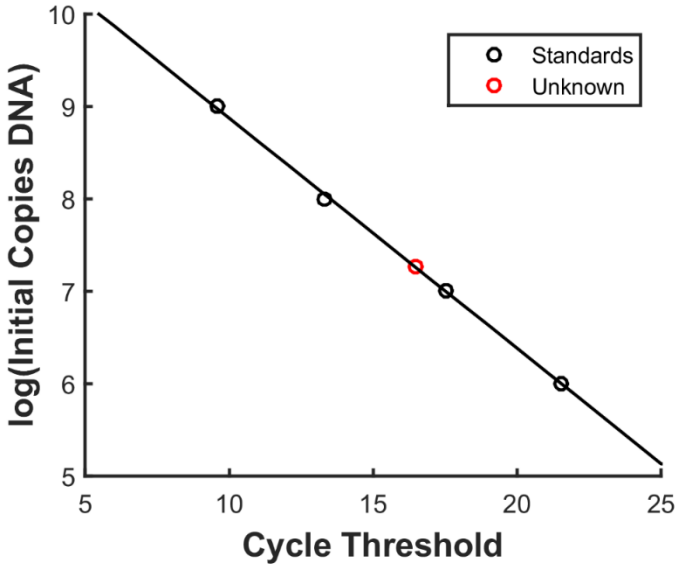


**Figure 2.2 qPCR calibration curve.** The cycle thresholds of pUC19 standards (*black circles*) from Figure 2.1 were plotted with the log of the initial copies of pUC19. A calibration curve was fit to the standards (*black line*, $y = -0.2492x + 11.364$, $R^2 = 0.9994$), and used to quantify the amount of DNA in the unknown sample (*red circle*).

Droplet PCR is similar to qPCR except the reaction is carried out in droplet microreactors so that the local DNA concentration is increased. Droplets amplified together in an emulsion is termed emulsion PCR. In this case, the emulsion is broken and amplified DNA is analyzed after thermal cycling because real time fluorescence during thermal cycling is impossible due to light scattering. Droplet PCR is termed digital PCR when the average number of copies of DNA per droplet is less than 1 and follows a Poisson distribution (most likely 1 or 0 copies in a given droplet). In contrast to qPCR, DNA is absolutely quantified by counting the number of droplets which amplified and fluoresced. Reverse transcription PCR (RT-PCR, not to be confused with real time PCR or qPCR), is used to detect RNA expression. A reverse transcriptase polymerizes complementary DNA

strands from RNA strands in the reaction. Then PCR is used to amplify the target complementary DNA. All of these variants of PCR, utilize Taq Pol to amplify DNA.

## 2.3 Taq Pol

Taq Pol is a polymerase derived from a thermophillic bacteria, Thermus aquaticus. As such, it can withstand extremely high temperatures that would denature typical proteins. A large relative volume of Taq Pol is hydrophobic, typical of proteins structurally stable at high temperatures. Thus at 95 °C, the polymerase has a half-life of 45 to 50 minutes (Lawyer et al. 1993). The optimal active temperature of Taq Pol is between 75 and 80 °C, and can polymerize 1000 base pairs in 10 s. The polymerase also requires a cofactor, magnesium, to be active. Typically, $MgCl_2$ is supplied in the reaction at around 2 mM. Normally, Taq Pol has a relatively low proof reading ability, committing an error every 9000 bases (Eun 1996). High fidelity mutants of Taq Pol are widely available, though they are more expensive. Taq Pol functions by binding to dsDNA and extending primers in the 3' to 5' direction. Premature polymerization during reaction setup is stopped by using a "hot start" polymerase which is basically Taq Pol bound to a specific antibody that stops polymerization. Functionality is restored by heating the polymerase to 95 °C for 3 minutes in the initial step of the reaction, which melts the antibody but leaves Taq Pol intact. Taq Pol also exhibits 5' to 3' exonuclease activity, meaning hybridized DNA that is in the path of polymerization is hydrolyzed.

## 2.4 Primers

The specificity of PCR is derived from the primer sets used to identify the target DNA as shown in Figure 2.3. They are short sequences of oligosaccharides, 18 to 22 base

pairs in length that are complementary in sequence to targeted DNA. There is a forward and reverse primer per set that indicate the start and end of the amplified portion of DNA, or amplicon. It is important that the melting temperature of the primers are between 52 and 58 °C. Higher melt temperatures lead to insufficient hybridization with target DNA and poor amplification. Lower melt temperatures leads to hybridization with off target DNA and unspecific amplification. Also, the primer pair should have similar melt temperatures. Primers should be cross checked to ensure they are uniquely specific to DNA target of interest. The NIH provides a free online primer design tool to aide in finding good primer sequences specific to inputted DNA targets (Ye et al. 2012). Custom primers are cheap and can be ordered through vendors such Integrated DNA Technologies. They are usually supplied at 100 to 500 nM in PCR mixtures.


**Figure 2.3 PCR primers.** The amplification specificity for PCR is derived from primers. Forward and reverse primers bind upstream and downstream of the targeted gene. The main amplified product or amplicon from PCR is the region bracketed by the primers.

## 2.5 Thermal cycling

PCRs are typically cycled between three temperature regimes as illustrate in Figure 2.4. In the first step of a cycle, the melt, the reaction is heated to about 95 °C. At this temperature dsDNA is melted into two separate ssDNA molecules. Next, in the annealing step, the temperature of the reaction is rapidly cooled to about 55 °C. At this low temperature of the cycle, primers are able to bind to ssDNA. In the last step of the thermal cycle, the elongation or extension step, the reaction is heated to about 75 °C. This is the optimal temperature for Taq Pol to extend primes and create new amplicons. A two-step cycle may be used in place of a three step cycle where annealing and extension are combined at around 55 °C (Eun 1996). Additionally, a "hot start" may be employed prior to thermal cycling to activate specific Taq Pol mutants designed to not prematurely elongate primers. Bulk scale PCR, in central lab environments with benchtop thermal cycles, is carried out in 20–50 μL reaction volumes using 48 or 96 well plates. It takes about 1 hour to complete a bulk scale reaction. Ultrafast droplet PCR has been achieved with integrated heaters, where 40 thermal cycles have been conducted in under 6 minutes (Neuzil et al. 2006).

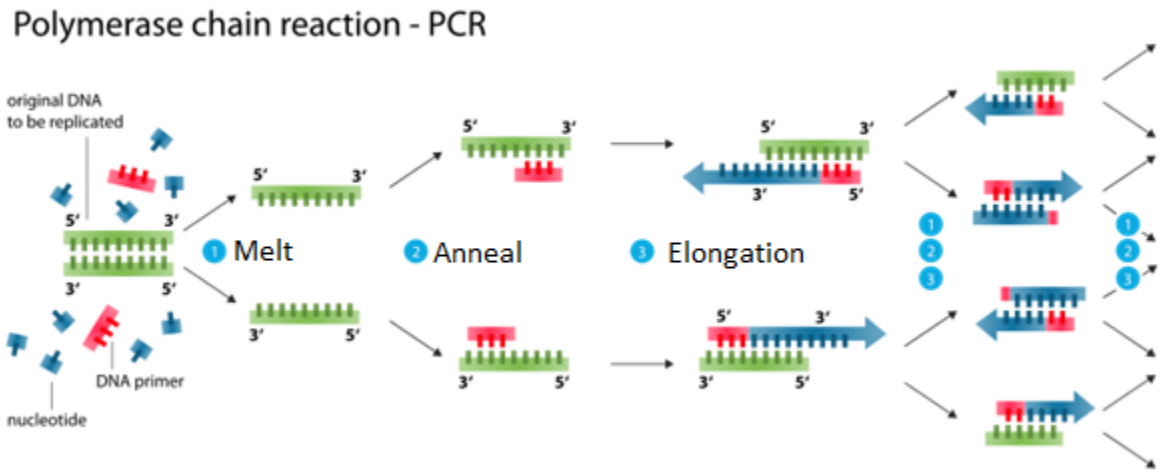


**Figure 2.4 PCR amplification scheme.** Each PCR cycle consists of three step. First dsDNA is melted into ssDNA at around 95 °C. Then forward and reverse primers are annealed to ssDNA at around 55 °C. Lastly, primers are elongated and nucleotides are polymerized from the 5' end to the 3' end in a sequence complimentary to the ssDNA by Taq Pol. Image modified from Wikipedia.

## 2.6 Fluorescent measurements

Real time fluorescence is measured by incorporating an intercalating dye or complementary probe into the PCR mixture. Intercalating dyes indiscriminately fluoresce in the presence of any dsDNA. The most common PCR dye is SYBR Green I. The dye, when intercalated in dsDNA, is excited with blue light ($\lambda_{max}$ = 497 nm) and emits green light ($\lambda_{max}$ = 520 nm). The final concentration of SYBR Green I in PCR mixtures is between 0.5 – 0.7 X (it is supplied as 10,000 X), greater concentrations inhibits the reaction. A less used PCR dye is LCGreen. It was developed specifically to saturate DNA for high resolution melt analyses of PCR products. As such it is not inhibitory to the reaction. The

optimal excitation and emission of LCGreen is 440 – 470 nm and 470 – 520 nm respectively.

In contrast to intercalating dyes, complementary probes, such as TaqMan probes, only fluoresce when PCR products are polymerized. The probes consist of an oligosaccharides, 20 to 30 base pairs in length (ideally with a melt temperature 10 °C greater than the primer melt temperatures), complementary to sequences in the middle of the gene of interest. A quencher, such as TAMRA, and donor, such as FAM, are covalently attached to opposite ends of the oligosaccharide. Through fluorescence resonant energy transfer, florescence from the donor is absorbed by the quencher when the two are in close proximity to each other, i.e. covalently attached to an oligosaccharide. Hybridized complementary probes are hydrolyzed during polymerization, due the 5’ to 3’ exonuclease activity of Taq Pol. Hydrolyzed probes release the quencher and donor from one another allowing the donor to fluoresce without absorption. Thus fluorescence increases during PCR is only a result of product amplification when measuring the emitter fluorescence.

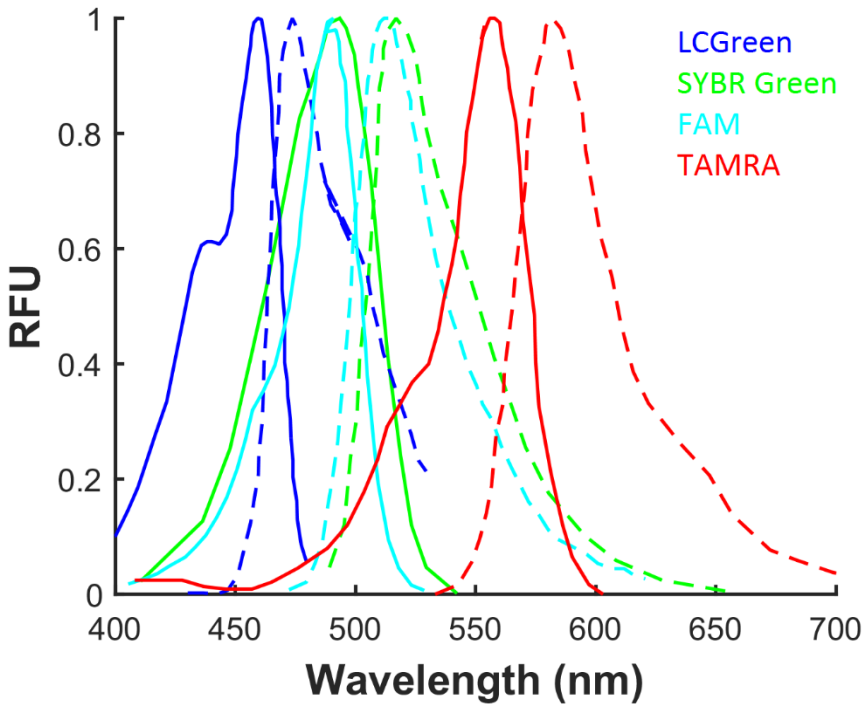


**Figure 2.5 PCR dye spectra.** Excitation (*solid curves*) and emission (*dashed curves*) spectra of fluorescent dyes commonly used with PCR.

## 2.7 Hardware

We conducted the majority of qPCR reactions using the Biorad Mini MJ Opticon (Figure 2.7). It is a small and compact benchtop real time PCR thermal cycler. The Mini MJ Opticon is easily programmed to heat and cool PCR reactions to 99 °C and 30 °C below ambient temperature respectively. The heating block is controlled by thermoelectric peltiers and can ramp the temperature up to 2.5 °C per second. The block holds up to 48 wells, each with a capacity of 200 µL in volume. Every well is sequentially illuminated from above by a dedicated blue LED (470 to 500 nm). Fluorescence from an illuminated

well is split into two beams and passed through separate filters to be measured by photodiodes. Channel 1 detects light between 532 to 543 nm (used with SYBR Green) and channel 2 detects light between 540 and 700 nm (Figure 2.7).


**Figure 2.6 BioRad MJ Mini Opticon.** The BioRad MJ Mini Opticon is advertised as a portable thermal cycler and can be programmed with the user interface on the machine or a connected computer. The thermal block can hold up to 48 wells. In this photograph, two conical 200 µL low profile 8-well-strips are inserted in the thermal block and one strip is placed outside the thermal block. The optics are house in the swinging lid of the thermal cycler.

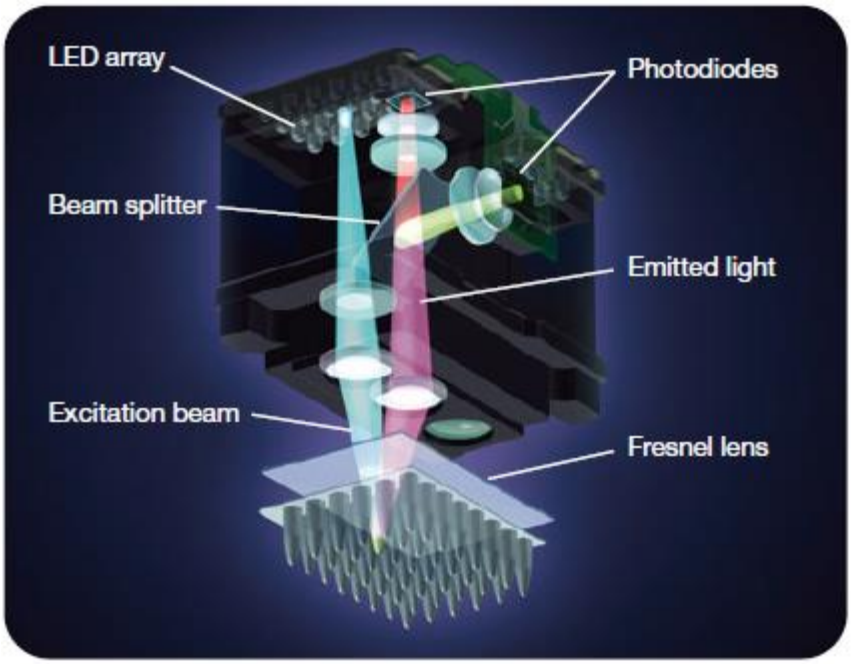


**Figure 2.7 Mini MJ Opticon optics.** Each PCR well is illuminated one at time a by a dedicated blue LED (470 to 500 nm). The light emitted from each well is split into two beams, filtered (532 to 543 nm and 540 to 700 nm), and measured by photodiodes. Image from biorad.com.

## 2.8 Challenges

The biggest challenge to bulk and droplet scale PCR is the sample preparation prior to amplification. Currently, the protocols for sample preparation at the bench scale are time intensive and require constant attention by a trained technician. Clinically, raw samples are first collected from sources such as blood, tissue, buccal swabs, saliva, and hair. Then cells from these samples need to be sorted and concentrated using a centrifuge. Next, cells are lysed by rupturing the membrane through any one of a number of methods (e.g.

enzymatically or sonicating). Afterwards, DNA is extracted from the lysate, most likely with a silica spin column which requires multiple wash steps with 3-4 different buffers. Then, DNA samples are mixed with PCR reagents using a vortexer. Finally the PCR mixture is pipetted into wells and thermal cycled.

Lab-on-chip devices have the potential to miniaturize and integrate sample preparation with PCR on a simple chip (Figure 2.6). However, the complexity of integration and automation of sample preparation increases with the number of steps involved. For example, a valve and pressure system must be incorporated for each buffer that is required for DNA solid phase extraction. Additionally, a valve system would need to be incorporated to direct the waste and DNA eluent. Typically, valve systems involve a pneumatically operated flexible control layer which needs to be aligned with the main channels. Design and large scale production of such a system is difficult. So instead robotic systems are preferred to automate to sample preparation.

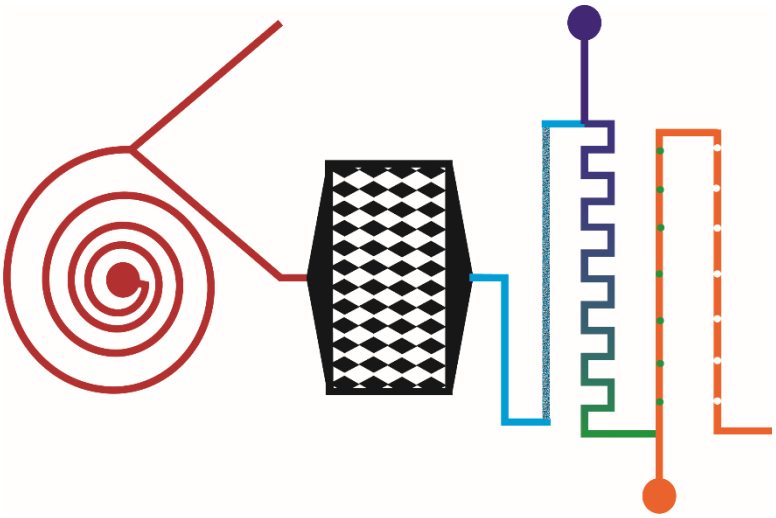

**Figure 2.6 Theoretical lab-on-chip device.** A basic device to accept cells and output PCR amplified droplets. From left to right, cells could sorted and concentrated using spiral inertial filtration (*red*). Then cells would be lysed using nozzles that expand and contract cells causing them to rupture (*black*). Next, DNA would be extracted from cell lysates using a packed silica bead channel (*light blue,* inlets and outlet for different buffers and waste are too complicated to show). Afterwards, PCR reagents would be passively mixed with purified DNA samples by periodically turning the laminar flow (*purple to green*). Finally PCR mixtures would apportioned into droplets and thermal cycled with integrated heaters (*orange*).

Another challenge specific to droplet PCR is the loss of polymerase to oil-water interfaces. The decreased length scale of droplet microreactors enables faster heat transfer and increases the local DNA concentration. Unfortunately, it also enables significant irreversible adsorption of polymerase from solution to the interface. To accomplish PCR in droplets, additional Taq Pol is necessary, even with surface blocking agents such as BSA and surfactants. Commercial digital PCR systems make use of expensive and proprietary

fluorinated oils and fluorosurfactants. A protocol for droplet PCR in a commonly available oil using bulk concentrations of Taq Pol has not been reported.

Also, performing droplet PCR without an oil phase has never been examined. This is a radical idea because the oil phase prevents droplets from evaporating while thermal cycling during PCR. However, it may be possible to seal droplets on-chip using other methods to prevent evaporation. Then the benefits of droplets could be taken advantage of without the loss of polymerase. Droplet microfluidics in confined channels with an air continuous phase is a nascent field with a lot of space for innovation. Other challenges, in addition to sealing the droplets on-chip, include on-chip droplet generation and on-chip droplet immobilization.

# Chapter 3 DNA EXTRACTION IN A SINGLE BUFFER WITH CHITOSAN MICROPARTICLES

The text and figures presented here have been adapted from a manuscript in preparation.

## 3.1 Introduction

Nucleic acid amplification (NAA) methods are powerful tools for biological research, as well as for disease diagnostics, in particular for genetic and infectious diseases. While the amplification steps are mostly automated and straight-forward, sample preparation can be complex, as DNA or RNA targets are normally diluted in a complex lysate or mixture from food, environment, or clinical samples. Nucleic acids must be purified prior to amplification because sample DNA can by digested by nucleases, polymerases can be hydrolyzed by proteases, lysis chemicals such as EDTA inhibit NAA, and other unknown materials in the complex mixture can interfere with NAA. Ultimately, it is the complexity of the sample preparation that prevents NAA techniques to be widely adopted away from the central laboratory.

Traditionally, nucleic acid purification is carried out using a silica solid phase extraction technique (Boom et al. 1990; D. N. Miller et al. 1999; Haugland, Brinkman, and Vesper 2002). The most commonly used format is a spin column with a silica membrane designed for use with a centrifuge (Naccache et al. 2014). First, the tissue or cellular sample is lysed to release DNA with a chemical lysis buffer and agitation. Then, binding, washing, and elution solutions are driven through the column by centrifugal force in a series of steps. Nucleic acids in samples are denatured by chaotropic salts, such as guanidine hydrochloride, which cause adsorption to the silica. Alcohol is then used to wash away the

salts and cellular debris, which would otherwise inhibit PCR. Purified nucleic acids are then eluted off of the silica in a moderate salt buffer and added to the PCR mixture to be amplified.

There are several inherent disadvantages to using silica membranes to purify nucleic acids. For one, typically three to four different solvents are necessary to extract nucleic acids from complex samples. Performing each wash step can be time consuming, while automation of washes increases in complexity with increasing number of solvents. In addition, the chaotropic agents and alcohols required for DNA adsorption to silica, are inhibitory to amplification methods. Furthermore, commercial spin columns can process only relatively small samples, i.e., on the order of 500 µL in volume. To capture dilute DNA or RNA from a rare target, the sample volume must be increased, leading to volumes that are impractical for spin columns.

Recently, the steps for solid phase extraction have been adapted for silica microbeads. The surface of the microbeads takes the place of the silica membrane; meanwhile, microbeads enable the elimination of one step from the process by lysing cells and capturing the released DNA under vortex in the presence of a high concentration of chaotropic salts. In addition, the use of magnetic microbeads may simplify the procedure (Roy et al. 2014). Nonetheless, even with the elimination of a step, the method is still relatively complex and time consuming, and does not position NAA methods for use away from the central lab.

Another method that has been reported to reduce the number of sample preparation steps is charge switching. In this approach, nucleic acids are adsorbed onto a pH-responsive

material in a moderately low pH (which positively charges the binding surface) and then released into a moderately high pH (compatible with NAA), which neutralizes the binding material (Kneuer et al. 2000). Therefore, in the charge switching methodology, inhibitory salt concentrations, chaotropic salts, or alcohols are not necessary. Instead, two buffers compatible with NAA are used for the release, which reduces steps and eliminates the use of inhibiting reagents (Cao et al. 2006). Also, the charge switching format can be easily adapted to a bead geometry to process large volumes (Hagan et al. 2009; C.-J. Liu et al. 2009).

Chitosan is a particularly useful polycation with amine groups that can be modulated by pH. It is derived from crustacean shells, so it is readily available, cheap, and biocompatible. The amine group of chitosan has a pKa of about 6.4. Thus, the negative phosphate backbone of nucleic acids are electrostatically attracted to chitosan when it is predominately positively charged in buffers below pH 6.4. Silica beads functionalized with low molecular weight chitosan efficiently elute DNA at a moderately high pH (~8.5) compatible with PCR. Chitosan coated silica beads under aqueous conditions have been shown to extract RNA from cancer cells more efficiently than bare silica beads (Hagan et al. 2009). Chitosan coated silica beads have also been used to purify genomic DNA from blood (Cao et al. 2006) and soybeans (C. Jiang et al. 2012) for PCR analysis. The use of charge switching implies a reduction in steps (lyse, bind, elute) as compared to silica membranes; however, as with silica beads (lyse, bind, wash, elute), the number of steps continues to imply complexity in attempts for automation.

Further simplification can be achieved by eliminating the elution step altogether. In this paradigm, the surface would bind DNA and retain DNA during any washes, such

that the binding material could be directly transferred to a NAA reaction with the nucleic acids still bound. For example, aluminum oxide membranes have been shown to bind nucleic acids at high salt concentrations similarly to solid silica supports. Although it is difficult to elute the nucleic acid off, bound DNA can be amplified with the membrane in the reaction solution (J. Kim et al. 2010; Oblath et al. 2013). This technique could be adapted to alumina microbeads, further improving the simplicity. However, it was also shown in that same work that alumina inhibits NAA, and thus the exposed surface area must be minimized. This limits its potential for practical implementation.

Commercially available polystyrene magnetic beads have also been demonstrated to capture nucleic in a high pH and high salt buffer (i.e. pH 12 and1.2 M NaCl, (Lacy and Voss Jr. 1989)). Recently they were used to retain the nucleic acids in a wash with a PCR pH compatible buffer (Yingnan Sun, Zhou, and Yu 2014). After the beads are vortexed with concentrated cell samples, they form gelatinous complexes with DNA. Then DNA can be eluted off by washing the complex in a low ionic strength buffer or by heating the complex at 65 °C for 5 minutes. Alternatively, a small amount of microbeads can be added directly to a NAA reaction without significant inhibition. Thus, lysis and binding steps can be combined while the elution step can be eliminated. However, it is recommended by the manufacturer (Life Technologies) to use only 10% of extracted DNA for PCR and no more than 50% when using 1 unit of the beads due to adverse effects of the beads on PCR. While this approach is significantly simpler than conventional solid phase extraction, elimination of the requirement for a high-pH NaOH binding solution would lead to a protocol that can be very simply automated and utilized away from the central laboratory.

The buffering capacity of chitosan can be used to adsorb DNA at a pH optimal for PCR. Recently, chitosan has also been proposed as a gene delivery vector, where DNA is complexed with chitosan to form nanoparticles in dilute acidic solutions (Agirre et al. 2014; Alameh et al. 2012). Nanoparticles are delivered into cells via endocytosis, whereby the cell membrane encapsulates the nanoparticle in a vesicle. It is thought that particle escape from the vesicle is due to the proton sponge effect. Basically, endosome pH is regulated to be 6.3 – 6.5, but chitosan absorbs hydrogen ions and becomes charged instead of the endosome compartment acidifying. Then increasingly ionized chitosan burst the vesicle due to osmotic effects, releasing endosome contents into the cell. DNA complexed to chitosan reduces the proton sponge effect, because the buffering capacity of chitosan is reduced from DNA ionizing chitosan (Richard et al. 2013). Furthermore, in a dense chitosan microenvironment, the degree of ionization of chitosan in complex with DNA at pH 7.4 is equal to the degree of ionization of free chitosan at pH 5.5 (Ma et al. 2009).

We leverage this phenomenon to perform (i) adsorption of DNA in a solution that is optimized for polymerase chain reaction (PCR) and (ii) subsequent amplification of the captured DNA directly from the chitosan. To accomplish this, we utilized magnetic microparticles fabricated from chitosan; the core of the microparticles was shown to maintain a positive charge at NAA-compatible pH, thus retaining genomic DNA captured under vortex conditions, while the outer surface was shown to exhibit the characteristic charge switching properties of chitosan, thereby not inhibiting the NAA reaction. We demonstrated that plasmid DNA is captured at pH 8.5 and is amplified directly from the microparticle substrate with PCR, despite permanent adsorption to the microparticle.

## 3.2 Materials and Methods

### 3.2.1 Microparticle fabrication

Chitosan microparticles were fabricated by creating chitosan droplets in oil and then crosslinking the droplets into microparticles. Stock solutions of 2% w/w low molecular weight chitosan (Sigma) in 2% v/v acetic acid (Fisher) and an oil solution of 2% w/w Span 80 (Sigma) in hexadecane (Sigma) were prepared and stored at room temperature. Prior to bead fabrication an aqueous solution of 1% w/w low molecular weight chitosan and 0.5% w/w magnetic iron (III) oxide nanoparticles, 20-40 nm in diameter (Alfa Aesar) in 1% v/v acetic acid was prepared. A crosslinking mixture of 0.44 g glutaraldehyde (grade 1, 70% in $H_2O$, Sigma) in oil solution was also prepared. Chitosan was emulsified in a 100 mL beaker by dripping 1 mL of the aqueous solution into 19 mL of the oil solution under constant mixing with an IKA T25 digital ULTRA-TURRAX homogenizer set at 1600 rpm. After emulsifying for 3 minutes, the crosslinking mixture was added dropwise and then further mixed with the homogenizer for an additional 5 minutes. Microparticles were cross-linked by glutaraldehyde, which reacts with chitosan amine groups to form Schiff bases (Hermanson 2008). Next the microparticles were transferred to a 50 mL tube and cross-linked for a different amounts of time on a nutating rocker. The crosslinking reaction was stopped by removing the glutaraldehyde-laden hexadecane after the microparticles were centrifuged at 1000 rpm for 2 minutes.

To prepare the microparticles for DNA adsorption assays they were first washed twice with oil solution. Then the microparticles were resuspended in oil solution and dried with an air stream bubbling through the solution overnight. The oil solution was removed by washing the beads twice, first in decanol (Alfa Aesar), then ethanol (Pharmco-AAPER),

and finally 10 mM Tris (Sigma). Schiff bases, which cross-linked the microparticles, were then reduced to secondary amines in 1% w/w NaBH4 (Sigma) in 10 mM Tris overnight (Hermanson 2008). After reduction, the microparticles were washed twice in 10 mM Tris. Finally they were dried overnight at room temperature under vacuum. Chitosan microparticles were stored in 10 mM Tris at a concentration of 40 mg/mL at 4 °C.

### 3.2.2 DNA capture below pKa

Quantitative DNA capture assays at pH 6 were performed by a series of buffer changes in 600 µL microtubes with qPCR quantification of DNA in each supernatant. First, 40 µg of chitosan microparticles (cross-linked for 30 minutes) were washed twice with loading buffer (pH 6, 10 mM MES, 0.1% Triton X-100 (Sigma)). Next, 1 µL of pUC19 plasmid DNA (Sigma) or E. coli genomic DNA (Sigma) diluted in de-ionized (DI) $H_2O$ was added to 99 µL of loading buffer with containing the chitosan microspheres. Then the microparticles were washed in 100 µL of loading buffer. Lastly, the beads were vortexed in 100 µL elution buffer (pH 9, 10 mM Tris, 0.1% Triton X-100 and 50 mM KCl) on the highest speed for 3 minutes. All buffer changes were facilitated by a magnetic tube stand that pulled and held the magnetic chitosan microparticles to one side of the tube. Supernatants from each step were saved for qPCR analysis.

### 3.2.3 PCR-optimal-pH capture

DNA adsorption assays at PCR-compatible pH (8.5) were similar to the assay at lower pH. First, 40 µg of chitosan beads cross-linked for 30 minutes were prewashed twice in pH 8.5 loading buffer (10 mM Tris, 0.1% Triton X-100). DNA was loaded onto the beads by adding 1 µL of pUC19 plasmid DNA or E. coli genomic DNA diluted in DI $H_2O$

to 99 µL of load buffer (pH 8.5). Lastly, the beads were washed in 100 µL of loading buffer (pH 8.5). The amount of DNA in the supernatants at each step was quantified with qPCR.

### 3.2.4 Primer adsorption to microspheres

Primer adsorption to chitosan microspheres was investigated by conducting PCR with a primer solution that had been mixed with chitosan microspheres. First, 40 µg of chitosan microspheres cross-linked for 30 minutes were prewashed twice in pH 8.5 loading buffer. Then 100 µL of 10 mM Tris, 2.5 µM forward primer, 2.5 µM reverse primer, and 0.1% Triton X-100 at pH 8.5 was repeatedly aspirated with the microspheres via pipette to mix the solution. The supernatant (containing primers that did not bind to the microspheres) was removed and used for qPCR. Reaction mixtures consisted of 10 µL iQ SYBR Green Supermix, 2 µL of primer solution, 2 µL DI H2O, and 6 µL of pUC19 standards.

### 3.2.5 Amplicon adsorption to microspheres

Amplicon adsorption to chitosan microspheres cross-linked for 30 minutes was investigated with a pH 8.5 capture assay. First, 40 µg of chitosan microspheres were prewashed twice in pH 8.5 loading buffer. Amplicons (1 µL diluted in DI $H_2O$) were added to 99 µL of pH 8.5 load buffer. The solutions were mixed via pipette aspiration (note that in the plasmid DNA adsorption assay, the DNA was vortexed with the microspheres, as would be done with cell lysis, but in the amplicon adsorption study, gentle mixing was used, as would be the case in a reaction). The amplicons added were generated from a standard pUC19 PCR used to create a calibration curve and diluted by a factor of $10^4$ or $10^6$. DNA that remained in the supernatant (i.e., unbound amplicons) was quantified with qPCR and an amplicon calibration curve.

### 3.2.6 qPCR

To quantify the amount of DNA captured or released in each step, the respective supernatants were analyzed with qPCR using an MJ MiniOpticon thermal cycler (BioRad). Reactions consisted of 10 µL of iQ SYBR Green Supermix (BioRad), 2 µL of 2.5 µM forward primer (GTC TCA TGA GCG GAT ACA A), 2 µL of 2.5 µM reverse primer (CTC GTG ATA CGC CTA TTT TT, primers purchased from IDT), and 6 µL of samples. Reactions consisted of a hot-start at 95 °C for 3 minutes followed by 30 thermal cycles. Each cycle included a melt step at 95 °C for 3 s and an anneal step at 56 °C for 30 s. Serial dilutions of pUC19 plasmid DNA in load and elution buffers were used to generate a calibration curve to quantify the unknown samples.

### 3.2.7 Elution under extreme conditions

To investigate the binding strength of DNA to the chitosan microparticles, multiple elution steps, high ionic strength, high pH, and high temperature elution washes were performed after microparticles (cross-linked for 30 minutes) were loaded with pUC19 plasmid DNA and washed. Additional washes with elution buffer were performed to increase the probability of eluting DNA. High ionic strength conditions were examined by overtaxing particles in 100 µL of pH 8.5, 10 mM Tris, 0.1% Triton X-100, and up to 500 mM KCl for 3 minutes. High pH conditions were examined by vortexing particles in Tris, bicarbonate, or sodium hydroxide buffers at a concentration of 10 mM and up to pH 12.5 for 3 minutes. High temperature elution was examined by suspending the particles in 100 µL of elution buffer and thermal cycling them according to the qPCR protocol with an additional 95 °C hold step at the end. The supernatant was removed during the hold step and released DNA was quantified with qPCR.

### 3.2.8 High pH capture

High pH DNA adsorption assays were similar to low pH assays. First, 40 µg of chitosan beads cross-linked for 0.5 hour were prewashed twice in high pH loading buffer; pH 8.5, 10 mM Tris, 0.1% Triton X-100. DNA was loaded onto the beads by adding 99 µL of high pH load buffer and 1 µL of pUC19 or E. coli genomic DNA diluted in DI H2O. Lastly, the beads were washed in 100 µL of high pH load buffer. The amount of DNA in the supernatants at each step was quantified with qPCR and averaged from 3 trials.

### 3.2.9 Adsorption mechanism assays

The adsorption of brilliant yellow (Sigma), BY, to chitosan particles at increasing pH was measured to investigate electrostatic interactions. Solutions of BY in 10 mM buffers and 0.1 % Triton X-100 from pH 5 to 12.5 were made as standards and load samples. First, 40 µg of chitosan particles cross-linked for 0.5 or 24 hours were prewashed twice in buffer without BY. Then 100 µL of 50 µM BY was loaded onto the particles. After vortexing for 3 min., BY remaining in the supernatant was quantified by comparing the absorbance at 397 nm with an Evolution 60 spectrophotometer to standard solutions. The adsorption of methylene blue (Sigma) and gold nanoparticles to chitosan particles cross-linked for 0.5 hour (absorbance measured at 670 nm and 530 nm respectively) was also measured at pH 6 and pH 8.5.

### 3.2.10 Bead PCR

PCR was conducted with chitosan bead cross-linked for 0.5 hour in the reaction to verify DNA was absorbed onto the beads. The reaction mixture consisted of 1X iQ SYBR Green Supermix, 0.36 nM forward primer, and 0.36 nM reverse primer. Following a high pH capture, the beads were re-suspended in 30 µL of high pH loading buffer and transferred

to a PCR well. The loading buffer was replaced with 20 µL of reaction mixture and then aspirated via pipette. Bubbles in the wells were removed by centrifugation. A magnet was used to disperse beads throughout the well after centrifugation and ensure they were not tightly packed at the bottom. Magnets were also placed adjacent to wells during PCR which held beads to one side of a well and allowed for real time fluorescent measurements. Each data point on the calibration curve was an average of 3 trials. The slopes of the linear portions (change in slope < 0.005 RFU/cycle) of the exponential phase of the real time fluorescence amplification curves were also calculated.

### 3.2.11 PCR product identification

Thermal melt analysis and gel electrophoresis was utilized on the supernatants obtained following PCR reactions with chitosan microparticles. The melt analysis was conducted immediately after PCR within the same thermal cycler. The temperature was increased from 65 to 95 °C every 5 s by 0.5 °C and the fluorescence was measured at each temperature step. Also, the supernatant from microsphere-based PCR was separated on a 1% agarose (BioRad) and 1.6 X SYBR Green I (Lonza) gel at 75 V for 1.5 hours.

## 3.3 Results & Discussion

### 3.3.1 Bead characterization

Aldehydes readily react with amines to form labile Schiff bases. Thus intermolecular and intramolecular bonds between chitosan amine groups are formed when exposed to glutaraldehyde (Figure 1). These bonds are reduced to covalent bonds with a reducing agent such as $NaBH_4$. We utilized these reactions by immersing aqueous chitosan droplets

in glutaraldehyde laden oil. Thus the droplets were cross-linked into beads, where the reaction began at the oil-water interface and continued into the core of the bead over time.

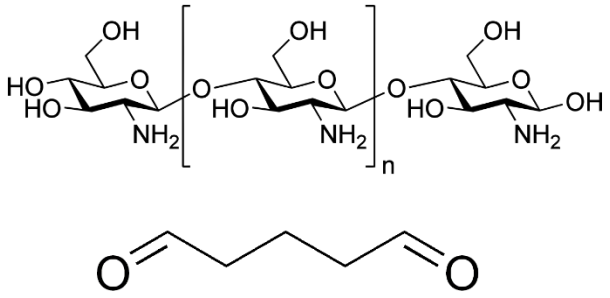


**Figure 3.1 Chitosan and glutaraldehyde structures.** (Top) Structure of chitosan. (Bottom) Structure of glutaraldehyde.

Whole chitosan magnetic beads were fabricated using a facile emulsion cross-linking methodology. We observed the beads to be dispersed while cross-linking, washing, and drying in hexadecane. However the beads aggregated into larger particles when washed with solvents other than hexadecane. Furthermore, large clusters of beads were formed after drying under vacuum, which were broken down by sonication. SEM images of the final freeze dried chitosan bead product showed individual microbeads clustered into larger particles (Figure 3.2). Individual beads were narrowly polydisperse and ranged in diameter from 0.5 to 8 μm. A large majority of the beads were clustered into particles on the order of 10 μm, although single beads were not uncommon. Magnetic iron nanoparticles, 20-40 nm in diameter, were found embedded within individual microbeads. The beads were very

responsive to magnets in close proximity, which allowed for quick buffer changes. Also, the beads were opaque and rust colored from the magnetic nanoparticles, and fluoresced under blue light.

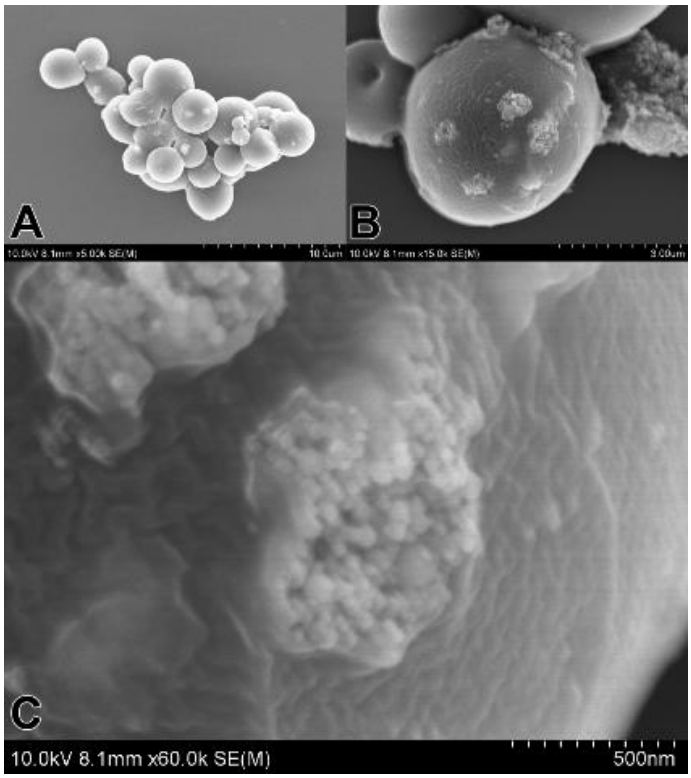


**Figure 3.2 Chitosan particle SEMs.** SEM images of whole chitosan particles cross-linked for 0.5 hour. (A) Individual beads ranged in diameter from 0.5 to 8 microns. A majority of the particles were clustered into aggregates on the order of 10 µm. (B) A cluster of beads with iron(III) oxide nanoparticles, 20 to 40 nm in diameter, visible. (C) Magnified view of iron (III) oxide nanoparticles embedded within the chitosan matrix of the particle.

### 3.3.2 DNA adsorption onto chitosan microparticles

Consistent with previously published work on chitosan for DNA purification, the chitosan microparticles efficiently captured DNA from acidic buffers (Figure 3). However, the microparticles did not elute DNA at a pH above the pKa (e.g., 8.5) as had been demonstrated with solid supports functionalized with oligomeric chitosan (Cao et al. 2006; Reedy et al. 2011). Also, further washing the microparticles with elution buffer multiple times did not result in pUC19 in solution. It has also been reported that densely coated microporous chitosan monoliths exhibited poor pUC19 elution (Kendall, Wienhold, and DeVoe 2014). We attempted to elute DNA off of the microparticles at more extreme elution conditions by (i) increasing the ionic strength, (ii) increasing the pH, and (iii) increasing the temperature by subjecting the beads to 30 PCR thermal cycles including a hot-start step. None of the enhanced elution conditions resulted in free DNA that could be measured via qPCR. This indicated that extreme elution conditions did not diminish the interactions between the chitosan microparticles and DNA and that the interaction was strong. Since the DNA chitosan interaction was preserved at high pH we attempted to capture DNA at pH 8.5.

Capture of pUC19 and E. coli genomic DNA in a pH 8.5 Tris buffer using whole chitosan particles was just as efficient at low pH (Figure 3.3). Using just 40 µg of particles, up to 700 ng of pUC19 and 0.6 ng of genomic E. coli DNA were separately loaded onto the particles (large amount of E. coli genomes were not tried). The full loading capacity of

the particles was not reached. The partial loading capacity of the beads was two orders of magnitude greater than previously reported for chitosan coated and bare silica beads(Cao et al. 2006). DNA captured onto chitosan at high pH has previously not been reported before, and is significant because nucleic acid assays are performed at a pH around 8.5. Thus, DNA extraction could be performed on a sample using the same buffer that could be used for PCR, next generation sequencing, isothermal amplification techniques, aptamer based assays, or enzymatic assays. Extracting DNA with a single buffer would reduce reagents, decrease sample preparation time, and simplify micro-total-analytical-systems by minimizing valving. As with low pH capture, pUC19 and E. coli genomic DNA could not be eluted off the particles using extreme elution protocols.

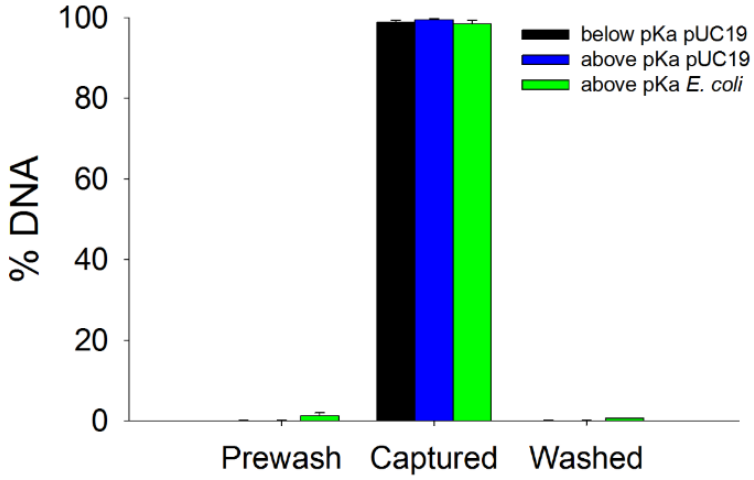


**Figure 3.3 DNA adsorption onto chitosan microparticles.** Below pKa extraction of $10^8$ copies of pUC19 plasmid, above pKa extraction of $10^{12}$ copies of pUC19 plasmid and above pKa $10^5$ copies of *E. coli* genomic DNA. All of the DNA was captured and could not be eluted or washed off the particles, using a pH 8.5 buffer of 10 mM Tris and 0.1% Triton X-100. Attempts to elute DNA via (i) increased washes (ii) increased pH, (iii) increased ionic strength and (iv) increased temperature were unsuccessful.

### 3.3.3 Chemical mechanism for capture above pKa

Adsorption of DNA to chitosan at high pH was counterintuitive to previously published chitosan DNA extraction techniques. Previous work has shown capture of DNA to be effective only at pHs lower than 7.5 and at pH 8 a sharp increase in DNA elution was observed (Cao et al. 2006). We aimed to elucidate the mechanism behind the pH 8.5 capture phenomenon by measuring the adsorption of an anionic dye, brilliant yellow (BY), as function of pH (Figure 3.4). It was found that chitosan microparticles were still pH-responsive, but with an apparent shift to a higher effective pKa, approximately 7.5 (as compared to the pKa of free chitosan in solution, 6.4). The microparticles captured nearly 100% of the added dye below pH 7.5, while above pH 7.5 BY adsorption decreased. The magnitude of the pH response was enhanced by cross-linking the beads for 24 hours, where at pH > 8, significantly less BY was adsorbed as compared to microparticles cross-linked for 30 minutes. Also, the adsorbed dye did not desorb from either microparticle when washed in higher pH buffers. In control experiments, methylene blue, a cationic dye, did not adsorb at all, verifying that BY interactions were electrostatic. The results indicate that increased cross-linking reacted away protonable chitosan amine groups, which limits possible electrostatic interactions.

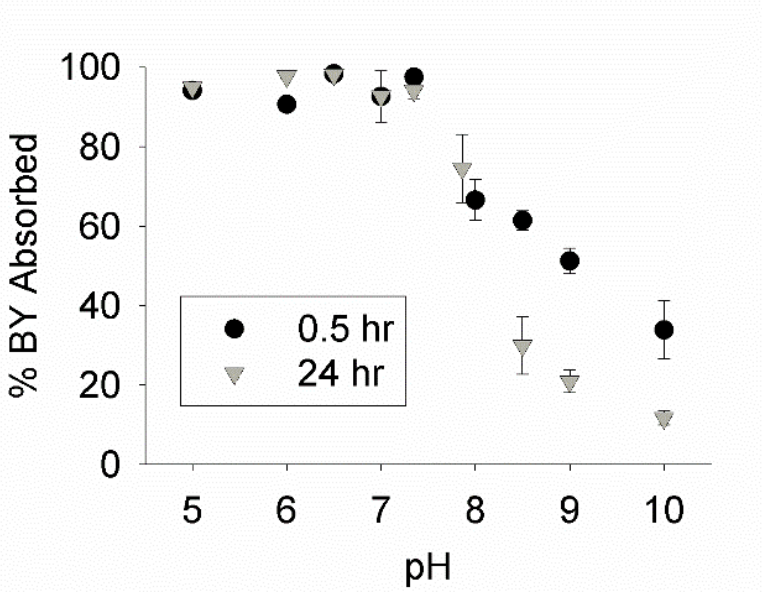


**Figure 3.4 Brilliant yellow adsorption to chitosan particles.** Adsorption of brilliant yellow dye onto chitosan particles cross-linked for 0.5 hour (*black circles*) and 24 hours (*gray inverted triangles*).

BY is a small molecule and thus has the potential to diffuse into the microparticles to adsorb. To distinguish the electrostatic potential at the outer surface from the inner core of the microparticles, we investigated the absorption of negatively charged gold nanoparticles, 40 – 50 nm in diameter. Gold nanoparticles are not be able to penetrate into a cross-linked chitosan matrix of embedded iron nanoparticles, they would be restricted to the outer surface of the beads. At pH 6, 20% of nanoparticles added were adsorbed while only 5% of the nanoparticles adsorbed at pH 8.5. Since glutaraldehyde cross-linking occurs from the outer surface inward, there are a fewer number of protonated amines available at the surface as compared to the core of the microparticles. Interestingly, it appears that the limited unreacted amines on the outer surface of the beads are charged at pH 6 but mostly

uncharged at pH 8.5, exhibiting a behavior similar to chitosan in solution (e.g., a pKa of 6.4).

While BY may penetrate well into the core of the microparticle, plasmid DNA would not be expected to penetrate deeply. The pore size radius of a glutaraldehyde cross-linked chitosan membranes has been approximated to be 1 nm by measuring solute diffusion (Krajewska and Olech 1996). The radius of gyration of supercoiled pUC19 is reported to be 65.6 nm (Störkle et al. 2007), so it would not be possible for the entire plasmid to be absorbed into the core of the bead. Instead, a small fragment of a DNA chain could condense, interact with unreacted amines below the outer surface (where the density of amine groups is greater), and become entangled with chitosan chains. Indeed, it has been reported that pUC19 in complexes with chitosan does compact to less than one half the size of free pUC19 (Lai and van Zanten 2001). We believe that DNA is permanently bound below the surface of the microparticle through a combination of electrostatic and steric interactions.

The microparticles were produced by glutaraldehyde cross-linking from the outside in. Therefore, as microparticles were cross-linked for longer times, the thickness of the shell of reacted amines around the microparticle increased. A large shell thickness of reacted amines would increasingly make it difficult for DNA to access the ionizable amines. The decrease in capture efficiency of pUC19 at pH 8.5 as a result of increasingly cross-linked chitosan microparticles is shown in Figure 3.5. The capture efficiency remained high with up to 16 hours of cross-linking. Cross-linking longer, up to 22 hours, resulted in about 50% pUC19 capture, while with 24 hours of cross-linking, pUC19 capture was reduced to an insignificant 7%. This suggests that the shell of reacted amines after

cross-linking for 16 hours was too thick for pUC19 to penetrate into a region with a shifted pKa. Long cross-linking times with glutaraldehyde to diminish pUC19 adsorption were because the cross-linker is partially soluble in oil. The oil-water partition coefficient of glutaraldehyde, $\log K_{ow}$, has been reported to be -0.18 (Emmanuel et al. 2005). Transport of glutaraldehyde is limited from mineral oil, through surfactant surrounding droplets, and into the chitosan droplets/particles.

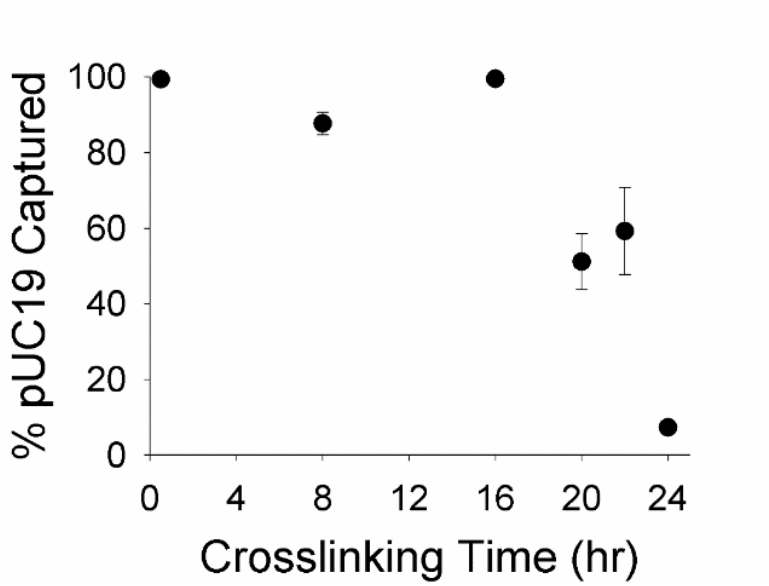


**Figure 3.5 DNA capture efficiency vs cross-linking time.** Capture efficiency of pUC19 as a function of cross-linking time. Over time an appreciable shell of amines were cross-linked around the chitosan particle and pUC19 was not absorbed.

### 3.3.4 qPCR directly from chitosan microparticles

The aim of this work is to simplify the PCR preparation process to the minimal number of steps, which can be accomplished if DNA can be amplified directly from the microparticle (i.e., without no elution or multiple buffers). For efficient PCR, however,

PCR primers and amplicons must not absorb to the particles such that the PCR reaction can propagate. Primer absorption was measured by performing PCR reactions with the supernatant of a primer solution that was mixed with chitosan microparticles. Solutions of primers vortexed with the microparticles for 3 minutes did not amplify DNA, suggesting that primers were permanently captured by the chitosan microparticles. However, mixing the primers and microparticles by triturating with a pipette (i.e., no vortexing), which is which is a typical method to mix primers into a PCR mixture, the primers efficiently amplified pUC19, indicating that the gentler mixing prevented DNA from effectively penetrating and absorbing onto the beads below the surface (Figure 3.6).

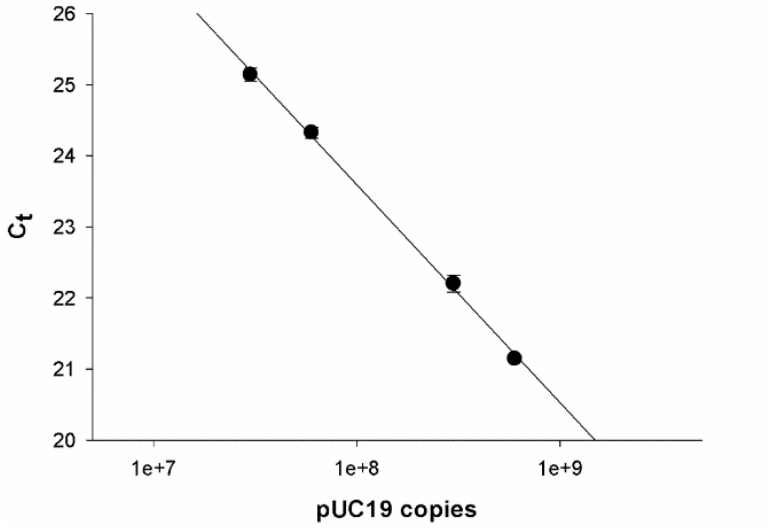


**Figure 3.6 Primer adsorption.** PCR calibration curve constructed from primers aspirated with chitosan particles cross-linked for 0.5 hr. The efficiency of the reaction was 112%, therefore minimal primers were absorbed.

Amplicon absorption was measured by triturating diluted samples of thermal-cycled PCR reactions with chitosan beads and using qPCR to measure amplicons remaining in solution. Half of the amplicons added to the beads were captured, even with gentle mixing. Since amplicons absorbed more easily than primers, PCR efficiency of reactions with microparticles could be due lost due to amplicon adsorption as they were polymerized.

Amazingly DNA was captured below the surface of chitosan microparticles, was still accessible by polymerase for qPCR. Only one recently published technique has shown amplification directly off of a solid DNA extraction phases which released the template DNA in the reaction. The template DNA remained bound to our beads after amplification which could be incredibly useful to perform serial PCRs especially on rare targets. The results of one PCR could inform the primer set selection for the next PCR which to aid in identifying the template DNA.

However to successfully amplify DNA off the microparticles, the concentrations of all the reagents in the reaction mixture were slightly increased. Also, to allow for real time fluorescence imaging, beads were held to one side of the PCR well with a magnet during thermal cycling. The PCR products were verified by gel electrophoresis and melt analyses (Figures 3.7 and 3.8 respectively). The calibration curve, shown in Figure 3.9, was constructed from standard samples of pUC19, and found to be linear over 4 orders of magnitude. The efficiency of PCR with DNA adsorbed to particles was diminished to 67.6%. Conversely, the efficiency of amplifications with pUC19 directly added to the reaction was 90.6%. In PCR with microparticles about 8-4 extra cycles were needed than without microparticles, which only translates to about an extra 10-5 minutes of hands off

reaction time. As stated earlier, the decrease in efficiency is most likely attributed to the adsorption of PCR product during amplification.

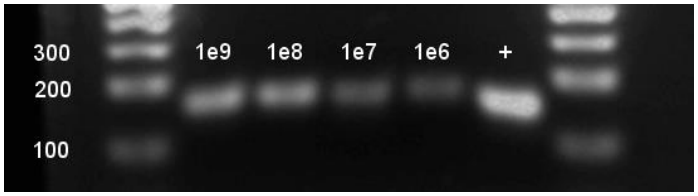


**Figure 3.7 Gel of particle PCR products.** Bead PCR products ran on a 1% agarose gel and stained with SYBR Green I. Copies of pUC19 captured by beads in reactions from Figure 3.9 are listed above each lane, the positive control lane (+) contains product from a PCR without beads, and DNA ladders are in the first and last lanes.

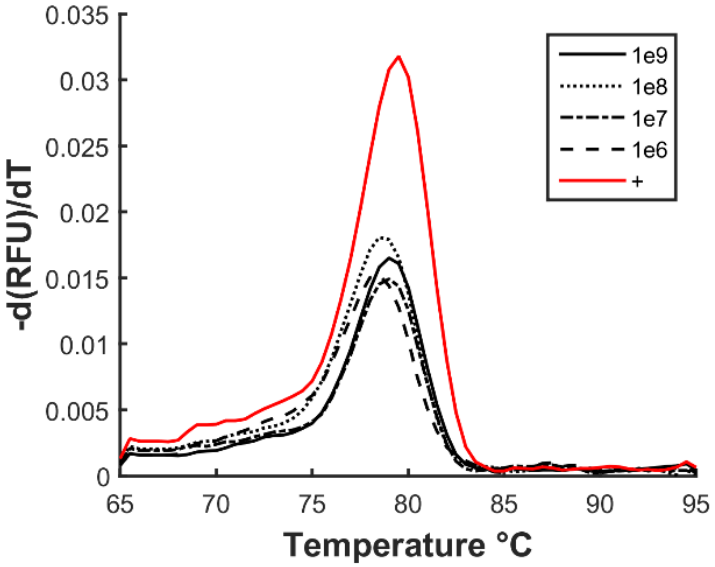


**Figure 3.8 Melt analysis of particle PCR products.** Melt peaks from one calibration curve of PCR products from Figure 6. The melt temperatures, 79.0 ± 0.5 °C, of the amplicons with beads in solution (1e9 – 1e6) match the melt temperature, 79.5 °C, of amplicons generated without beads (+).

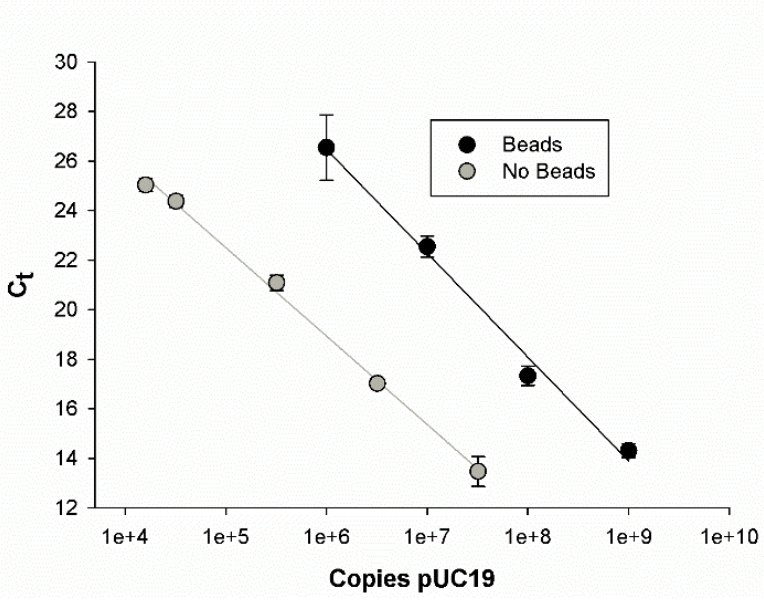


**Figure 3.9 Particle calibration curve.** PCR calibration curves of reactions with beads (*black circles*) and reactions without beads (*gray circles*). Addition of chitosan beads into the reaction resulted in less efficient PCR, E = 67.6%, than reactions without beads, E = 90.6%.

It is interesting to note that the amplification plots between reactions with particles and reactions particles were different (Figure 3.10). In general, the exponential phase of reactions without particles increased in fluorescence faster than reaction with particles. The slope of the exponential phase as a function of initial pUC19 copies is plotted in the inset of Figure 3.10. For normal reactions, there is no correlation to the slope of the exponential phase to the initial amount of DNA. However, in reactions with particles, the slope increases with less initial DNA. This is probably because particles with less adsorbed DNA can more easily adsorb PCR products as they are amplified. On the other hand, particles

with more adsorbed DNA, such at $10^9$ copies pUC19, amplify DNA just as quickly as normal reactions in the exponential phase.

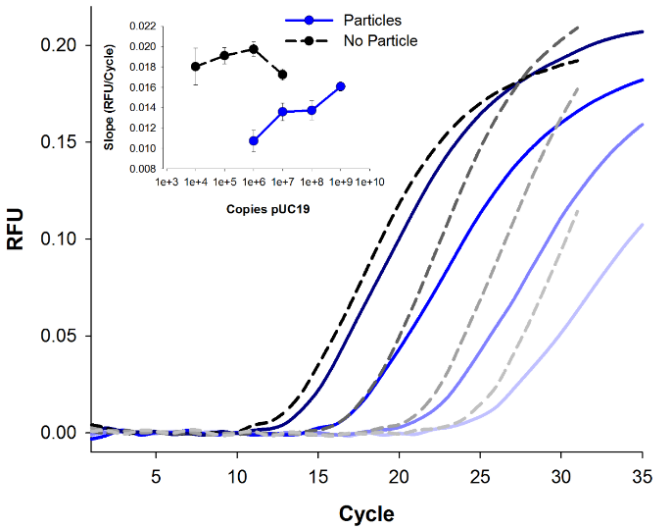


**Figure 3.10 Amplification slope.** Fluorescence intensity at each cycle from sets of calibration curves in Figure 7. The amplification of reactions with 0.5 hour cross-linked particles with $10^9$, $10^8$, $10^7$, and $10^6$ initial adsorbed copies of pUC19 from left to right are shown in *blue*. The amplification of $10^7$, $10^6$, $10^5$, and $10^4$ copies pUC19 initially added to the reaction from left to right are shown in *black*. The exponential amplification is slower with particles than in normal reactions. The slope of the linear portion of the exponential phase of each amplification is shown as a function of the initial amount of DNA in the inset. The slope does not correlate to initial pUC19 copies in reactions without particles. However, the slope increases with initial amount of adsorbed pUC19 on particles. Particles with 1e9 copies pUC19 amplify as quickly as normal reactions.

## 3.4 Conclusion

Whole chitosan magnetic particles were produced by an emulsion cross-linking process. These particles were capable of DNA extraction but behaved drastically different from previously published charge switching extraction schemes of chitosan modified surfaces. Whole chitosan particles absorbed DNA at a pH optimal for PCR and did not elute the DNA after (i) high salt, (ii) high pH or (iii) high temperature treatments. After glutaraldehyde crosslinking for 0.5 hour, the particles were still found to be pH responsive but an apparent shift from the reported chitosan pKa of 6.4 to 7.5 was observed. Further crosslinking longer than 16 hours resulted in decreased DNA adsorption. We believe DNA was electrostatically and sterically bound to particle subsurface. Although DNA was not eluted off the particles, qPCR was performed with the particles directly in the reaction mixture. DNA extraction with a single extraction buffer greatly simplifies sample preparation methods, especially in micro-total-analytical-systems.

# Chapter 4 PCR SURFACTANT ASSESSMENT USING THE PENDANT DROP TECHNIQUE

The text and figures presented here have been adapted from the following journal article and reprinted with permission from Elsevier.
Kunal R. Pandit, Paul E. Rueger, Richard V. Calabrese, Srinivasa R. Raghavan, and Ian M. White, Assessment of surfactants for efficient droplet PCR in mineral oil using the pendant drop technique, *Journal of Colloids and Surfaces B: Biointerfaces*, 126, 489-495, 2015. DOI:10.1016/j.colsurfb.2015.01.001

## 4.1 Introduction

Droplet PCR uses microfluidic techniques to apportion PCR reaction mixtures into aqueous droplets ("microreactors") surrounded by an oil phase. Typically, droplet volumes range from nanoliters to picoliters. At the larger size range, DNA is quantified using a cycle threshold calibration curve. In comparison, for picoliter droplets, DNA can be absolutely quantified using digital PCR (Beer et al. 2007). Digital PCR has been shown to quantify extremely rare targets, such as HIV DNA in infected patients undergoing effective treatment (Strain et al. 2013).

Though impactful, droplet PCR is in need of technical improvement. Microreactors less than microliters in volume are dominated by surface effects (Angione, Chauhan, and Tripathi 2012). The increase in surface area relative to the volume of the droplet is advantageous for rapid heat transfer and reaction kinetics. However, adsorption of proteins to the oil-water interfaces hinders droplet PCR. Specifically, Taq polymerase (Taq Pol), an enzyme derived from thermophillic bacteria, is used in PCR to catalyze the reaction. Taq Pol is a relatively hydrophobic enzyme and thus is especially prone to adsorption at interfaces. The aliphatic index characterizes the relative hydrophobic volume of a protein

and, in general, thermophillic bacterial proteins have large relative hydrophobic volumes to aid in structural stability at high temperatures (Ikai 1980). The aliphatic index of Taq Pol is 98.6; in comparison, the aliphatic index of bovine serum albumin (BSA), a protein commonly used for surface blocking in molecular biology techniques, is 76.1. Indeed, Taq Pol is incredibly stable; even at DNA melting temperatures of 95 °C, the half-life of Taq Pol is 45 to 50 minutes (Lawyer et al. 1993).

Several techniques have been reported in the literature to overcome Taq Pol adsorption in microfluidic droplets. One obvious method is to increase the Taq Pol concentration to replace adsorbed enzyme (Angione, Chauhan, and Tripathi 2012). However, this is a wasteful approach since Taq Pol is the most expensive reagent in PCR (~ $1.00 per unit) and accounts for greater than 95% of the cost per bulk reaction. It has been shown to require up to 7 times (7X) the Taq Pol needed for bulk PCR to perform successful droplet PCR in contact with oil without any blocking agents (Wang and Burns 2009).

Obviously, adding cheaper blocking agents is preferred, such as nonionic surfactants (ionic surfactants are extremely toxic to PCR.). While surfactants are needed to stabilize the water droplets in oil, they can also competitively bind to the interface and thus reduce Taq Pol adsorption. Typically, nonionic surfactants such as NP-40, Triton X-100 or Tween 20 in concentrations of about 0.1 % w/w are added to PCR reactions to stimulate the enzyme (Innis et al. 1988). However, these surfactants are not sufficient in stabilizing droplets and preventing coalescence. Excess concentrations of nonionic surfactants, greater than 5% w/w, are inhibitory to PCR.

Instead, a surfactant must be added to the oil phase to prevent loss of polymerase to the interface and to prevent droplet coalescence at high temperatures. A popular surfactant to use with mineral oil as the continuous phase is ABIL EM90 because it is stable at high temperatures. It is a silicone based surfactant with a polyethylene glycol head group (Figure 4.1A). Normally, it is added to the oil at a concentration of 1-4 % w/w (Hatch et al. 2011; Baret 2012; Williams et al. 2006). It is important to note increasing the bulk surfactant concentration past the critical micelle concentration increases the number of micelles in solution. It does not increase the surfactant surface concentration to block the interface. Nonionic surfactants with long hydrophobic tails have small critical micelle concentrations on the order of 0.01 mM (Mattei, Kontogeorgis, and Gani 2013). In any case, extra Taq Pol is normally required to perform PCR even with significant surfactant concentrations in the surrounding oil phase (Schaerli et al. 2009).

Similarly, inactive proteins like BSA may be included in the PCR mixture to competitively bind to the interface (Yingnan Sun, Zhou, and Yu 2014; Beer et al. 2008). BSA is usually added to PCR reaction mixtures at large concentrations of about 5% w/w, to outcompete Taq Pol adsorption. When using mineral oil as the continuous phase, a combination of BSA in the aqueous phase and ABIL EM90 in the oil phase is usually employed simultaneously (Kumaresan et al. 2008). Since the adsorption is competitive, significant polymerase will still bind to the interface, and extra Taq Pol is necessary. For example in one protocol, with droplets created on ice with 2.0% v/v ABIL EM90 and 0.05% v/v Triton X-100 in mineral oil and 1.5% w/w BSA in the PCR mixture, the amount of Taq Pol used was twice the concentration used in bulk reactions.

Commercialized digital PCR technologies (RainDrop from RainDance or QX series from BioRad) utilize fluorinated oils instead of mineral oil as the continuous phase. Also proprietary fluorosurfactants are used in conjunction with fluorinated oils to stabilize droplets and prevent protein adsorption for digital PCR (Pekin et al. 2011). In particular, oil soluble fluorinated alkanes capped with triethylene glycol head groups were shown be excellent in preventing adsorption of proteins such as BSA and fibrinogen at fluorinated oil-water interfaces (Roach, Song, and Ismagilov 2005). However, this required proprietary fluorocarbon specialty chemicals not readily available, which increases costs. A system that relies on a cheap and widely available oil phase, such as mineral oil, is preferred.

In this chapter, we focus on the use of surfactants to prevent the adsorption and loss of polymerase in droplet PCR with mineral oil. Previous studies verified surfactants were compatible with droplet PCR through a trial and error methodology. A more systematic and quantitative approach is missing from literature. As proteins adsorb to the oil-water interface, the interfacial tensions between the two phases decreases in response. A trusted method to quantifying protein and surfactant adsorption by measuring interfacial tension is the pendant drop technique (R. Miller, Fainerman, Makievski, Krägel, Grigoriev, et al. 2000; R. Miller, Fainerman, Makievski, Krägel, and Wüstneck 2000). However, dynamic protein absorption studies have been limited to proteins such as albumins, casein, insulin, lysozyme, and IgG (Tornberg 1978; Voigt et al. 1991; Beverung, Radke, and Blanch 1999). Only limited investigations of Taq Pol adsorption to oil-water interfaces have been conducted.

Most researchers who have published work with droplet PCR have only just acknowledged extra Taq Pol was necessary for successful amplification. Wang & Burns were the first to characterize the optimal concentration of Taq Pol in nanoliter droplets. They found 0.175 U/μL of polymerase was necessary to perform droplet PCR as efficiently as in bulk reactions with only 0.025 U/μL (Wang and Burns 2009). Later, Angionne, Chauhan, and Tripathi measured the amount of DNA amplified in microliter droplets and bulk reactions with varying amounts of Taq Pol, and assumed active concentrations of Taq Pol were related to the amount of DNA after a fixed number of PCR cycles. They estimated the concentration of active polymerase in droplets by matching the decrease of DNA polymerized in droplets to bulk reactions with a smaller concentration of Taq Pol. They also calculated how much Taq Pol would be required to form a monolayer of denatured protein in a droplet of a given radius assuming the rate limiting step was diffusion to the interface. Although, there is no particular reason to assume adsorption is diffusion controlled. In the end, they estimated that 60 ± 10% of the polymerase they added was lost to adsorption to the oil-water interface (Angione, Chauhan, and Tripathi 2012).

We established the use of the pendant drop technique for quantitative assessment and comparison of surfactants in droplet PCR. In this technique, an aqueous drop is suspended in oil at the tip of a syringe. The geometry of the drop is correlated to the interfacial tension. By performing the pendant drop test with an aqueous drop of Taq Pol suspended in mineral oil with surfactant, we measure the adsorption of enzyme and/or surfactant at the droplet interface. Thus, this simple test can assess the capability of a surfactant to inhibit the adsorption of Taq Pol in a quantitative manner rather than a trial and error PCR based method.

Our studies show that Taq Pol forms a high surface pressure film within seconds at oil-water interface that is not controlled by diffusion in contrast to the previously published assumption. Furthermore, we found ABIL EM90 is unable to prevent significant Taq Pol adsorption and loss. On the other hand, as an alternative, we have identified a simple, inexpensive surfactant, Brij L4 (Figure 4.1B), which has an alkyl tail attached to an oxyethylene head group. Brij L4 ensures negligible adsorption of Taq Pol at the droplet interface. In turn, when PCR is conducted in picoliter droplets in the presence of Brij L4, fewer cycles and less Taq Pol are needed to reach the fluorescence threshold compared to the case of ABIL EM90. Brij L4 is thus a superior alternative for droplet PCR. To our knowledge, this is the first report of Brij L4 for this purpose.

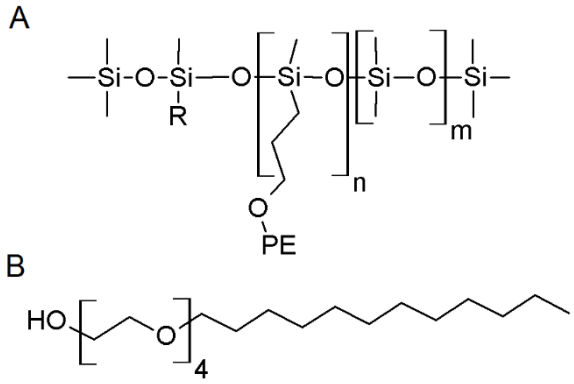


**Figure 4.1 Surfactant structures.** Structure of the surfactants used in this study. (A) ABIL EM90, a silicone-based surfactant where R is an *n*-alkyl chain and PE is $–(CH_2)_3–O–(C_2H_4O)_x–(C_3H_6O)_y–H$. (B) Brij L4, a nonionic surfactant with a head group composed of 4 polyethylene units and an *n*-dodecyl tail.

## 4.2 Materials and Methods

### 4.2.1 Interfacial tension measurement

Interfacial tension measurements were taken using a dynamic pendant drop technique. An aqueous drop with an initially clean interface was formed in oil. As time proceeded, enzyme and/or surfactants adsorbed at the interface, lowering the interfacial tension until the equilibrium interfacial tension was achieved. Transient drop shape factors were determined from images by measuring in millimeters the largest width of the drop $D_e$ and the width of the drop $D_s$ at a distance equal to $D_e$ from the bottom of the drop (Figure 4.2).

These were empirically correlated to the interfacial tension $\gamma$ in dynes per centimeter using Equation 4.1,

$$\gamma = 3.17\, g\, \Delta\rho\, D_e^{-0.08} D_s^{2.08} \qquad (4.1)$$

where $g$ is the acceleration due to gravity in meters per second squared, and $\Delta\rho$ is the difference in density between the water and oil phases in kilograms per meter cubed (Adamson 1976).

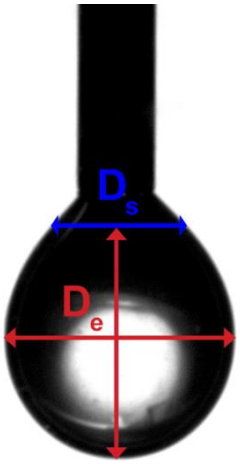


**Figure 4.2 Pendant drop width measurements.** Measurement of interfacial tension between water and oil from the shape of a pendant droplet. The photograph shows an aqueous droplet (diameter ~ 1 – 5 mm) hanging from a needle in a solution of mineral oil. Droplet width is measured at two points, as shown: the largest equatorial width De, and the width Ds at a distance of De from bottom of the droplet. The interfacial tension is correlated with De and Ds using Equation 4.1.Stock solutions of 1.5% w/w (≈ 200 mM) ABIL EM90 (Evonik Industries) and 0.5% w/w (≈ 1300 mM) Brij L4 (Sigma-Aldrich) in mineral oil (light oil, BioReagent, suitable for mouse embryo cell culture, Sigma Aldrich) were stored at room temperature. The ABIL EM90 concentration was chosen based on previous studies (Williams et al. 2006). The Brij L4 concentration was the highest that allowed for sufficiently sized droplets that would not detach from the needle tip over an hour. Aqueous solutions of Taq Pol (BioRad) consisting of 20 mM Tris-HCl, 50 mM KCl, and 1.5 mM MgCl2 were made the day of experiments and stored on ice. The concentration of Taq Pol in the aqueous droplet phase ranged from 0 to 8X, where 1X was 0.025 U/µL (the concentration prescribed by the manufacturer for a 50 µL reaction).

Mineral oil solutions were preheated and maintained at 55 °C with a water bath during all experiments to obtain measurements at relevant elevated PCR temperatures. Higher temperatures caused observable bubble formation in the water bath which obscured

the droplet. The density of mineral oil at 55 °C was measured to be 0.806 ± 0.005 g/mL. The density of the aqueous solutions was taken to be 0.986 g/mL, the density of water at 55 °C (Lemmon, McLinden, and Friend 2012). The viscosity of the light mineral oil at 55 ˚C was measured using an Advanced Rheometer 2000 thermally controlled cone-and-plate rheometer and found to be 9.2 mPa·s.

Hanging aqueous droplets were formed in mineral oil solutions at the tip of either 16, 18, or 26 gauge syringe needles to form the largest non-spherical droplets that would not pinch off. No difference was seen in γ with different sized needles. Syringes were rinsed thoroughly with ultrapure deionized water and dried with nitrogen between experiments. Interfacial tensions for each time point were calculated from 5 images of the pendant droplet acquired using a Pulnix TM-1405GE CCD camera. The images were analyzed using ImageJ and Matlab software packages (Rueger and Calabrese 2013). All equipment was setup on a vibration isolation table to minimize droplet movement, with the exception of the camera, which was stabilized on a tripod. The apparatus and experimental details are described elsewhere (Rueger and Calabrese 2013; Rueger 2013). Each experimental condition was observed for at least 1 h and conducted in triplicate. The Bond number, defined as $Bo = \rho g L^2/\sigma$, was greater than 0.48 for all measured droplets, ensuring they were sufficiently non-spherical to allow for accurate measurements (Alvarez, Walker, and Anna 2009). The maximum error in γ at each time point was 0.1 dyn/cm and the maximum error from drop to drop was 0.5 dyn/cm.

### 4.2.2 Real-time droplet PCR

To validate interfacial tension measurements, real-time PCR was performed, in which the change in fluorescence of individual PCR droplets was measured over each

thermal cycle. The PCR master mix consisted of 20 mM Tris-HCl, 50 mM KCl, 1.5 mM MgCl2, 200 μM of each deoxynucleotide triphosphate (dNTP), 200 nM forward and reverse primers (forward primer: ACA GAG TTC TTG AAG TGG TGG; reverse primer: TGG TTT GTT TGC CGG GAT CAA), LC Green (Biofire Diagnostics), and varying concentrations of Taq Pol. The pUC19 (Thermo) plasmid served as the template for amplification. LC Green as supplied was diluted by a factor of 10 in the master mix. The initial concentration of pUC19 was 5 x $10^6$ copies/μL. Wells were fabricated by creating holes in 2.5 mm thick cured Sylgard 184 polydimethylsiloxane (PDMS, Dow Corning) using a 5 mm biopsy punch. Individual wells were separated and bonded to cover glass slips; bonding of the PDMS to glass was performed by spinning PDMS at 3000 rpm for 30 s on the glass to form a thin layer that served as an adhesive and as a hydrophobic bottom surface. Droplets, 20 ± 2 μm in diameter (~ 4 pL in volume) were formed in PDMS microfluidic chips using a 20 μm square channel flow focusing geometry (oil flow rate = 10 μL/min; aqueous flow rate = 2 μL/min) and then captured in wells filled with mineral oil solutions. Care was taken to capture single droplets in wells when using Brij L4 as the surfactant due to droplet coalescence during changes in temperature when thermal cycling. Wells were sealed with cover glass slips before thermal cycling on an aluminum plate heated and cooled with a peltier.

The reaction in the droplets was initialized with a hot start at 95 °C for 3 minutes and then thermal cycled for 35 cycles. Each thermal cycle consisted of 30 s at 55 °C for annealing, 30 s at 72 °C for extension, and 30 s at 95 °C for melting. Real time amplification results were obtained after every extension step by exciting fluorescence using a blue LED (Innovations in Optics) with a 424 – 438 nm bandpass filter (Brightline), while capturing

fluorescence emission with a CCD (Allied Vision) fitted with a 67 mm working distance lens (Edmund Optics) and a high pass filter with a 475 nm cut-off (Omega Optical). The cycle threshold was defined as the cycle where the fluorescence during the extension step of a given cycle was greater than the fluorescence during the extension step of the first cycle by 10 standard deviations. Data was taken from at least 3 droplets for each experimental condition.

### 4.2.3 Emulsion stability

Stable emulsions with Brij L4, a hydrophilic surfactant, were created by modifying the hydrophile−lipophile balance (HLB) with the addition of Span 80, a lipophilic surfactant. A ratio of 4:1 Span 80 to Brij L4 is required to form stable water in mineral oil emulsions at room temperature (*The HLB SYSTEM a Time-Saving Guide to Emulsifier Selection* 1980), though upon thermal cycling the emulsion broke. To find the optimal surfactant concentrations, emulsions with varying ratios of Span 80 : Brij L4 in mineral oil were thermal cycled and then inspected under magnification to verify stability. A mixture of 5.0 wt% Span 80 and 0.5 wt% Brij L4 formed stable emulsions that withstood thermal cycles.

### 4.2.4 Oil extraction

The mineral oil/surfactant mixtures were separated from the aqueous phase using a liquid-liquid extraction technique (Schaerli et al. 2009). First, emulsions were broken by centrifugation at 13000×g for 5 minutes and then excess upper oil phases were removed. Next, the remaining oil was extracted twice by addition of 0.5 mL of water-saturated diethyl ether, sample vortexing, and upper organic phase disposal. Finally, the residual organic phase was evaporated in a fume hood at room temperature for 10 minutes.

### 4.2.5 PCR for amplification factor determination

Emulsions of various mineral oil and surfactant mixtures with PCR master mix were thermal cycled to validate interfacial tension measurements with droplets in contact with one another. The PCR master mix consisted of 20 mM Tris-HCl, 50 mM KCl, 1.5 mM MgCl2, 200 µM of each dNTP, 200 nM forward and reverse primers (forward primer: GTC TCA TGA GCG GAT TAC A; reverse primer: CTC GTG ATA CGC CTA TTT TT), SYBR Green I (Lonza), and 1X or 2X Taq Pol. SYBR Green I as supplied was first diluted by a factor of 1000/3 in dimethylsulfoxide and then by a factor of 60 in the master mix. The pUC19 plasmid was again used as the template. The initial concentration of pUC-19 was 5 x $10^6$ copies/µL. Mineral oil/surfactant mixtures used to create emulsions included 5.0 % Span 80 and 0.5% Brij L4, 1.5% Span 80 & 0.5% Brij L4, and 1.5% ABIL EM90. PCR master mix was apportioned into droplets with the oil mixtures as the continuous phase as described in section 4.2.3. Droplets were directed into plastic conical PCR tubes where 20 µL of total droplet volume was collected in 10 minutes. Bulk PCRs were amplified by layering 100 µL of oil and surfactant mixtures on top of 20 µL of PCR master mix in plastic conical PCR tubes.

A MiniOpticon Real-Time PCR system (BioRad) was used to thermal cycle bulk and emulsion PCR reactions. The thermal cycles consisted of a 95 ˚C melt for 3 s followed by a 56 ˚C anneal for 30 s. The initial hot start was at 95 ˚C for 3 minutes and was followed by 20 cycles. To better differentiate effects of various oil/surfactant mixtures, the number of thermal cycles was chosen so that the amplification of DNA in bulk reactions would not reach the exponential phase. Each oil mixture and Taq Pol concentration was amplified in triplicate.

### 4.2.6 Amplification factor measurement

The amount of DNA amplified after 20 thermal cycles was quantified using qPCR. The PCR reaction mixture consisted of iQ SYBR Green Supermix (BioRad) diluted by a factor of two, 200 nM forward and reverse primers (same as used in the amplification factor determination), and the amplified DNA samples diluted by a factor of 10000/3. The thermal cycle conditions were the same as the amplification factor determination.

## 4.3 Results and Discussion

### 4.3.1 Interfacial tension measurements

In our pendant drop experiments, we suspended an aqueous droplet in mineral oil at 55 °C (this temperature is relevant to an annealing step in a PCR thermal cycle). The interfacial tension of the oil-water interface $\gamma$ was measured as a function of time. Typically, $\gamma$ decreased with time, reaching an equilibrium within 45 minutes. Figure 3 shows plots of $\gamma(t)$ for various cases.

In the absence of surfactants or enzyme, $\gamma$ of the oil-water interface has a value of 36.4 dyn/cm at equilibrium (we denote this as $\gamma_0$). The decrease in $\gamma$ over time is not surprising because of possible surface active contamination in the mineral oil. In any case, $\gamma_0$ was used as a reference point to determine further adsorption of surfactants or proteins. When either surfactant or enzyme is present, $\gamma$ is much lower. Specifically, when 1X Taq Pol is present in the aqueous phase and there is no surfactant in the oil, $\gamma$ is 15.3 dyn/cm at $t = 0$ and decreases to 9.6 dyn/cm at equilibrium. On the other hand, when the buffer with no Taq Pol is contacted with oil containing 1.5 wt% of the silicone surfactant ABIL EM90, $\gamma$ is 3.8 dyn/cm at $t = 0$ and 2.2 dyn/cm at equilibrium (we denote the latter value as $\gamma_{A0}$).

Lastly, when the buffer with no Taq Pol is contacted with oil containing 0.5 wt% of Brij L4, $\gamma$ is at 1.82 dyn/cm, and is nearly constant with time (we denote this value as $\gamma_{B0}$).

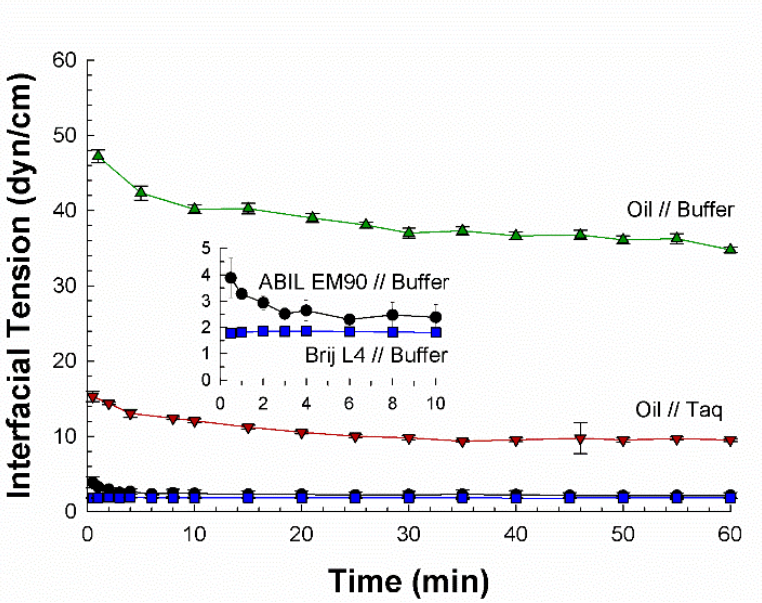


**Figure 4.3 Dynamic interfacial tension.** Interfacial tension $\gamma$ at the oil-water interface as a function of time $t$ for various cases. At $t = 0$, the aqueous drop is suspended in mineral oil. The *green triangles* correspond to aqueous buffer (with no enzyme) in oil (with no surfactant). The *red triangles* represent the case where the Taq Pol enzyme is in the buffer (at a 1X concentration) and there is no surfactant in the oil. Finally, data are shown for two surfactants in the oil: 1.5 wt% of ABIL EM90 (*black circles*) and 0.5 wt% Brij L4 (*blue squares*); in each case the buffer contains no enzyme. The surfactants reduce $\gamma$ and the equilibrium is reached rapidly, especially in the case of Brij L4. Points are averages of 3 trials. Error bars represent the standard deviation.

The dynamic measurements reflect the adsorption of enzyme and surfactant at the droplet interface. As soon as the droplet is formed, surfactant or enzyme molecules migrate to the interface, causing the interfacial tension $\gamma$ to decrease relative to its value without surface active molecules (i.e., $\gamma_0$). For the case of Taq Pol alone (no surfactant), the decrease

in $\gamma$ from its initial to steady-state value occurs quite slowly (over about 30 min). This shows that Taq Pol adsorption at the interface continues well after droplet formation. In comparison, when using ABIL EM90 (in the oil), $\gamma$ has a lower initial value and also reaches its equilibrium faster (in about 10 min). In this case, the interface will initially have adsorbed surfactant, but it is evidently not saturated. The decrease in $\gamma$ with time likely reflects additional adsorption of surfactant from the oil. Lastly, when using Brij L4 (in the oil), we note that $\gamma$ reaches an equilibrium very quickly (in < 2 min), implying that the interface is rapidly saturated with surfactant molecules.

The initial interfacial tension $\gamma$ of surfactant or protein systems was very low compared to $\gamma_0$, thus the interface was under a high surface pressure $\Pi = \gamma_0 - \gamma$. Adsorption to a high $\Pi$ film is limited by penetration to the interface, where there is a considerable surface excess concentration of amphiphiles. The kinetics of adsorption at liquid-liquid interfaces in the presence of excess amphiphile is usually interpreted in terms of the model of Ward and Tordai (Ward and Tordai 1952). According to this model, for the case of adsorption limited kinetics, the variation of the surface pressure $\Pi$ with time is given by Equation 4.2:

$$\frac{d\Pi}{dt} = k_f \nu \cdot C \cdot \exp\left(-\frac{\Pi \Delta A}{k_B T}\right) \tag{4.2}$$

where $k_f$ is the adsorption rate constant, $\nu$ is the number of adsorbing groups, $C$ is the bulk concentration of the amphiphile, $\Delta A$ is the area created in the interfacial film to adsorb the species, and $\Pi \Delta A$ is the work to create the area $\Delta A$ in a film under surface pressure $\Pi$. The above equation assumes that the adsorption of the amphiphile is irreversible and it can be

rewritten in the following form:

$$\ln\left(\frac{d\Pi}{dt}\right) = \ln\left(k_f \nu \cdot C\right) - \frac{\Pi \Delta A}{k_B T} \tag{4.3}$$

Figure 4.4 shows a plot of ln(dΠ/d*t*) as a function of Π for the case of 1X Taq Pol in the aqueous droplet and no surfactant in the oil. The initial linear portion of the plot at low surface pressures is fitted to Equation 4.3 using a linear least squares fit. The slope of the line is proportional to Δ*A*, which is the area occupied by a Taq Pol molecule on the interface (Tornberg 1978). We calculate $\Delta A = 4 \pm 1$ nm$^2$. For comparison, $\Delta A = 2$ nm$^2$ for BSA, a much smaller protein. The significance of this parameter is that if a space in the interfacial film of 4 nm$^2$ is cleared, Taq Pol would still be able to migrate from solution and adsorb at the interface.

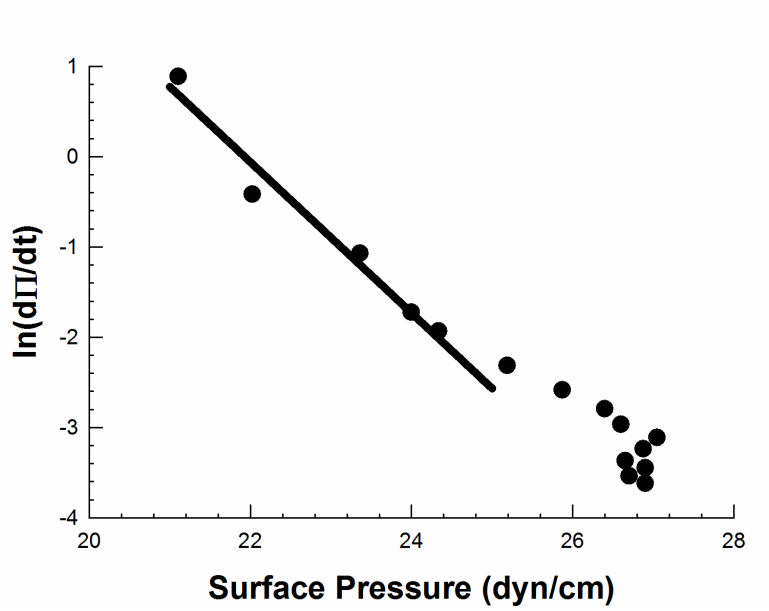


**Figure 4.4 Adsorption limited kinetics.** Dynamics of Taq Pol adsorption to the oil-water interface in the absence of surfactant. The $\gamma(t)$ from Figure 2 (*red triangles*) is replotted in terms of the surface pressure $\Pi = \gamma_0 - \gamma$, where $\gamma_0$ is the interfacial tension at steady state of a bare interface. The plot above is a semi log plot of $d\Pi/dt$ vs. $\Pi(t)$, as suggested by Equation 4.3. A straight line fit to the initial linear region at low $\Pi$ yields the value of $\Delta A$, which is the area occupied by Taq Pol at the interface.

Previously, Angione, et al., estimated adsorption of Taq Pol based on diffusion limited adsorption theory and correlating production of DNA to Taq Pol concentrations in bulk reactions (Angione, Chauhan, and Tripathi 2012). Our results indicate that the protein film is under a high surface pressure $\Pi$, and therefore is not diffusion limited but kinetically limited. Furthermore, Angione, et al., determined that the area per molecule of Taq Pol at the oil-water interface reasonably agreed with an estimate of the radius of gyration of the polymerase in a denatured conformation (116 Å). However our interfacial tension data suggests that Taq Pol could further adsorb between gaps in the film that are smaller than

the enzyme in size (native radius of gyration = 38.3 Å). This minimal area required for adsorption is likely due to the enzyme's large hydrophobic content. Only a small hydrophobic portion of Taq Pol is necessary to interact with the interface for the enzyme to irreversibly adsorb.

Next, we proceeded to measure the interfacial tension $\gamma$ vs. time for different concentrations of Taq Pol in the aqueous phase and 1.5 wt% ABIL EM90 in the oil phase. Figure 4.5a plots $(\gamma_{A0} - \gamma)$ for representative polymerase concentrations (data at other concentrations is shown in the Supplementary data, Figure S1). Note that $\gamma_{A0}$ is the equilibrium interfacial tension for mineral oil with 1.5 wt% ABIL EM90 in contact with aqueous buffer (as measured in Figure 3). At low Taq Pol (0.1X) and moderate Taq Pol (1.4X), $\gamma(t)$ shows a monotonic behavior, and equilibrium is reached within 20 minutes. When the polymerase concentration was greater than or equal to 2X, a nonmonotonic trend was seen, as indicated in Figure 4.5a, for the case of 8X Taq Pol. Here, the function initially shows an overshoot from its initial value before decreasing to a steady-state within about 20 minutes. The overshoot is likely due to the displacement of surfactant molecules from the interface by protein.

Similarly, we measured the interfacial tension $\gamma$ vs. time for various concentrations of Taq Pol in the aqueous phase and 0.5 wt% Brij L4 in the oil phase. Plots of $(\gamma_{B0} - \gamma)$ for representative protein concentrations are shown in Figure 4.5b (data at other concentrations is shown in the Supplementary data, Figure S2). Note that $\gamma_{B0}$ is the steady-state interfacial tension for mineral oil with 0.5 wt% Brij L4 in contact with buffer (as measured in Figure 4.3). The plots are all nearly flat, i.e., the interfacial tension is nearly constant over time at all polymerase concentrations. This suggests that the interface is rapidly saturated with Brij

L4 and that the Taq Pol does not displace the surfactant from the interface. In other words, Brij L4 is able to prevent the adsorption of polymerase over the course of our experiments.

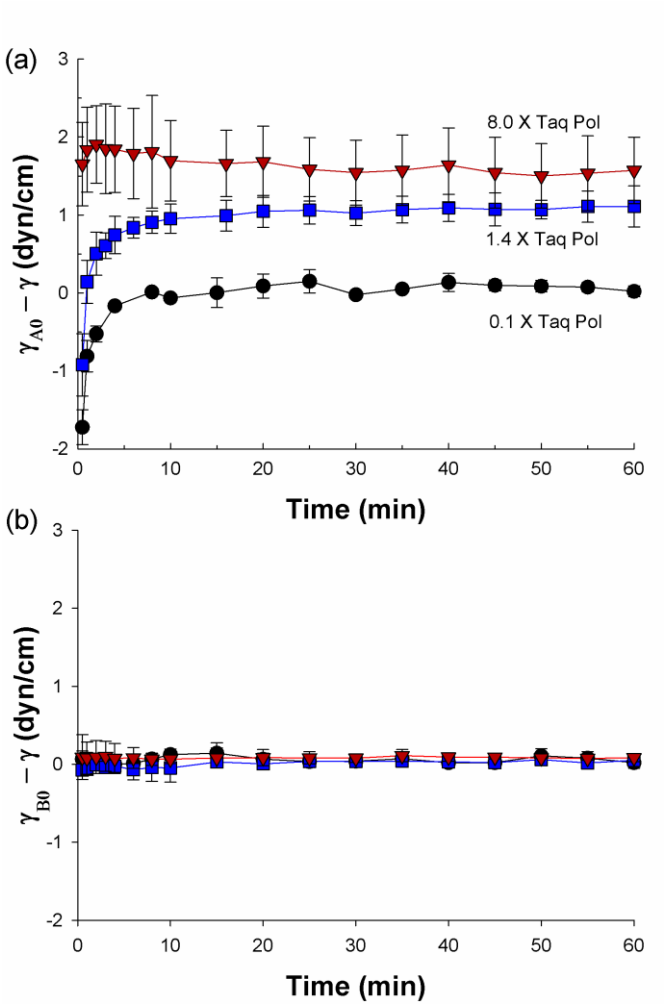


**Figure 4.5 Dynamic surface pressure.** Interfacial tension as a function of time t with surfactant in the oil phase and protein in the aqueous phase. (a) 1.5 wt% ABIL EM90 in the oil phase and various concentrations of Taq Pol in the aqueous phase. The data is plotted as the deviation from the steady state interfacial tension $\gamma_{A0}$ for mineral oil with 1.5 wt% ABIL EM90 in contact with buffer (from Figure 3). In all cases, a steady state is reached within about 20 minutes. (b) 0.5 wt% Brij L4 in the oil phase and various concentrations (same as in (a)) for Taq Pol in the aqueous phase. In this case the data is plotted as the deviation from the steady state interfacial tension $\gamma_{B0}$ for mineral oil with 0.5 wt% Brij L4 in contact with buffer (from Figure 3). The steady state is reached immediately in all cases.

The surface pressure $\Pi_S$ at equilibrium as a function of Taq Pol concentration is shown in Figure 4.6 for both surfactants (i.e., these are the equilibrium data from Figures 4.5, S1, and S2). When 1.5% of ABIL EM90 is in the oil, $\Pi_S$ increases with polymerase concentration before levelling out. This indicates that both Taq Pol and ABIL EM90 adsorb at the interface. It is only when 4X Taq Pol is in solution that the interface is fully saturated at $\Pi_S$ = 35.2 dyn/cm. These results are in sharp contrast to the case when 0.5% Brij L4 is present in the oil; $\Pi_S$ is constant at 34.6 dyn/cm over all polymerase concentrations. In other words, Brij L4 rapidly saturates the oil-water interface and thus prevents significant adsorption of the enzyme. These results suggest that Brij L4 is likely to be a better surfactant for droplet PCR than ABIL EM90. It should be noted that the droplet size in the pendant drop measurements is in the millimeter range (volumes in the microliters). If the droplets are instead in the microscale range of diameters (picoliter volumes), the surface-to-volume ratios would be even higher and therefore even at 4X Taq Pol, much of the enzyme could be adsorbed at the interface and thereby rendered non-functional.

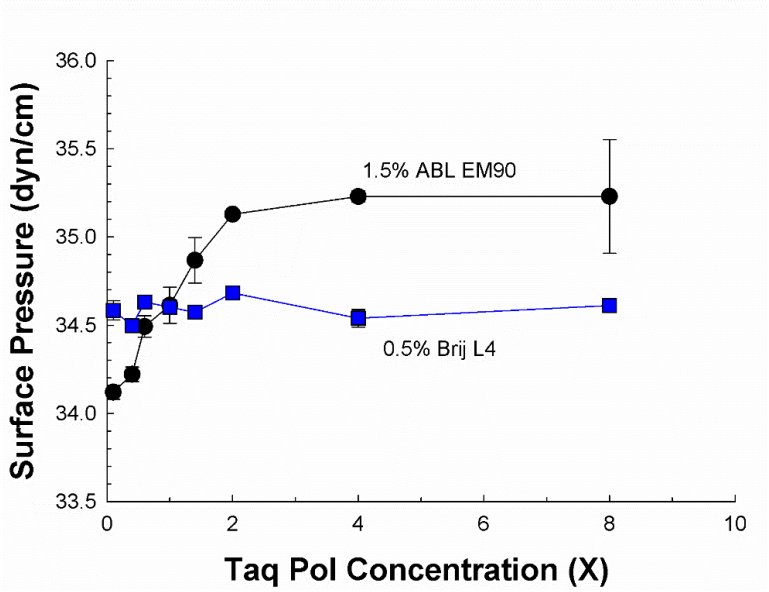


**Figure 4.6 Equilibrium surface pressure.** Influence of surfactants on Taq Pol adsorption, measured for different polymerase concentrations. The surface pressure $\Pi_s$ at equilibrium is shown as a function of polymerase concentration (denoted by the multiple X, where 1X is 0.025 U/µL) for the two different surfactants, 1.5 wt% ABIL EM90 (*black circles*) and 0.5 wt% Brij L4 (*blue squares*). In the case of ABIL EM90, $\Pi_s$ increases with Taq Pol, indicating that both the surfactant and the enzyme adsorb at the interface. In the case of Brij L4, $\Pi_s$ is independent of Taq Pol, indicating that the surfactant saturates the interface, thereby minimizing adsorption of the enzyme.

### 4.3.2 Real-time droplet PCR validation

To examine whether Brij L4 is indeed a superior surfactant for PCR, we performed droplet PCR with droplets of 20 µm diameter (~4 pL volume). Aqueous droplets containing the pUC19 plasmid, Taq Pol, and the rest of the components of the PCR master mix were captured in wells filled with mineral oil containing dissolved surfactant (ABIL EM90 or Brij L4). At this droplet size, the number of initial copies of pUC19 per droplet vary

probabilistically with an average of 20 initial plasmids. Droplets were thermal cycled (as described above), and fluorescence from the droplets was measured in real-time. When the PCR was successful, all the droplets observed amplified. If the PCR is efficient, all template-primer pairs are extended every cycle and the copies of amplicons roughly double over each cycle. This is achieved only if sufficient active polymerase is in solution to catalyze the extension of bound primers. An excess of Taq Pol would have no effect on the cycle threshold, whereas a depletion of Taq Pol would decrease the cycle efficiency of PCR and thus increase the cycle threshold.

Figure 4.6 shows the cycle threshold for droplet PCR as a function of Taq Pol for the two surfactants under study. The results confirm that the PCR cycle efficiency is significantly better when 0.5 wt% Brij L4 is used than when 1.5 wt% ABIL EM90 is used. Using 1.5% ABIL EM90 and 8X Taq Pol, 16 ± 2 cycles are necessary to reach the fluorescence threshold. In contrast, with 0.5% Brij L4, and at the same polymerase concentration, only 7 ± 1.5 cycles are required to reach the same threshold. Furthermore, PCR with ABIL EM90 could not be conducted to an appreciable level using less than 8X Taq Pol. On the contrary, when Brij L4 is present, efficient PCR was achieved with polymerase concentrations as low as 2X, with the threshold in this case being 7 ± 1.5 cycles as well. Even with 1X Taq Pol and with Brij L4, PCR could be performed, but 21 ± 5 cycles were necessary to reach the fluorescence threshold. Thus, when the enzyme concentration is very low, a fraction of it may still be lost due to competitive adsorption. Though a significant amount of Taq Pol was still in solution that allowed for successful PCR. However, it is sufficient to use 2X Taq Pol to completely overcome any such losses due to adsorption.

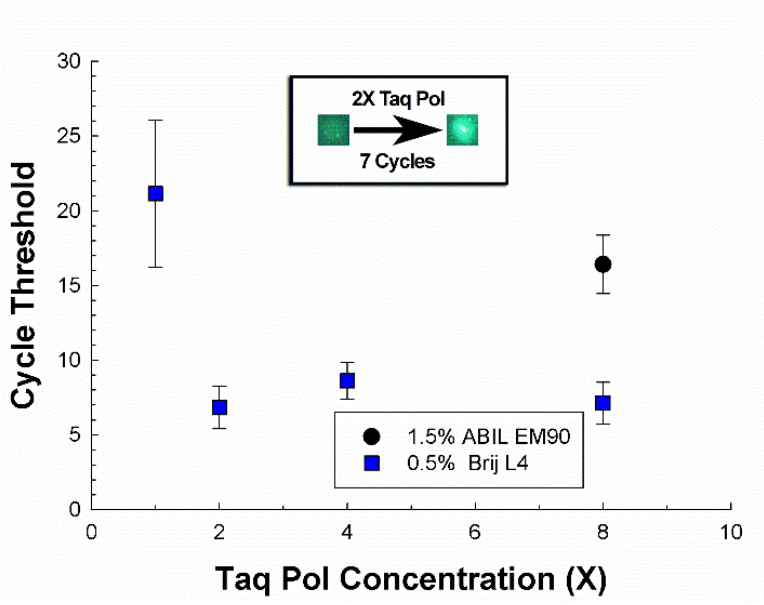


**Figure 4.7 Real time droplet PCR.** Cycle threshold during droplet PCR for various Taq Pol concentrations and in the presence of surfactant. The data show that efficient PCR can be accomplished when 0.5% Brij L4 (*blue squares*) is used in the oil phase. For Taq Pol concentrations from as little as 2X to 8X, only ~ 7 cycles are necessary to reach the threshold. In comparison, with 1.5 wt% ABIL EM90 as the surfactant (*black circles*), PCR could not be performed with less than 8X Taq Pol, and even for that case, more cycles (~ 16) were needed. The inset shows raw images of a 20 μm diameter droplet revealing the increase in fluorescence from the initial cycle to the 7th cycle using 2X Taq Pol and 0.5% Brij L4.

Overall, we can conclude that using 0.5% Brij L4 significantly eliminates Taq Pol adsorption, as predicted by the pendant drop technique and as validated by droplet PCR. With 2X Taq Pol, the use of Brij L4 enables the fluorescence threshold to be reached in about half as many thermal cycles as compared to ABIL EM90 with 8X Taq Pol.

Furthermore, successful PCR with Brij L4 also confirms that surfactant was not appreciably degraded during thermal cycling.

### 4.3.3 Emulsion PCR amplification factor validation

The above work demonstrated that Brij L4 was highly effective at preventing Taq Pol adsorption at the droplet interface, but it was noted that care was required to prevent coalescence when using Brij L4. While many microfluidic droplet systems maintain control over the droplets such that coalescence is not an issue (J. A. Kim et al. 2006), some droplet PCR systems, including emulsion PCR, are subject to coalescence. We found that stable water-in-mineral-oil emulsions at PCR temperatures with 0.5% Brij L4 required the addition of 5.0% Span 80 to achieve stability. We compared this oil and surfactant mixture with 1.5% ABIL EM90, 1.5% Span 80 & 0.5% Brij L4, and bulk PCR by measuring the amplification factor after 20 thermal cycles using 1X Taq Pol in the aqueous phase (Figure 8). Amplification factors of bulk PCRs were measured to be independent of the upper phase oil mixtures. An emulsion with 5% Span 80 in addition to 0.5% Brij L4 amplified about 3 orders of magnitude more DNA than bulk PCR. The droplet amplification was much more efficient due to the presence of nonionic surfactants which have stabilize and stimulate polymerase activity (Eun 1996). However, this increase in efficiency would only be possible with significant enzyme in solution. The emulsion with 1.5 % ABIL EM90 amplified about as much DNA as the bulk reaction. The 1.5% Span 80 and 0.5% Brij L4 emulsions broke whilst thermal cycling, thus amplification factors similar to bulk PCR were recorded.

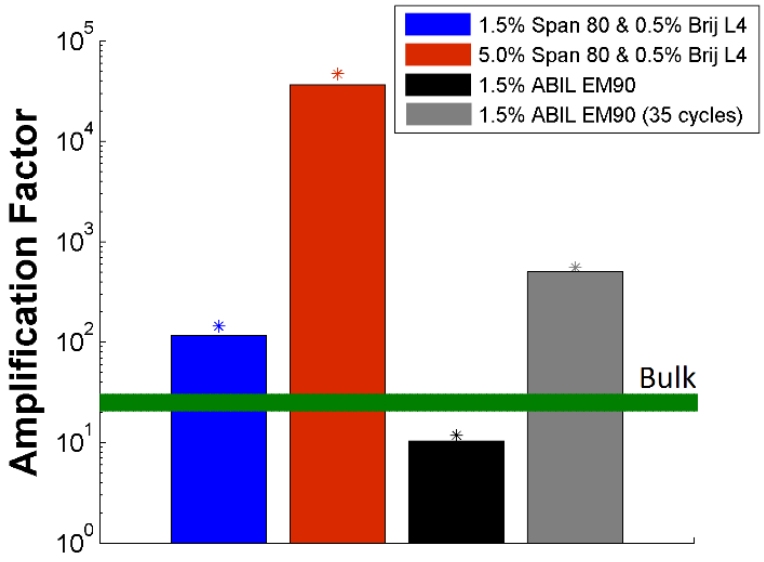


**Figure 4.8 PCR amplification factor.** Amplification factor of various emulsion PCRs with 1X Taq Pol. Amplification factor = copies of pUC19 product amplified after 20 thermal cycles / initial copies of pUC19. The *green line* provides a bulk PCR reference, which was independent of the different overlaid oil/surfactant mixtures. The 1.5% Span 80 & 0.5% Brij L4 emulsion (*blue bar*) was stable at room temperature but broke upon thermal cycling. Therefore, the amplification factor was similar to bulk PCR. The 1.5% ABIL EM90 emulsion (*black bar*), also had amplification factors similar to bulk PCR. When the PCR was extended to 35 cycles with 1.5% ABIL EM90 (*gray bar*), the amplification factor increased. However, the amount of DNA amplified was 3 orders of magnitude less than the bulk at 35 cycles. Amplification factors of 5.0% Span 80 & 0.5% Brij L4 (*red bars*) were about 3 orders of magnitude greater than that of bulk PCR.

Although 1.5% ABIL EM90 amplified about as much DNA as bulk PCR, our interfacial tension measurements and real-time droplet PCR results indicated that the amplification factor should be much less than bulk conditions. After we verified that the emulsion did not break during thermal cycling, we investigated the matter further by

thermal cycling the emulsion for 35 cycles and comparing it to a bulk reaction. The amplification factors of the emulsion and bulk reactions after 35 cycles were 500 and $4 \times 10^5$ respectively. Thus the 1.5% ABIL EM90 emulsion PCR was severely inhibited by a lack of functional Taq Pol in solution as suggested by our results in the previous sections. The lack of active Taq Pol was balanced by the increase in activity by a nonionic surfactant and enabled the amplification factor at 20 cycles of the emulsion to be similar to the bulk.

The exponential increase in pUC19 product after 20 cycles using 5% Span 80 & 0.5% Brij L4 with as little as 1X Taq Pol indicates that active Taq Pol is sufficiently blocked from the oil-water interface. However, our real-time droplet PCR results indicated 1X Taq Pol inefficiently amplified DNA. This discrepancy is probably due to optimal thermal cycling in the emulsion PCR, which was performed in a commercial thermal cycler instead of a custom-made system for microdevices. Furthermore, we believe the superior performance of this oil/surfactant mixture was attributed to the immediate saturation of the oil-water interface mostly by Brij L4 rather than Span 80. Without Brij L4, the 5 wt% Span 80 mineral oil emulsion broke during thermal cycling. The stabilization by a small amount of Brij L4 suggests that a large fraction of the interface was made up of Brij L4. Additionally, although a large amount of Span 80 was required, it is a lipophilic surfactant, and thus much of the surfactant likely formed micelles in the oil phase (Campanelli and Wang 1998).

In summary, the stable PCR emulsion with Brij L4 amplified orders of magnitude more DNA than the ABIL EM90 emulsion using only 1X Taq Pol. This is consistent with the surface tension measurements in Section 3.1 and validates the droplet PCR results of Section 3.2. Furthermore, this demonstration proved that droplet PCR with standard Taq

Pol concentration is feasible with mineral oil, as opposed to fluorinated oils and surfactants, as done commercially today.

## 4.4 Conclusion

We have shown that the commercially available nonionic surfactant Brij L4 greatly enhances the efficiency of droplet PCR compared to a surfactant that is commonly used for this purpose, ABIL EM90. The superior effectiveness of Brij L4 is demonstrated by measurements of the oil-water interfacial tension using the pendant drop technique. When 0.5% Brij L4 is present in the oil, it rapidly migrates to and saturates the oil-water interface, in turn greatly inhibiting the adsorption of the Taq Pol enzyme from the water droplet to the same interface. In comparison, ABIL EM90 competes with the Taq Pol for the interface, and considerable enzyme is thus lost due to interfacial adsorption. These differences predict the performance of the surfactants in PCR experiments with picoliter droplets. Efficient DNA amplification is achieved in droplets coated with Brij L4 using standard concentrations of Taq Pol (as little as 1X or 2X Taq Pol relative to its standard concentration for bulk PCR). In contrast, 8X Taq Pol is needed to reach the cycle threshold in the case of ABIL EM90, and the threshold cycle number was significantly higher than that of Brij L4 with 2X Taq (16 vs. 7). Furthermore, stable Brij L4 emulsions akin to digital PCR methods were demonstrated and amplified 3 orders of magnitude more DNA than ABIL EM90 emulsions using standard concentrations of Taq Pol. Given that the cost of polymerase is ~$10^6$ times that of Brij L4, a reduction in Taq Pol by a factor of 4 or more corresponds to at least an 80% reduction in material costs.

# Chapter 5 DROPLET MICROFLUIDICS WITHOUT AN OIL CONTINOUS PHASE

The text and figures presented here have been adapted from a manuscript in preparation.

## 5.1 Introduction

In the previous chapter, surfactants were necessary to block proteins from adsorbing at oil-water interfaces and prevent droplets from coalescing to perform droplet PCR. Could the oil interface be removed? Would it be possible to conduct droplet PCR in an air continuous phase? In this chapter, first the benefits and challenges associated with replacing the oil phase with an air phase are examined. Then current techniques compatible with air continuous phases are reviewed. Lastly, solutions to generating and immobilizing droplets on-chip are presented.

There are several benefits to removing the oil phase when conducting droplet PCR. An immediate and obvious benefit is that there are less material and storage costs. From a practical standpoint, oils tend to coat everything, rendering them greasy and slippery. Besides oils, surfactants would no longer be needed. Water under low surface tension from the addition of surfactants would wet solid surfaces instead of forming droplets on them (surface tension of water in air is similar to the interfacial tension of water in oil, $\approx 0.05$ and 0.07 N/m respectively). Surfactants would also not prevent droplet coalescence in an air phase. Instead, droplets would have to be physically separated when using air as the continuous phase.

Furthermore, surfactants are not necessary to prevent protein adsorption at air-water interfaces. At oil-water interfaces, proteins denature in contact with oil, causing irreversible adsorption. At air-water interfaces, proteins reversibly adsorb thereby increasing the duration of time an enzyme could be functional in solution. For example ovalbumin at a concentration of 1% w/w decreases the surface tension of a droplet after being in contact with heptane for 10 s. However in contact with air, the surface tension does not decrease until after 15 minutes (Beverung, Radke, and Blanch 1999). Protein adsorption dynamics on hydrophobic solid surfaces is complex, but depends on surface roughness and contact time. Hydrophobic walls with nanoscale roughness also adsorb little due to so called Cassie-Baxter wetting (Figure 5.1) where liquid sits atop gas bubbles between the rough solid nanoscale structures and the effective contact area with the solid surface is decreased (Koc et al. 2008). Therefore channel walls must be rougher when using air as the continuous phase than with oil to prevent protein adsorption.

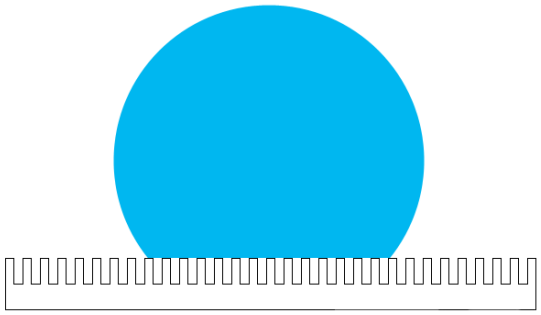

**Figure 5.1 Cassie-Baxter wetting.** In the Cassie-Baxter wetting model for rough hydrophobic surfaces, droplets sit atop gas pockets between the small scale structures. If the structures are small enough, protein adsorption to the hydrophobic surface is minimized because the effective solid-liquid area of contact is reduced.

Another benefit to using an air continuous phase rather than an oil continuous phase is that air, is much less viscous than oils (dynamic viscosity of air, $\mu$, $\approx 2\text{x}10^{-5}$ Pa·s vs $\mu$ of light mineral oil $\approx 0.01$ Pa·s). Therefore faster flowrates can be achieved with air than with oil in confined microchannels with less backpressure. Also, due to the length scale of microchannels, fluids flow at low Reynolds number which is defined as

$$\text{Re} = \frac{\rho \text{UL}}{\mu} \tag{5.1}$$

where $\rho$ is the fluid density, $U$ is the fluid velocity, $L$ is the hydraulic diameter of the channel and $\mu$ is as stated earlier, the fluid dynamic viscosity. For liquids the dynamics are characterized as Stokes or creeping flow (Re << 1), which deters mixing of reagents. However, faster gaseous flows have Re = 10-100. Although the flow is still laminar, it can facilitate mixing (Carroll and Hidrovo 2013a). Thus mixing of droplets surrounded by an air continuous phase is much easier than surrounded by an oil continuous phase.

Surfactant and oil free droplet microfluidics are an interesting concept. However, traditional multiphase disperse microfluidic flows use water in oil instead of water in air for good reasons. For one, water in air droplets are limited to very hydrophobic substrates. The contact angle between the gas-liquid-solid interfaces must greater than 90° to be characterized as a hydrophobic surface. Nanostructured surfaces with contact angles greater than 150° employ the lotus effect and are termed superhydrophobic. The lotus effect refers to the excellent water repellence and superhydrophobicity of the nanostructured leaves of lotus flowers. This superhydrophobicity is due to Cassie-Baxter wetting as

previously mentioned. If the surface is not hydrophobic enough, droplets will adhere and break apart into satellite droplets when traveling across it. This is important to prevent because of cross contamination with subsequent droplets flowing down the channel. A hydrophobic surface ensures the surface tension of the droplet will hold it together as it travels along the surface. Even when oil is used as a continuous phase, the channel walls must be hydrophobic to prevent droplets from adhering to the walls (Teh et al. 2008). Additionally, oil acts as a lubrication layer between the droplet and channel wall (Kuo et al. 2003). There is no lubrication layer with air as the continuous phase because it is not viscous enough. Therefore the walls must be even more hydrophobic than with oil to prevent droplets from adhering to the surface.

Another major concern of removing the oil continuous phase is the evaporation of droplets. As the size of a droplet decreases, the faster it will evaporate as compared to bulk solutions. This size effect is described by the Kelvin equation (Equation 5.2) where $p$ is the actual vapor pressure of the droplet,

$$ln\left(\frac{p}{p_0}\right) = \frac{2\sigma V_m}{rRT} \tag{5.2}$$

$p_0$ is the saturated vapor pressure of the bulk liquid, $\sigma$ is the surface tension, $V_m$ is the molar volume, $r$ is the droplet radius, $R$ is the gas constant, and $T$ is temperature. According to Equation 5.2, small water droplets evaporate quickly due to the high convex curvature of the surface. The effect of droplet size on vapor pressure for water is shown in Figure 5.2 Surrounding the droplet with oil seals the water in, preventing evaporation. A different method of sealing the water droplet will be necessary to perform droplet PCR with an air continuous phase.

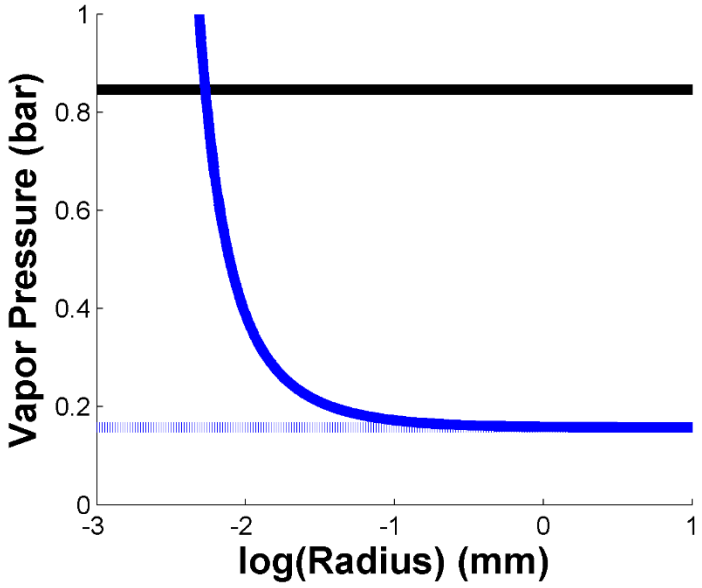


**Figure 5.2 Droplet evaporation.** The vapor pressure of bulk water at 55 and 95 °C is indicated by the *dashed blue line* and *solid black line* respectively. The *solid blue curve* shows the increase in vapor pressure of water at 55 °C as a function of droplet size according to Equation 5.2.

A lesser but very practical concern is the delivery of air into the chip. Normally a constant displacement pump, for example a syringe or peristaltic pump, is used in microfluidic systems. However they do not generate flows at constant pressure. This is acceptable with liquids where pressure variations are attenuated by the viscosity of the liquids. In gaseous flows though, the pressure waves are propagated throughout the continuous phase and results in poor control of droplets (Carroll and Hidrovo 2013b). Instead of pumps, a low pressure air source must be regulated to generate droplets on-chip.

Therefore custom control systems consisting of valves and high precision air regulators must be built to deliver air into the microchannel.

Droplets generated on-chip must also be able to be manipulated. At the very least for PCR, droplets need to be held stationary to be imaged for fluorescent measurements. Hydrodynamic capture of water droplets in oil has been demonstrated, but trapping of water droplets in air has never been investigated (Bithi and Vanapalli 2010). Droplets are captured in on-chip traps based on hydrodynamic resistances. Specifically, the hydrodynamic resistance of the upper fluid path which bypasses the trap, $R_U$, relative to the resistance of the lower fluid path which goes through the trap, $R_L$. Hydrodynamic resistances are defined by the geometry of the channels and traps. Traps are designed such that the exit of the trap is much narrower than the entrance. Thus to exit a trap, the captured droplet must overcome a large interfacial force to squeeze through the exit. Droplets follow the path of least resistance, therefore if $R_U/R_L < 1$, then the droplet bypasses the trap. If the opposite is true, and $R_U/R_L > 1$, then droplets are held in the trap. In order to perform droplet PCR without oil, a trapping system needs to be adapted to be compatible with continuous air flows.

Despite the limitations of continuous gas phase microfluidics, some preliminary progress has been made in the nascent field of confined water droplets with gas continuous phases. Mainly on droplet generation technique and mechanisms. Numerical simulations of droplet detachment at a T-junction were first performed to investigate water dynamics in fuel cells (Zhu, Sui, and Djilali 2007). It was found that droplet formation is incredibly sensitive to the hydrophobicity of the channel walls. Additionally fast air inlet velocities sheared droplets emerging from the T-junction along the adjacent channel wall. This was

later experimentally confirmed in PDMS devices (Carroll and Hidrovo 2013b). Furthermore, Carroll and Hidrovo determined that in slow continuous gas flows, Re < 100, large droplets (diameter > channel width) were formed. These droplets detached from the T-junction due to hydrostatic forces (the pressure drop across the droplet). In faster gas flows, Re > 100, smaller droplets (diameter < channel width) formed and detached due to inertial forces. Viscous shear forces were not enough to overcome surface tension forces pinning the droplet to the T-junction.

Recently in our lab and in collaboration with the Maryland MEMS & Microfluidic Laboratory (DeVoe research group), a simple co-flow device was used to generate droplets in hydrophobically modified quartz capillaries (K. Jiang et al. 2015). The results from our collaboration matched with Carroll and Hidrovo. As the gas flow rate increased, droplets became smaller and the droplet detachment mechanism were due to hydrodynamic pressure and inertial forces. It is also important to note our collaboration found droplets broke apart at low gas flow rates because of contact with the capillary side walls. Smaller droplets remained intact and were monodisperse in high gas flow rates.

Far more research has been conducted on droplet microfluidics not confined within a channel but on an open plane. One popular method utilizes a phenomenon known as electrowetting, where the interfacial tension or contact angle between polarizable droplets and segments of the plane are controlled by an applied voltage. The electric potential (DC or low frequency AC) is applied from a counter electrode, across a hydrophobic insulating layer, across the droplet, and to a ground electrode above. The applied voltage lowers the effective surface tension between the solid and liquid according to Equation 5.3 (Lippmann 1875) where

$$\gamma_{ws} = \gamma_{ws}^{0} - \frac{CV^2}{2} \quad (5.3)$$

$\gamma_{ws}$ is the total surface tension between the solid and liquid, $\gamma_{ws}^{0}$is the surface tension between the solid and liquid without the presence of an electric field, $C$ is the capacitance of the interface, $V$ and is the applied voltage. Essentially, the droplet wets the hydrophobic surface when it is polarized by the energy held in the droplet-insulator-electrode capacitor system. Cheap electrowetting systems can be made with printed circuit boards coated with thin layers of Teflon or parylene as the hydrophobic insulating layer (Sista et al. 2008). Electrowetting has been used to aliquot, transport, merge, split, and mix droplets surrounded by air (Moon et al. 2006). However to perform PCR with electrowetting, the droplets must surrounded in oil (Chang et al. 2006). Illumina (which acquired Advance Liquid Logic) has recently commercialized an oil filled chip/cartridge capable of droplet PCR to prepare DNA libraries for next generation sequencing technologies using electrowetting.

Surface acoustic waves microfluidics is another technique capable of droplet microfluidics without oil that has been recently started to attract attention. The technology utilizes interdigital transducers (a common electronic device component, for example found in all smart phones), fabricated on a hydrophobic piezoelectric substrate, which vibrate in response to an electrical signal. The interdigital transducers mechanically stresses the surface of the substrate which exhibit surface waves with displacement amplitudes on the order of 1 nm. Travelling surface waves propagate outward in all directions within the substrate surface plane and exert an acoustic force upon contact of droplets. Waves with small amplitudes induce streaming within droplets. Waves with large

amplitudes translate droplets in the direction of propagation. Acoustic forces can be controlled by the geometry of the interdigital transducers and the electric signal frequency (Bourquin and Cooper 2013). Droplet aliquoting, transport, merging, and mixing in air have all been demonstrated with surface acoustic wave microfluidics (Ding et al. 2013). However, oil is still necessary to prevent droplet evaporation during PCR thermal cycling (Guttenberg et al. 2005).

Although electrowetting and surface acoustic wave techniques are very capable of generating and manipulating droplets in an open air continuous phase, the droplets will always need to be sealed in oil during PCR to prevent evaporation. Instead in a confined microchannel it may be possible to seal in droplets with an impermeable solid surface. For example, captured droplets in hydrodynamic traps are already partially sealed by a solid surface. Could a liquid seal off the entrance and exits of the trap and potentially prevent evaporation during thermal cycling? We made significant advancements to answer that question, in order to demonstrate droplet PCR without oil or surfactants. First, our lab's co-flow droplet generator was adapted to function within a microfluidic channel. Droplets were formed with minimal breakup in hydrophobic and superhydrophobic channels at low gas flowrates. Then hydrodynamics traps were designed to capture droplets on-chip by two different modes. Finally, captured droplets were heated to verify if thermal cycling without evaporation was possible.

## 5.2 Materials and methods

### 5.2.1 Hydrodynamic trap design

Microfluidic chips were designed to directly or indirectly hydraulically trap droplets. The height of all the channels was 300 μm and the inlet of the chip was 500 μm wide to allow droplets generators to be easily inserted in. The channels were intentionally planned without concave corners and sharp curves which could break up droplets. The hydraulic traps consisted of a lower channel to trap droplets and an upper channel to bypass trapped droplets (Figure 5.3). The lower channel was comprised of various channel widths and geometries. The upper channel was comprised of rectangular channels at a constant width of 200 μm. Different hydraulic resistance ratios of the upper channel to the lower channel was achieved by varying the length of the upper channel and keeping the width of the lower channel set to 85 μm.

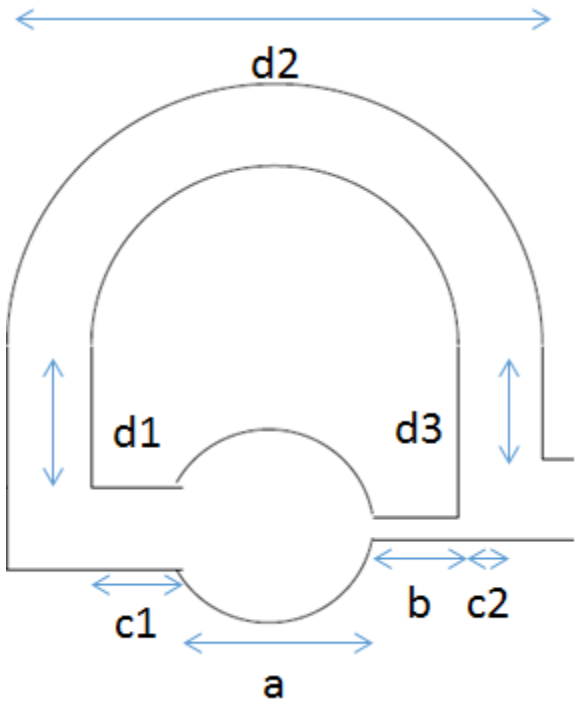


**Figure 5.3 Geometry of hydraulic traps.** The upper channel that bypasses the trap consists of channel segments d1, d2, and d3. The lower channel that goes through the trap consists of channel segments c1, a, b, and c2

.

To aide in the design of the traps, the hydraulic resistances, $R_n$, for different sections of the upper and lower path were first estimated using analytically derived equations. The following hydraulic resistance equations were derived under the assumption that the flow is incompressible, Newtonian, laminar, and fully developed (i.e. Poiseuille flow). The assumptions that the air flow is laminar and Newtonian are valid. However, air is compressible and may not be fully developed in the microchannel. To approximate the hydraulic resistance of (i) the upper channel sections (sections d1, d2, and d3), (ii) the trap

(section c1 and a), and (iii) the trap exit (section b and c2), the exact analytical solution for flow in a straight rectangular channel was used (Equation 5.4)

$$R_n = \frac{12\mu L}{hw}\left[1 - \sum_{n.odd}^{\infty} \frac{1}{n^5} \times \frac{192}{\pi^5} \times \frac{h}{w} \tanh\left(\frac{n\pi w}{2h}\right)\right]^{-1} \quad (5.4)$$

where $\mu$ is, as previously defined, the dynamic viscosity of air, $L$ is the length of the channel section, and $h$ and $w$ are the height and width of the channel ($w > h$) (Bithi and Vanapalli 2010). To estimate the hydraulic resistance of the square portions of the lower channel (sections c1 and c2), the approximate solution for flow in a square channel was used (Equation 5.5) where $h$ was set to 300 μm (Hsu et al. 2012). The total resistance of the upper and lower channels were just the sum of the resistances of the channel segments.

$$R_n = 28.47\frac{\mu L}{h^4} \quad (5.5)$$

Computational fluid dynamic simulations were performed using COMSOL 4.1, a finite element analysis solver, to obtain more accurate estimates of the hydraulic resistances. The channel geometry was finely meshed with tetrahedral cells calibrated for fluid dynamics. Laminar flow physics were implemented using air fluid properties from the software's library. The steady state flow was solved (default solver settings, generalized minimal residual method) with the inlet air velocity set to 1 m/s, the outlet set to 1 atm and no slip boundary conditions on the channel walls. The hydraulic resistances were calculated from the simulations using Equation 5.6

$$\Delta P_n = Q_n R_n \quad (5.6)$$

where $\Delta P_n$ is the pressure drop across the channel, and $Q_n$ is the average volumetric flowrate through the channel.

### 5.2.2 Chip fabrication

Master molds were fabricated on silicon wafers using SU-8 2075 (Microchem). The wafers were first cleaned in a piranha bath, rinsed, and then dehydrated at 120 °C for 10 minutes. A two-step spin coating process was used to achieve a 300 µm thickness. To apply the first coat, photoresist was spin coated to a thickness of 225 µm and then soft baked at 100 °C. The wafer was allowed to cool to room temperature and then a second layer of photoresist was spin coated to a thickness of 75 µm. The second layer was soft baked at 100 °C for 20 minutes. After the coating process, the wafer was rehydrated for 1 hr. at ambient temperature and humidity. Uncured SU-8 was removed with SU-8 developer by gentle agitation for 18 minutes. Lastly, the wafer was rinsed with IPA and DI water, and then baked overnight at 80 °C.

PDMS (Sylgard 184) chips were fabricated with the base and curing agent mixed in a 10:1 ratio. Top pieces, 5 mm in thickness, were cured on the SU-8 master mold for 10 minutes in an oven at 80 °C. Bottom pieces, 1 mm in thickness, were partially cured on a clean silicon wafer using a hotplate. The hotplate was initially at room temperature and then set to 90 °C after placing the wafer. While the PDMS was slightly tacky and not fully cured, after about 20 minutes, the top pieces were bonded to the bottom pieces and cured an additional 10 minutes.

### 5.2.3 Channel wall modifications

Sidewalls of the channels could be modified to be superhydrophobic, vapor resistant, or both. Superhydrophobic walls were created through the lotus effect and roughening the sidewalls with a PDMS etchant (3:1 N-Methyl-2-pyrrolidone (NMP) : Tetrabutylammonium fluoride (TBAF)) (Sigma). Channels in bonded chips were filled

with the etchant and then incubated for 2 minutes. The etchant was removed by flowing 1 mL of DI water through the chip.

Vapor resistant channels were made by coating assembled chips with 4 g of parylene C (Specialty Coating Systems) through a chemical vapor deposition process with a SCS Labcoter. Parylene was vaporized at 175 °C, pyrolyzed at 690 °C, and deposited at room temperature under medium vacuum for about 30 minutes. Channels could be made both superhydrophobic and vapor resistant by first etching the sidewalls and then coating them in parylene.

### 5.2.4 Continuous droplet generators

Continuous droplet generators were made by attaching capillary tubing to T-junction valves with 5 minute epoxy. First, the inner capillary (i.d. = 75 µm, o.d. = 100 µm) was inserted into the inlet of the T-junction straight through to the outlet. Then a seal around the inner capillary and within the inlet of the T-junction was made with epoxy so that fluid could only flow through the capillary when attached to a syringe. Next, outer tubing (300 µm i.d.) was threaded onto the unsealed end of the inner capillary. The outer tubing was held in place with an epoxy seal between the outer tubing and T-junction outlet. The inner capillary was trimmed so that it extended about 1 mm past the outer capillary. The droplet generator was inserted into PDMS devices parallel with the microchannels through 500 x 300 µm inlet. The continuous air phase, < 0.05 bar, was humidified before it was directed into the perpendicular inlet of the T-junction and out through the outer tubing. The droplet aqueous phase consisted of 0.2 µm filtered DI water. It was injected into the inner capillary at a rate of 10 µL/minute with a syringe pump (Harvard Apparatus).

### 5.2.5 Single droplet generation

Single droplet generators (Figure 5.4) were very similar to the continuous droplet generators. The end of an inner capillary (i.d. = 75 µm, o.d. = 200 µm) was attached to the outlet of a 10 µL pipette tip and inserted through the inlet of the T-junction straight to the outlet. Again, a seal around the inner capillary and within the inlet of the T-junction was made with epoxy. Also, outer tubing (300 µm i.d.) was threaded onto the inner capillary and an epoxy seal in between the outer tubing and T-junction outlet held it place. Aqueous solutions were drawn into the inner capillary and pipette tip using negative pressure with a 10 µL pipette. On demand low air pressure, < 0.05 bar and controlled with a solenoid valve, pneumatically pulsed aqueous solutions for 70 ms through the inner capillary.

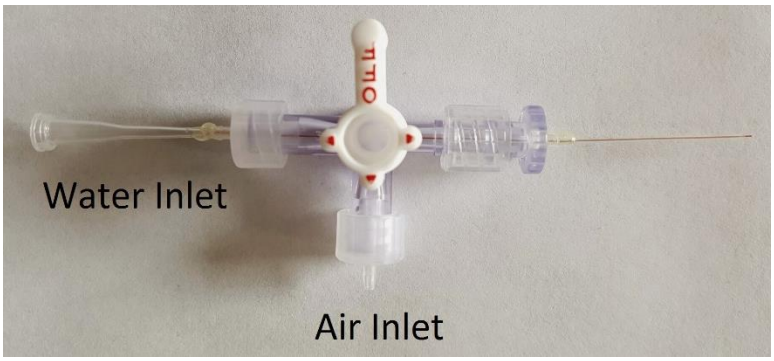


**Figure 5.4 Single droplet generator.** Water is drawn from the 75 µm i.d. capillary tip into the pipette tip with a pipette. The T-junction valve is filled with air at a low pressure which flows out the outer capillary, sheathing the inner capillary. The pipette tip is pulsed with low pressure to form a droplet at the capillary tip. Continuous flow droplet generators were similar. Instead of a pipette tip, a syringe was connected directly to the water inlet.

### 5.2.6 Droplet Heating

Continuously generated droplets were first captured in etched and parylene coated small indirect traps. Then DI water was pumped through the channels at a rate of 2 µL/min with a 25 G syringe inserted into the 300 x 300 µm chip exit. Once the channels were filled, the inlet and outlet of the chip were sealed with silicon vacuum grease. Then the chip was heated on top of a 1 x 3 in. polyimide resistive heater (Omega) with a 20 V power source. The set point temperature of the heater was measured with a calibrated infrared sensor and maintained with a tuned PID controller. The chip was equilibrated for 10 minutes at a set temperature and then quickly imaged on an optical microscope.

## 5.3 Results and Discussions

### 5.3.1 Hydrodynamic trap designs

Three different traps, (i) small indirect, (ii) large indirect, and (iii) direct traps were designed based on the estimates of the hydraulic resistances from analytically derived equations. The trap dimensions and geometry, are shown in Tables 5.1 and 5.2 and Figure 5.4. The first trap, the (i) small indirect trap, consisted of a wide upper channel which was calculated to have a small $R_U$ as compared to $R_L$ ($R_U/R_L$ = 0.44). The (ii) large indirect trap was an iteration of the (i) small indirect trap. The trap entrance and exit in the lower channel were elongated to further isolate captured droplets from other droplets flowing around it. Increasing the length of the narrow trap exit dramatically increased the resistance of the lower channel. Although the upper channel was also modified to be narrower and longer to also increase the hydraulic resistance, the $R_U/R_L$ = 0.58. The (iii) direct trap was

very similar to the (ii) indirect trap. The only difference was that the upper channel was elongated so that $R_U/R_L$ was just larger than 1. The reported hydraulic resistance ratios were calculated from computational fluid dynamics simulations. The analytical estimates were only used as a rough guide to help design the traps.

| Upper Section (length x width μm) | | | |
|---|---|---|---|
| **Trap** | **d1** | **d2** | **d3** |
| **small indirect** | — | 877 x 300 | — |
| **large indirect** | 500 x 200 | 2396 x 200 | 458 x 200 |
| **direct** | 1000 x 200 | 2396 x 200 | 958 x 200 |

**Table 5.1** Trap Dimensions of the upper channel in μm.

| Lower Section (length x width μm) | | | | |
|---|---|---|---|---|
| **Trap** | **c1** | **a** | **b** | **c2** |
| **small indirect** | 300 x 300 | 675 x 675 | 150 x 85 | 300 x 300 |
| **large indirect** | 450 x 300 | 675 x 675 | 300 x 85 | 300 x 300 |
| **direct** | 450 x 300 | 675 x 675 | 300 x 85 | 300 x 300 |

**Table 5.2** Trap Dimensions of the lower channel in μm.

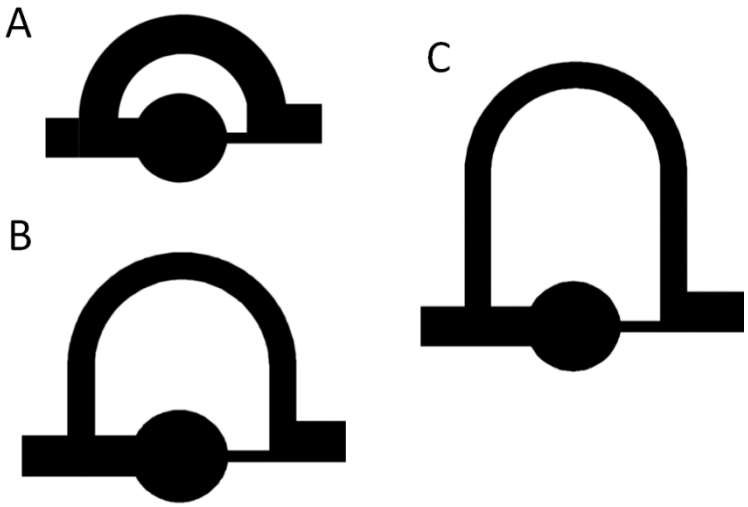


**Figure 5.5 Trap design geometries.** (A) small indirect (B) large indirect (C) direct designs.

PDMS microfluidic devices were made with the traps arranged as in Figure 5.6. The traps were serially connected in rows of three. It is also important to note the traps are connected in a step like fashion. The trap exit channel is extended into the trap connecting channel so that a concave corner is not formed. Concave corners were very prone to breaking apart droplets in preliminary trap designs. The rows were connected by a U-turn rather than three straight microchannels for the same reason. Devices with up to three rows of traps were tested.

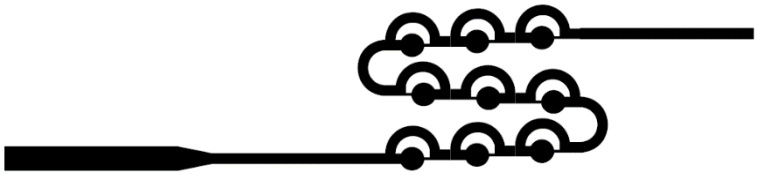

**Figure 5.6 Trap arrangements.** Typical arrangement of traps in whole chip. A 500 μm wide inlet that tapers down to 300 μm wide enables the co-flow device to be inserted into the microfluidic chip, parallel with the channels. U-turn channels connect rows of traps.

### 5.3.2 Indirect hydrodynamic trapping

We first demonstrated indirect hydraulic trapping of droplets in unmodified PDMS devices using the small indirect trap design and continuous droplet generator (Video can be download at http://ter.ps/krpV2). Droplets were continuously formed at the tip of the inner capillary and then traveled down the channel in a non-continuous motion. Newly formed droplets filled the microchannel and then detached from the capillary tip due to the increase of air pressure behind the droplets. Then they propelled down the channel a finite distance, because the air flow rate was quickly diminished by a forming droplet. Droplets briefly resumed motion again upon the detachment of a newly formed droplet. Droplets temporarily immobilized in the upper channel increased the hydraulic resistance of that channel relative to the lower channel. Subsequently, lagging droplets filled the lower channel trap until the exit was blocked. This increased the hydraulic resistance of lower channel relative to the upper channel. The leading droplet then continued through the upper channel. Also, subsequent lagging droplets bypassed the filled lower channel.

### 5.3.3 Superhydrophobic channels

Since PDMS is regarded as a very hydrophobic material (contact angle = 115°), droplets traveled smoothly across the unmodified hydrophobic walls without breaking apart. However small satellite droplets were formed at the entrance of the traps in a systematic fashion. The systematic satellite droplets were avoided by increasing the hydrophobicity of the channel walls. Superhydrophobic walls were achieved by mimicking the lotus effect and isotropically roughening the PDMS surface. This was illustrated by first coating channels in parylene, which has been used to create a moisture impermeable barrier in PDMS channels to prevent evaporation during PCR, however it is less hydrophobic than PDMS (contact angle = 92°). The difference in surface energy is clearly seen when generating and trapping droplets PDMS chips coated with parylene (Figure 2). Droplets were broken apart and satellite droplets were observed throughout the channels. The surface energy of parylene coated PDMS channels was lowered by roughening the sidewalls with a PDMS etchant prior to parylene deposition. The rough sidewalls were superhydrophobic due to the lotus effect. Droplets traveled smoothly along the roughened sidewalls without breaking apart (Video can be downloaded at http://ter.ps/krpv3).

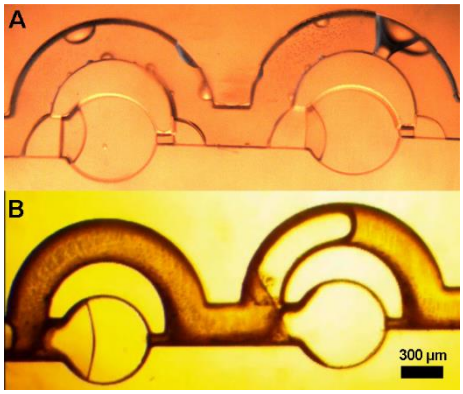


**Figure 5.7 Super hydrophobic PDMS.** (A) Parylene coated PDMS channels cause droplets to break apart. (B) Etched and parylene coated superhydrophobic channels allow droplets to travel smoothly along the roughened sidewalls. PDMS could be superhydrophobically modified by isotropically etching the walls with a 3:1 solution of NMP : TBAF for 2 minutes. The roughened channel walls mimic the lotus effect through Cassie-Baxter wetting.

The small indirect traps were capable of capturing droplets on-chip, but indirect hydraulic trapping is only effective for droplets of the same composition where a larger volume of liquid can be split into many droplets continuously. However, some applications require only a few or one droplet of a certain composition to be dispensed. For example, calibration standards could be incredibly difficult to aliquot into the traps with this mode of trapping. If the standards are aliquoted from different bulk solutions they could not be generated continuously. Indirect trapping is therefore difficult because the unsynchronized droplets need to be spatially and temporally coordinated to modify the $R_U/R_L$. Direct hydraulic trapping is more robust because droplet coordination is not required for trapping. Furthermore, the sequence of trapped droplets can be controlled. The first droplet is captured in the first trap, the next in the second trap, and so on.

### 5.3.4 Direct hydrodynamic trapping

We demonstrated direct hydraulic trapping of droplets with unmodified PDMS chips using the direct trap design. To ensure captured droplets were directly trapped, the continuous droplet generator was modified and optimized to generate a single droplet on-chip. Still frames of direct capture are shown in Figure 5.8. In the first frame an empty trap is observed. Next, the trap is quickly filled the fluorescent droplet. Since only one droplet was generated, the upper channel was empty and the observed droplet was directly captured. Subsequent droplet bypass the filled trap (Video can be downloaded at http://ter.ps/krpV1).

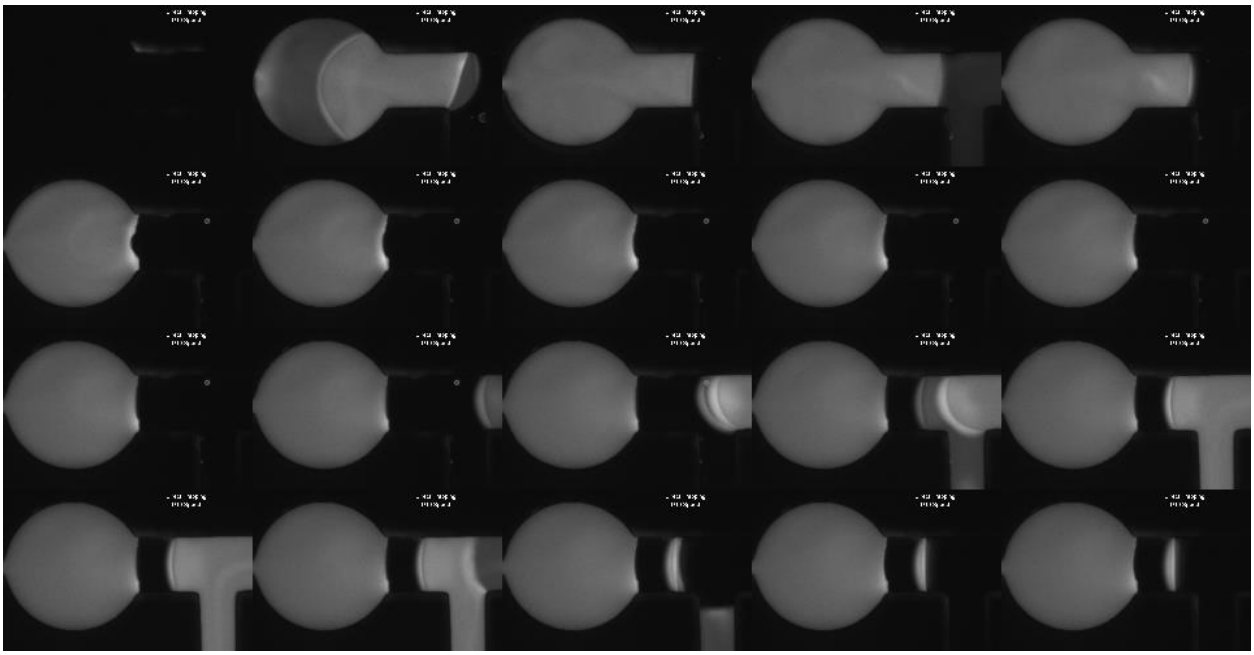

**Figure 5.8 Direct trapping.** Montage of http://ter.ps/krpV1, progress in time from left to right. Droplets were trapped using the direct design with the single droplet generator. Initially the trap was empty. The first droplet observed quickly filled the trap. The droplet

was directly captured, since only a single droplet was generated and the upper channels were empty.

### 5.3.5 Droplet Evaporation

Captured droplets were sealed in on-chip by backfilling the channels that connect and bypass traps with DI water. Sealed droplets only contacted the trap solid surface and pockets of air at the entrance and exit of the trap as shown in Figure 5.9 at T = 25 °C. Heating the chip to 35 °C expanded the pockets of air. Further heating the chip up to 55 °C evaporated the water in the channels connecting and bypassing traps. At 65 °C the water seal around the droplets was broken. Increasing the temperature above 65 °C evaporated trapped droplets and water in channels.

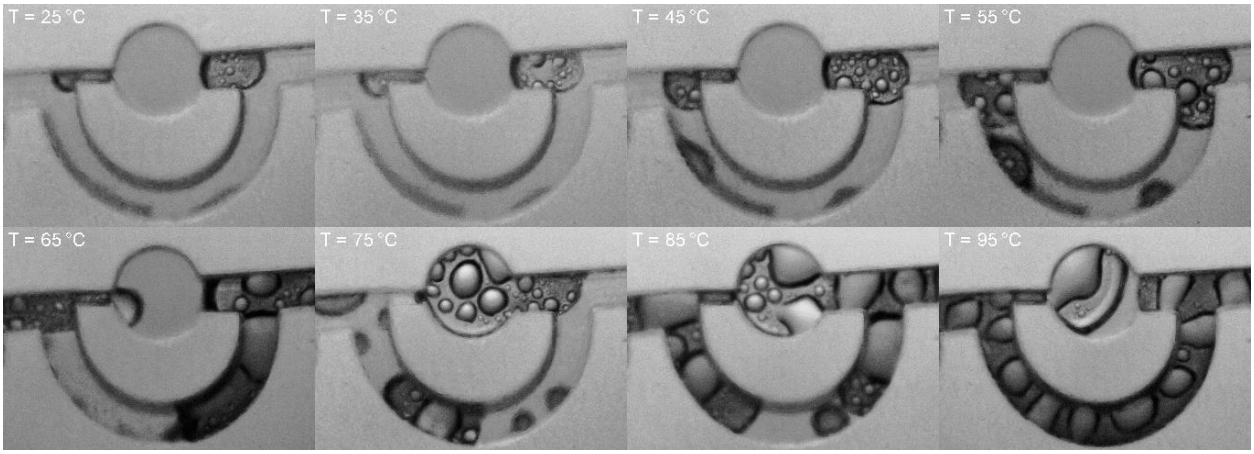


**Figure 5.9 Heating of sealed droplet.** A trapped and sealed droplet was heated at increasing temperatures. After equilibrating on the heater for 10 minutes, the droplet was quickly imaged on a microscope. Droplets were sealed in on-chip by filling the channels around the drop with DI water as seen at T = 25 °C. Initial heating to 25 °C expanded air bubbles at the entrance and exit of the traps. Further heating to 55 °C partially evaporated water in the channels surrounding the trapped droplet. The seal around the droplet was broken when heated to 65 °C. Raising the temperature further evaporated the trapped droplet.

Assembled and etched chips were coated in parylene C to prevent water vapor from escaping the PDMS device. Although the exterior of the device was coated effectively, the coating of the channels walls was limited to diffusion of parylene into the microfluidic channels. Therefore, the channel walls at a short distance away from the entrance or exit of the chips were coated in thicker films of parylene than channel walls in the center of the chip. For a sufficient vapor barrier, at least a 1 µm parylene film is necessary (Flueckiger et al. 2011). The amount of parylene used to coat the device would result in about a 1 µm film on the exterior of the device, but it is highly likely that the film was thinner throughout the interior channel walls. Therefore, water vapor could easily escape into the PDMS substrate. Furthermore, cracks in the exterior coating from handling the device could allow vapor to escape the device altogether. More parylene could be used to achieve a thicker

film. However, the surface roughness of channel walls may be lost in thicker parylene films, decreasing their hydrophobicity.

Since the droplets only evaporated after the seal around it was broken, we feel it may be possible to thermal cycle trapped droplets in an impermeable substrate. For example, cyclic olefin copolymer (COC) would be a more ideal substrate because it 160 times less permeable to water vapor than PDMS. COC could maintain the liquid seal around the droplet and prevent evaporation at high temperatures. However, satellite droplet formation could be a concern because COC is not as hydrophobic as PDMS or parylene (contact angle = 88°). The hydrophobicity could be enhanced by the lotus effect. For example, using high nitric acid wet etched silicon molds to impart roughened channels on molded COC.

## 5.4 Conclusion

We adapted a co-flow device, previously used to generate droplets in capillaries with an air continuous phase, for use in PDMS microfluidic chips. The chips consisted of hydrodynamic traps which were designed to directly or indirectly capture droplets based on the ratio of the hydraulic resistance of the channel bypassing the trap to the hydraulic resistance of the channel through the trap ($R_U/R_L$). Indirect droplet captured was demonstrated with continuous droplet generation in traps designed with $R_U/R_L < 1$. Direct droplet captured was demonstrated with single droplet generation in traps designed with $R_U/R_L > 1$. However, satellite droplets systematically formed at the entrances to traps in unmodified PDMS channels. Channel walls were easily modified to be superhydrophobic with isotropic micro-scale features using a PDMS etchant. Upon surface roughening, the formation of satellite droplets was eliminated, even after coating the channels with parylene C to lower the vapor permeability of the PDMS chips. Captured droplets were sealed in by the solid surface of the trap and pockets of humidified air by carefully filling the main channels surrounding the trap with water. Unfortunately, the seal was broken upon heating

when water in the main channels evaporated. Subsequently, the trapped droplets quickly evaporated. A more moisture impermeable chip substrate such as cyclic olefin copolymer may prevent sealed droplets from evaporating upon heating.

# Chapter 6 CONCLUSIONS

## 6.1 Summary of findings and contributions to the field

In this dissertation several new innovations for PCR lab-on-chip devices were discussed, (i) whole chitosan particles to extract DNA, (ii) characterization of the adsorption of Taq Pol to oil-water interfaces, (iii) and on-chip generation and immobilization of aqueous droplets with an air continuous phase.

In Chapter 3, whole magnetic chitosan particles were fabricated by an emulsion methodology. These particles interacted with DNA in a manner contradicting all known reports of charge switching DNA extraction schemes. Previously, at least two buffers were necessary to adsorb DNA and then elute DNA where the adsorption buffer was inhibitory to PCR. Multiple buffer protocols require complex integrated valves in lab-on-chip devices to direct control buffer washes, waste, and eluent. In our work, DNA was permanently adsorbed onto beads using a single buffer optimal for PCR. Although DNA was not eluted into solution, PCR products were directly and quantifiably amplified off the particles. For the first time, a DNA extraction scheme was performed with a single buffer. This innovation could lead to incredibly simplified lab-on-chip devices with minimal valves, less buffers, and elimination of an elution step. The invention of these beads could also lead to combined cell lysis and DNA extraction, further simplifying sample preparation. The permanent capture nature of the beads could also enable higher resolution melt curves of PCR products and informed multi-round PCR on the exact same sample.

In Chapter 4, the adsorption of Taq Pol was observed by measuring the change in interfacial tension over time with the pendant drop method. Previously, amplification efficiency of PCR in droplets was used to estimate the adsorption of Taq Pol with different surfactants. For the first time, a method to predict the ability of surfactants to prevent Taq Pol adsorption without PCR was demonstrated. Our results indicate that superior surfactants saturate the oil-water interface faster, which can be measured easily via the pendant drop method. For the first time, Brij L4 was identified as an ideal surfactant to conduct droplet PCR in mineral oil. Furthermore, the equilibrium surface pressures of droplets with increasing concentrations of Taq Pol and constant surfactant concentration in the surrounding oil phase, can be used to predict the amount of extra Taq Pol necessary to successfully amplify PCR products. Using Brij L4, an order of magnitude less Taq Pol was required to amplify DNA than using ABIL EM90, the most popular surfactant in the literature. Our work was the first to demonstrate droplet PCR in mineral oil with 1X Taq Pol. Also, previous calculations of Taq Pol adsorption to droplet oil-water interfaces were based on the assumption that the rate limiting step was diffusion to the oil-water interface. For the first time we showed that adsorption was not diffusion limited but kinetic adsorption limited where the rate limiting step was penetration into a film (either protein or protein and surfactant) at the oil-water interface under high surface pressure.

In Chapter 5, droplets were formed in confined microfluidic channels using a simple co-flow device with air as the continuous phase instead of oil for the first time. The vast majority of droplet microfluidics are performed with oil as the continuous phase. The only widespread techniques with air as a continuous phase suitable for PCR, are droplets manipulated on open planar surfaces using electrowetting or surface acoustic waves.

However, even those systems require oil to thermal cycle droplets to prevent evaporation. We attempted to thermal cycle droplets by sealing them in hydraulic traps without oil. For the first time droplets were immobilized in hydraulic traps using a gas continuous phase. Two modes of trapping were presented. The first mode was indirect hydraulic trapping compatible with continuous generation of droplets. The second mode was, direct hydraulic trapping compatible with continuous or single droplet generation. Although droplets sealed in parylene coated PDMS traps evaporated upon heating, our designs and technique could enable droplet PCR without oil in a more vapor impermeable substrate such as cyclic olefin copolymer. Satellite droplets were eliminated by modifying PDMS channels to be superhydrophobic, even after coating the walls with parylene. Previously, TBAF in NMP was used to fabricate PDMS channels or etch sacrificial layers of PDMS. For the time first time, we used this etchant to isotopically roughen PDMS channels with microscale features. This increased the hydrophobicity of the channel walls through the lotus effect.

## 6.2 Future work

### 6.2.1 Chitosan particles

Permanent adsorption of DNA to densely coated chitosan particles has incredibly useful applications to nucleic acid technologies. For example, serial rounds of PCR could be performed on the exact same DNA sample. Then the results of previous rounds of PCR would inform which primer sets to use for the next round. Also, the full functionality of the particles has yet to be explored. RNA chitosan interactions need to be investigated as well as the particle's compatibility in RT-PCR. The extraction efficiency in other complex real world samples should be examined. The actual implementation of the particles into droplet PCR devices will be exciting, especially digital PCR technologies. It will be

interesting to learn if the particles aide in suppressing background DNA, so that fluorescence measurements are only a result of amplification products. Lastly the lysis capabilities of the particles should be tested. Confirmation that the particles can mechanically lyse most cells and extract DNA with a single would cement these particles as the easiest tool to use for nucleic acid sample preparation.

### 6.2.2 Characterizing surfactants for PCR

We showed that surfactant performance for PCR can be predicted by measuring the change interfacial tension of oil and surfactant mixtures in contact with Taq Pol solutions. If the interfacial tension does not change with respect to time, then the surfactant has successfully outcompeted Taq Pol and blocked the interface. Further non-ionic surfactants and oil combinations could be explored. A database of predicted performance of oil and surfactant mixtures would be very welcomed by the droplet PCR community

### 6.2.3 Droplet PCR without oil

Our success with droplet microfluidics without oil is very promising. Although we were not able to perform PCR due to evaporation, our results indicated chips fabricated from a more impermeable material would most likely enable droplet PCR without oils or surfactants. Parylene coated PDMS was very permeable and allowed water vapor to diffuse out across the chip. A vapor impermeable material such as COC would be ideal to partially seal droplets in traps while thermal cycling. Our initial results of completing the partial seal by backfilling the bypass channels with water worked to a degree. The captured droplets did not evaporate out of the chip until the water in the bypass channels evaporated out first and broke the seal. Although COC is not as naturally hydrophobic as PDMS, it can be modified to be superhydrophobic. For example by mimicking the lotus effect using an

isotropically etched mold to imprint a submicron roughened channel wall. It is likely droplet generation and manipulation could be demonstrated in a superhydrophobic COC device with minimal satellite droplet formation. Furthermore, minimal proteins would adsorb at the rough channel walls and very little water would be lost to evaporation.

# BIBLIOGRAPHY


Adamson, Arthur W. 1976. *Physical Chemistry of Surfaces*. 3rd ed. New York: Wiley.

Agirre, Mireia, Jon Zarate, Edilberto Ojeda, Gustavo Puras, Jacques Desbrieres, and Jose Luis Pedraz. 2014. "Low Molecular Weight Chitosan (LMWC)-Based Polyplexes for pDNA Delivery: From Bench to Bedside." *Polymers* 6 (6): 1727–55. doi:10.3390/polym6061727.

Ahmad, Farhan, and Syed A. Hashsham. 2012. "Miniaturized Nucleic Acid Amplification Systems for Rapid and Point-of-Care Diagnostics: A Review." *Analytica Chimica Acta* 733 (July): 1–15. doi:10.1016/j.aca.2012.04.031.

Alameh, Mohamad, Diogo DeJesus, Myriam Jean, Vincent Darras, Marc Thibault, Marc Lavertu, Michael D Buschmann, and Abderrazzak Merzouki. 2012. "Low Molecular Weight Chitosan Nanoparticulate System at Low N:P Ratio for Nontoxic Polynucleotide Delivery." *International Journal of Nanomedicine* 7: 1399–1414. doi:10.2147/IJN.S26571.

Alvarez, Nicolas J., Lynn M. Walker, and Shelley L. Anna. 2009. "A Non-Gradient Based Algorithm for the Determination of Surface Tension from a Pendant Drop: Application to Low Bond Number Drop Shapes." *Journal of Colloid and Interface Science* 333 (2): 557–62. doi:10.1016/j.jcis.2009.01.074.

Angione, Stephanie L, Anuj Chauhan, and Anubhav Tripathi. 2012. "Real-Time Droplet DNA Amplification with a New Tablet Platform." *Analytical Chemistry* 84 (6): 2654–61. doi:10.1021/ac202532a.

Baret, Jean-Christophe. 2012. "Surfactants in Droplet-Based Microfluidics." *Lab Chip* 12 (3): 422–33. Accessed March 23. doi:10.1039/C1LC20582J.

Beer, N. Reginald, Benjamin J. Hindson, Elizabeth K. Wheeler, Sara B. Hall, Klint A. Rose, Ian M. Kennedy, and Bill W. Colston. 2007. "On-Chip, Real-Time, Single-Copy Polymerase Chain Reaction in Picoliter Droplets." *Analytical Chemistry* 79 (22): 8471–75. doi:10.1021/ac701809w.

Beer, N. Reginald, Elizabeth K. Wheeler, Lorenna Lee-Houghton, Nicholas Watkins, Shanavaz Nasarabadi, Nicole Hebert, Patrick Leung, Don W. Arnold, Christopher G. Bailey, and Bill W. Colston. 2008. "On-Chip Single-Copy Real-Time Reverse-Transcription PCR in Isolated Picoliter Droplets." *Analytical Chemistry* 80 (6): 1854–58. doi:10.1021/ac800048k.

Beverung, C.J., C.J. Radke, and H.W. Blanch. 1999. “Protein Adsorption at the Oil/water Interface: Characterization of Adsorption Kinetics by Dynamic Interfacial Tension Measurements.” *Biophysical Chemistry* 81 (1): 59–80. doi:10.1016/S0301-4622(99)00082-4.

Bithi, Swastika S., and Siva A. Vanapalli. 2010. “Behavior of a Train of Droplets in a Fluidic Network with Hydrodynamic Traps.” *Biomicrofluidics* 4 (4): 044110–11 – 044110–10. doi:doi:10.1063/1.3523053.

Boom, R., C. J. Sol, M. M. Salimans, C. L. Jansen, P. M. Wertheim-van Dillen, and J. van der Noordaa. 1990. “Rapid and Simple Method for Purification of Nucleic Acids.” *Journal of Clinical Microbiology* 28 (3): 495–503.

Bourquin, Yannyk, and Jonathan M. Cooper. 2013. “Swimming Using Surface Acoustic Waves.” *PLoS ONE* 8 (2): e42686. doi:10.1371/journal.pone.0042686.

Campanelli, John R., and Xiaohong Wang. 1998. “Comments on Modelling the Diffusion-Controlled Adsorption of Surfactants.” *The Canadian Journal of Chemical Engineering* 76 (1): 51–57. doi:10.1002/cjce.5450760107.

Cao, Weidong, Christopher J. Easley, Jerome P. Ferrance, and James P. Landers. 2006. “Chitosan as a Polymer for pH-Induced DNA Capture in a Totally Aqueous System.” *Anal. Chem.* 78 (20): 7222–28. doi:10.1021/ac060391l.

Carroll, Brian, and Carlos Hidrovo. 2013a. “Experimental Investigation of Inertial Mixing in Colliding Droplets.” *Heat Transfer Engineering* 34 (2-3): 120–30. doi:10.1080/01457632.2013.703087.

Carroll, Brian, and Carlos Hidrovo. 2013b. “Droplet Detachment Mechanism in a High-Speed Gaseous Microflow.” *Journal of Fluids Engineering* 135 (7): 071206–071206. doi:10.1115/1.4024057.

Chang, Yi-Hsien, Gwo-Bin Lee, Fu-Chun Huang, Yi-Yu Chen, and Jr-Lung Lin. 2006. “Integrated Polymerase Chain Reaction Chips Utilizing Digital Microfluidics.” *Biomedical Microdevices* 8 (3): 215–25. doi:10.1007/s10544-006-8171-y.

Chin, Curtis D., Tassaneewan Laksanasopin, Yuk Kee Cheung, David Steinmiller, Vincent Linder, Hesam Parsa, Jennifer Wang, et al. 2011. “Microfluidics-Based Diagnostics of Infectious Diseases in the Developing World.” *Nature Medicine* 17 (8): 1015–19. doi:10.1038/nm.2408.

Chin, Curtis D., Vincent Linder, and Samuel K. Sia. 2012. “Commercialization of Microfluidic Point-of-Care Diagnostic Devices.” *Lab on a Chip* 12 (12): 2118–34. doi:10.1039/C2LC21204H.

Cho, Sung Kwon, Hyejin Moon, and Chang-Jin Kim. 2003. “Creating, Transporting, Cutting, and Merging Liquid Droplets by Electrowetting-Based Actuation for Digital Microfluidic Circuits.” *Journal of Microelectromechanical Systems* 12 (1): 70–80. doi:10.1109/JMEMS.2002.807467.

Ding, Xiaoyun, Peng Li, Sz-Chin Steven Lin, Zackary S. Stratton, Nitesh Nama, Feng Guo, Daniel Slotcavage, et al. 2013. “Surface Acoustic Wave Microfluidics.” *Lab on a Chip* 13 (18): 3626–49. doi:10.1039/C3LC50361E.

Emmanuel, Evens, Khalil Hanna, Christine Bazin, Gérard Keck, Bernard Clément, and Yves Perrodin. 2005. “Fate of Glutaraldehyde in Hospital Wastewater and Combined Effects of Glutaraldehyde and Surfactants on Aquatic Organisms.” *Environment International* 31 (3): 399–406. doi:10.1016/j.envint.2004.08.011.

Eun, Hyone-Myong. 1996. *Enzymology Primer for Recombinant DNA Technology*. San Diego, CA: Academic Press, Inc.

Flueckiger, Jonas, Vahid Bazargan, Boris Stoeber, and Karen C. Cheung. 2011. “Characterization of Postfabricated Parylene C Coatings inside PDMS Microdevices.” *Sensors and Actuators B: Chemical* 160 (1): 864–74. doi:10.1016/j.snb.2011.08.073.

Gubala, Vladimir, Leanne F. Harris, Antonio J. Ricco, Ming X. Tan, and David E. Williams. 2012. “Point of Care Diagnostics: Status and Future.” *Analytical Chemistry* 84 (2): 487–515. doi:10.1021/ac2030199.

Guttenberg, Zeno, Helena Müller, Heiko Habermüller, Andreas Geisbauer, Jürgen Pipper, Jana Felbel, Mark Kielpinski, Jürgen Scriba, and Achim Wixforth. 2005. “Planar Chip Device for PCR and Hybridization with Surface Acoustic Wave Pump.” *Lab on a Chip* 5 (3): 308–17. doi:10.1039/B412712A.

Hagan, Kristin A., Whitney L. Meier, Jerome P. Ferrance, and James P. Landers. 2009. “Chitosan-Coated Silica as a Solid Phase for RNA Purification in a Microfluidic Device.” *Anal. Chem.* 81 (13): 5249–56. doi:10.1021/ac900820z.

Hatch, Andrew C., Jeffrey S. Fisher, Armando R. Tovar, Albert T. Hsieh, Robert Lin, Stephen L. Pentoney, David L. Yang, and Abraham P. Lee. 2011. “1-Million Droplet Array with Wide-Field Fluorescence Imaging for Digital PCR.” *Lab on a Chip* 11 (22): 3838–45. doi:10.1039/C1LC20561G.

Haugland, Richard A., Nichole Brinkman, and Stephen J. Vesper. 2002. “Evaluation of Rapid DNA Extraction Methods for the Quantitative Detection of Fungi Using Real-Time PCR Analysis.” *Journal of Microbiological Methods* 50 (3): 319–23. doi:10.1016/S0167-7012(02)00037-4.

Hermanson, Greg. 2008. *Bioconjugate Techniques*. 2nd ed. London: Elsevier Inc.

Hsu, Yu-Hsiang, Monica L. Moya, Parinaz Abiri, Christopher C. W. Hughes, Steven C. George, and Abraham P. Lee. 2012. "Full Range Physiological Mass Transport Control in 3D Tissue Cultures." *Lab on a Chip* 13 (1): 81–89. doi:10.1039/C2LC40787F.

Ikai, Atsushi. 1980. "Thermostability and Aliphatic Index of Globular Proteins." *Journal of Biochemistry* 88 (6): 1895–98.

Innis, M. A., K. B. Myambo, D. H. Gelfand, and M. A. Brow. 1988. "DNA Sequencing with Thermus Aquaticus DNA Polymerase and Direct Sequencing of Polymerase Chain Reaction-Amplified DNA." *Proceedings of the National Academy of Sciences* 85 (24): 9436–40.

Jiang, Cheng, Shen Xu, Sheng Zhang, and Li Jia. 2012. "Chitosan Functionalized Magnetic Particle-Assisted Detection of Genetically Modified Soybeans Based on Polymerase Chain Reaction and Capillary Electrophoresis." *Analytical Biochemistry* 420 (1): 20–25. doi:10.1016/j.ab.2011.09.004.

Jiang, Kunqiang, Annie Xi Lu, Panagiotis Dimitrakopoulos, Don L. DeVoe, and Srinivasa R. Raghavan. 2015. "Microfluidic Generation of Uniform Water Droplets Using Gas as the Continuous Phase." *Journal of Colloid and Interface Science* 448 (June): 275–79. doi:10.1016/j.jcis.2015.02.023.

Kendall, Eric L., Erik Wienhold, and Don L. DeVoe. 2014. "A Chitosan Coated Monolith for Nucleic Acid Capture in a Thermoplastic Microfluidic Chip." *Biomicrofluidics* 8 (4): 044109. doi:10.1063/1.4891100.

Kim, Jeong Ah, Ji Youn Lee, Shimyoung Seong, Seung Hwan Cha, Seung Hwan Lee, Jae Jeong Kim, and Tai Hyun Park. 2006. "Fabrication and Characterization of a PDMS–glass Hybrid Continuous-Flow PCR Chip." *Biochemical Engineering Journal* 29 (1–2): 91–97. doi:10.1016/j.bej.2005.02.032.

Kim, Jitae, Michael Mauk, Dafeng Chen, Xianbo Qiu, Jungkyu Kim, Bruce Gale, and Haim H. Bau. 2010. "A PCR Reactor with an Integrated Alumina Membrane for Nucleic Acid Isolation." *Analyst* 135 (9): 2408–14. doi:10.1039/C0AN00288G.

Kneuer, Carsten, Mohammad Sameti, Eleonore G Haltner, Thomas Schiestel, Hermann Schirra, Helmut Schmidt, and Claus-Michael Lehr. 2000. "Silica Nanoparticles Modified with Aminosilanes as Carriers for Plasmid DNA." *International Journal of Pharmaceutics* 196 (2): 257–61. doi:10.1016/S0378-5173(99)00435-4.

Koc, Y., A. J. de Mello, G. McHale, M. I. Newton, P. Roach, and N. J. Shirtcliffe. 2008. "Nano-Scale Superhydrophobicity: Suppression of Protein Adsorption and Promotion of Flow-Induced Detachment." *Lab on a Chip* 8 (4): 582–86. doi:10.1039/B716509A.

Krajewska, Barbara, and Andrzej Olech. 1996. “Pore Structure of Gel Chitosan Membranes. I. Solute Diffusion Measurements.” *Polymer Gels and Networks* 4 (1): 33–43. doi:10.1016/0966-7822(95)00015-1.

Kumaresan, Palani, Chaoyong James Yang, Samantha A. Cronier, Robert G. Blazej, and Richard A. Mathies. 2008. “High-Throughput Single Copy DNA Amplification and Cell Analysis in Engineered Nanoliter Droplets.” *Analytical Chemistry* 80 (10): 3522–29. doi:10.1021/ac800327d.

Kuo, Jason S., Paolo Spicar-Mihalic, Indalesio Rodriguez, and Daniel T. Chiu. 2003. “Electrowetting-Induced Droplet Movement in an Immiscible Medium.” *Langmuir* 19 (2): 250–55. doi:10.1021/la020698p.

Lacy, Michael J., and Edward W. Voss Jr. 1989. “Direct Adsorption of ssDNA to Polystyrene for Characterization of the DNA/anti-DNA Interaction, and Immunoassay for Anti-DNA Autoantibody in New Zealand White Mice.” *Journal of Immunological Methods* 116 (1): 87–98. doi:10.1016/0022-1759(89)90316-5.

Lai, Eva, and John H. van Zanten. 2001. “Monitoring DNA/Poly-L-Lysine Polyplex Formation with Time-Resolved Multiangle Laser Light Scattering.” *Biophysical Journal* 80 (2): 864–73. doi:10.1016/S0006-3495(01)76065-1.

Lawyer, F. C., S. Stoffel, R. K. Saiki, S. Y. Chang, P. A. Landre, R. D. Abramson, and D. H. Gelfand. 1993. “High-Level Expression, Purification, and Enzymatic Characterization of Full-Length Thermus Aquaticus DNA Polymerase and a Truncated Form Deficient in 5’ to 3’ Exonuclease Activity.” *Genome Research* 2 (4): 275–87. doi:10.1101/gr.2.4.275.

Lemmon, E.W., M.O. McLinden, and D.G. Friend. 2012. “Thermophysical Properties of Fluid Systems.” In *NIST Standard Reference Database Number 69*. Gaithersburg, MD: National Institute of Standards and Technology. http://webbook.nist.gov.

Lippmann, Gabriel. 1875. “Relations Entre Les Phénomènes Électriques et Capillaires.” Gauthier-Villars.

Liu, Chien-Ju, Kang-Yi Lien, Ching-Yi Weng, Jyh-Wei Shin, Tsuey-Yu Chang, and Gwo-Bin Lee. 2009. “Magnetic-Bead-Based Microfluidic System for Ribonucleic Acid Extraction and Reverse Transcription Processes.” *Biomedical Microdevices* 11 (2): 339–50. doi:10.1007/s10544-008-9240-1.

Liu, Peng, Xiujun Li, Susan A. Greenspoon, James R. Scherer, and Richard A. Mathies. 2011. “Integrated DNA Purification, PCR, Sample Cleanup, and Capillary Electrophoresis Microchip for Forensic Human Identification.” *Lab on a Chip* 11 (6): 1041–48. doi:10.1039/C0LC00533A.

Lounsbury, Jenny A., Anne Karlsson, Daniel C. Miranian, Stephen M. Cronk, Daniel A. Nelson, Jingyi Li, Doris M. Haverstick, Paul Kinnon, David J. Saul, and James P.

Landers. 2013. “From Sample to PCR Product in under 45 Minutes: A Polymeric Integrated Microdevice for Clinical and Forensic DNA Analysis.” *Lab on a Chip* 13 (7): 1384–93. doi:10.1039/C3LC41326H.

Ma, Pei Lian, Marc Lavertu, Françoise M. Winnik, and Michael D. Buschmann. 2009. “New Insights into Chitosan−DNA Interactions Using Isothermal Titration Microcalorimetry.” *Biomacromolecules* 10 (6): 1490–99. doi:10.1021/bm900097s.

Mattei, Michele, Georgios M. Kontogeorgis, and Rafiqul Gani. 2013. “Modeling of the Critical Micelle Concentration (CMC) of Nonionic Surfactants with an Extended Group-Contribution Method.” *Industrial & Engineering Chemistry Research* 52 (34): 12236–46. doi:10.1021/ie4016232.

Miller, D. N., J. E. Bryant, E. L. Madsen, and W. C. Ghiorse. 1999. “Evaluation and Optimization of DNA Extraction and Purification Procedures for Soil and Sediment Samples.” *Applied and Environmental Microbiology* 65 (11): 4715–24.

Miller, R., V.B. Fainerman, A.V. Makievski, J. Krägel, D.O. Grigoriev, V.N. Kazakov, and O.V. Sinyachenko. 2000. “Dynamics of Protein and Mixed Protein/surfactant Adsorption Layers at the Water/fluid Interface.” *Advances in Colloid and Interface Science* 86 (1–2): 39–82. doi:10.1016/S0001-8686(00)00032-4.

Miller, R, V.B Fainerman, A.V Makievski, J Krägel, and R Wüstneck. 2000. “Adsorption Characteristics of Mixed Monolayers of a Globular Protein and a Non-Ionic Surfactant.” *Colloids and Surfaces A: Physicochemical and Engineering Aspects* 161 (1): 151–57. doi:10.1016/S0927-7757(99)00333-7.

Moltzahn, Felix, Adam B. Olshen, Lauren Baehner, Andrew Peek, Lawrence Fong, Hubert Stöppler, Jeffry Simko, Joan F. Hilton, Peter Carroll, and Robert Blelloch. 2011. “Microfluidic-Based Multiplex qRT-PCR Identifies Diagnostic and Prognostic microRNA Signatures in the Sera of Prostate Cancer Patients.” *Cancer Research* 71 (2): 550–60. doi:10.1158/0008-5472.CAN-10-1229.

Moon, Hyejin, Aaron R. Wheeler, Robin L. Garrell, Joseph A. Loo, and Chang-Jin “CJ” Kim. 2006. “An Integrated Digital Microfluidic Chip for Multiplexed Proteomic Sample Preparation and Analysis by MALDI-MS.” *Lab on a Chip* 6 (9): 1213–19. doi:10.1039/B601954D.

Naccache, Samia N., John Hackett, Eric L. Delwart, and Charles Y. Chiu. 2014. “Concerns over the Origin of NIH-CQV, a Novel Virus Discovered in Chinese Patients with Seronegative Hepatitis.” *Proceedings of the National Academy of Sciences* 111 (11): E976–E976. doi:10.1073/pnas.1317064111.

Neuzil, Pavel, Chunyan Zhang, Juergen Pipper, Sharon Oh, and Lang Zhuo. 2006. “Ultra Fast Miniaturized Real-Time PCR: 40 Cycles in Less than Six Minutes.” *Nucleic Acids Research* 34 (11): e77. doi:10.1093/nar/gkl416.

Niemz, Angelika, Tanya M. Ferguson, and David S. Boyle. 2011. “Point-of-Care Nucleic Acid Testing for Infectious Diseases.” *Trends in Biotechnology* 29 (5): 240–50. doi:10.1016/j.tibtech.2011.01.007.

Oblath, Emily A., W. Hampton Henley, Jean Pierre Alarie, and J. Michael Ramsey. 2013. “A Microfluidic Chip Integrating DNA Extraction and Real-Time PCR for the Detection of Bacteria in Saliva.” *Lab on a Chip* 13 (7): 1325–32. doi:10.1039/C3LC40961A.

Pekin, Deniz, Yousr Skhiri, Jean-Christophe Baret, Delphine Le Corre, Linas Mazutis, Chaouki Ben Salem, Florian Millot, et al. 2011. “Quantitative and Sensitive Detection of Rare Mutations Using Droplet-Based Microfluidics.” *Lab on a Chip* 11 (13): 2156–66. doi:10.1039/C1LC20128J.

Peter, Trevor, Anne Badrichani, Emily Wu, Richard Freeman, Bekezela Ncube, Fabiana Ariki, Jennifer Daily, Yoko Shimada, and Maurine Murtagh. 2008. “Challenges in Implementing CD4 Testing in Resource-Limited Settings.” *Cytometry Part B: Clinical Cytometry* 74B (S1): S123–30. doi:10.1002/cyto.b.20416.

Pollack, M. G., A. D. Shenderov, and R. B. Fair. 2002. “Electrowetting-Based Actuation of Droplets for Integrated Microfluidics.” *Lab on a Chip* 2 (2): 96–101. doi:10.1039/B110474H.

Pompano, Rebecca R., Weishan Liu, Wenbin Du, and Rustem F. Ismagilov. 2011. “Microfluidics Using Spatially Defined Arrays of Droplets in One, Two, and Three Dimensions.” *Annual Review of Analytical Chemistry* 4 (1): 59–81. doi:10.1146/annurev.anchem.012809.102303.

Reedy, Carmen R., Carol W. Price, Jeff Sniegowski, Jerome P. Ferrance, Matthew Begley, and James P. Landers. 2011. “Solid Phase Extraction of DNA from Biological Samples in a Post-Based, High Surface Area Poly(methyl Methacrylate) (PMMA) Microdevice.” *Lab on a Chip* 11 (9): 1603. doi:10.1039/c0lc00597e.

Richard, Isabelle, Marc Thibault, Gregory De Crescenzo, Michael D. Buschmann, and Marc Lavertu. 2013. “Ionization Behavior of Chitosan and Chitosan–DNA Polyplexes Indicate That Chitosan Has a Similar Capability to Induce a Proton-Sponge Effect as PEI.” *Biomacromolecules* 14 (6): 1732–40. doi:10.1021/bm4000713.

Roach, L. Spencer, Helen Song, and Rustem F. Ismagilov. 2005. “Controlling Nonspecific Protein Adsorption in a Plug-Based Microfluidic System by Controlling Interfacial Chemistry Using Fluorous-Phase Surfactants.” *Analytical Chemistry* 77 (3): 785–96. doi:10.1021/ac049061w.

Roy, Emmanuel, Gale Stewart, Maxence Mounier, Lidija Malic, Régis Peytavi, Liviu Clime, Marc Madou, Maurice Bossinot, Michel G. Bergeron, and Teodor Veres.

2014. “From Cellular Lysis to Microarray Detection, an Integrated Thermoplastic Elastomer (TPE) Point of Care Lab on a Disc.” *Lab on a Chip* 15 (2): 406–16. doi:10.1039/C4LC00947A.

Rueger, Paul E. 2013. “Liquid-Liquid Dispersions in Batch and In-Line Rotor Stator Mixers.” College Park: University of Maryland.

Rueger, Paul E., and Richard V. Calabrese. 2013. “Dispersion of Water into Oil in a Rotor–stator Mixer. Part 1: Drop Breakup in Dilute Systems.” *Chemical Engineering Research and Design* 05. Accessed October 23. doi:10.1016/j.cherd.2013.05.018.

Schaerli, Yolanda, Robert C. Wootton, Tom Robinson, Viktor Stein, Christopher Dunsby, Mark A. A. Neil, Paul M. W. French, Andrew J. deMello, Chris Abell, and Florian Hollfelder. 2009. “Continuous-Flow Polymerase Chain Reaction of Single-Copy DNA in Microfluidic Microdroplets.” *Analytical Chemistry* 81 (1): 302–6. doi:10.1021/ac802038c.

Sista, Ramakrishna, Zhishan Hua, Prasanna Thwar, Arjun Sudarsan, Vijay Srinivasan, Allen Eckhardt, Michael Pollack, and Vamsee Pamula. 2008. “Development of a Digital Microfluidic Platform for Point of Care Testing.” *Lab on a Chip* 8 (12): 2091–2104. doi:10.1039/B814922D.

Störkle, Dominic, Sabrina Duschner, Nils Heimann, Michael Maskos, and Manfred Schmidt. 2007. “Complex Formation of DNA with Oppositely Charged Polyelectrolytes of Different Chain Topology: Cylindrical Brushes and Dendrimers.” *Macromolecules* 40 (22): 7998–8006. doi:10.1021/ma0711689.

Strain, Matthew C., Steven M. Lada, Tiffany Luong, Steffney E. Rought, Sara Gianella, Valeri H. Terry, Celsa A. Spina, Christopher H. Woelk, and Douglas D. Richman. 2013. “Highly Precise Measurement of HIV DNA by Droplet Digital PCR.” *PLoS ONE* 8 (4): e55943. doi:10.1371/journal.pone.0055943.

Sun, Yingnan, Xiaoguang Zhou, and Yude Yu. 2014. “A Novel Picoliter Droplet Array for Parallel Real-Time Polymerase Chain Reaction Based on Double-Inkjet Printing.” *Lab on a Chip* 14 (18): 3603–10. doi:10.1039/C4LC00598H.

Sun, Yi, Than Linh Quyen, Tran Quang Hung, Wai Hoe Chin, Anders Wolff, and Dang Duong Bang. 2015. “A Lab-on-a-Chip System with Integrated Sample Preparation and Loop-Mediated Isothermal Amplification for Rapid and Quantitative Detection of Salmonella Spp. in Food Samples.” *Lab on a Chip* 15 (8): 1898–1904. doi:10.1039/C4LC01459F.

Teh, Shia-Yen, Robert Lin, Lung-Hsin Hung, and Abraham P. Lee. 2008. “Droplet Microfluidics.” *Lab on a Chip* 8 (2): 198–220. doi:10.1039/B715524G.

*The HLB SYSTEM a Time-Saving Guide to Emulsifier Selection*. 1980. Wilmington, DE: ICI Americas Inc.

Tornberg, Eva. 1978. "The Application of the Drop Volume Technique to Measurements of the Adsorption of Proteins at Interfaces." *Journal of Colloid and Interface Science* 64 (3): 391–402. doi:10.1016/0021-9797(78)90382-X.

Urdea, Mickey, Laura A. Penny, Stuart S. Olmsted, Maria Y. Giovanni, Peter Kaspar, Andrew Shepherd, Penny Wilson, et al. 2006. "Requirements for High Impact Diagnostics in the Developing World." *Nature* 444 (November): 73–79. doi:10.1038/nature05448.

Voigt, A., O. Thiel, D. Williams, Z. Policova, W. Zingg, and A. W. Neumann. 1991. "Axisymmetric Drop Shape Analysis (ADSA) Applied to Protein Solutions." *Colloids and Surfaces* 58 (3): 315–26. doi:10.1016/0166-6622(91)80231-C.

Wang, Fang, and Mark A. Burns. 2009. "Performance of Nanoliter-Sized Droplet-Based Microfluidic PCR." *Biomedical Microdevices* 11 (5): 1071–80. doi:10.1007/s10544-009-9324-6.

Ward, A. F. H., and L. Tordai. 1952. "Time-Dependence of Boundary Tensions of Solutions: IV. Kinetics of Adsorption at Liquid-Liquid Interfaces." *Recueil Des Travaux Chimiques Des Pays-Bas* 71 (6): 572–84. doi:10.1002/recl.19520710605.

Williams, Richard, Sergio G. Peisajovich, Oliver J. Miller, Shlomo Magdassi, Dan S. Tawfik, and Andrew D. Griffiths. 2006. "Amplification of Complex Gene Libraries by Emulsion PCR." *Nature Methods* 3 (7): 545–50. doi:10.1038/nmeth896.

Ye, Jian, George Coulouris, Irena Zaretskaya, Ioana Cutcutache, Steve Rozen, and Thomas L. Madden. 2012. "Primer-BLAST: A Tool to Design Target-Specific Primers for Polymerase Chain Reaction." *BMC Bioinformatics* 13 (1): 134. doi:10.1186/1471-2105-13-134.

Zhu, Xun, P. C. Sui, and Ned Djilali. 2007. "Numerical Simulation of Emergence of a Water Droplet from a Pore into a Microchannel Gas Stream." *Microfluidics and Nanofluidics* 4 (6): 543–55. doi:10.1007/s10404-007-0209-9.